JUSTUS-LIEBIG-UNIVERSITÄT GIESSEN

Justus-Liebig-Universität Gießen

Fachbereich 08: Biologie und Chemie

Institut für Anorganische und Analytische Chemie

Investigation on the Reactivity of Copper(I) and Copper(II) Complexes Supported by Triethylenetetramine Ligands Toward Dioxygen and Peroxides

Kumulativ-Dissertation zur Erlangung

des Doktorgrades der Naturwissenschaften

– Dr. rer. nat. –

Vorgelegt von

Chiara Eleonora Campi

Aus Solaro

June 2026

Selbstständigkeitserklärung

„Ich erkläre: Ich habe die vorgelegte Dissertation selbstständig und ohne unerlaubte fremde Hilfe und nur mit den Hilfen angefertigt, die ich in der Dissertation angegeben habe. Alle Textstellen, die wörtlich oder sinngemäß aus veröffentlichten Schriften entnommen sind, und alle Angaben, die auf mündlichen Auskünften beruhen, sind als solche kenntlich gemacht. Ich stimme einer evtl. Überprüfung meiner Dissertation durch eine Antiplagiat-Software zu. Bei den von mir durchgeführten und in der Dissertation erwähnten Untersuchungen habe ich die Grundsätze guter wissenschaftlicher Praxis, wie sie in der „Satzung der Justus-Liebig-Universität Gießen zur Sicherung guter wissenschaftlicher Praxis "niedergelegt sind, eingehalten."

Angaben zu auf künstlicher Intelligenz (KI) basierender Hilfen wie ChatGPT oder SchulKI von OpenAI oder Gemini von Google zur Erstellung meiner Dissertation (Zutreffendes angekreuzt):

☐ Ich habe bei der Erstellung dieses Textes kein KI-Tool verwendet.

☐ Ich habe ein KI-Tool in den folgenden Bereichen eingesetzt (Mehrfachnennungen möglich):

☐ Ideen finden, meine Kreativität anregen

☐ Verstehen von Konzepten, Recherche von Fakten und Definitionen

☐ Optimierung eines von mir verfassten Textes

☐ Erstellen ganzer Textpassagen nach meinen Vorgaben

Folgende KI-Tools habe ich verwendet, damit aufgeführte Teile meines Textes von dem Tool wie folgt profitiert haben: Grammarly & ChatGPT zur Optimierung eines von mir verfassten Textes.

Datum: _____ Unterschrift: _____

Erstgutachter: Prof. Dr. Siegfried Schindler

Zweitgutachter: Prof. Dr. Richard Göttlich

Acknowledgements

First and foremost, I would like to thank Prof. Dr. Siegfried Schindler for giving me the opportunity to pursue my doctoral studies within his research group and for his continuous support throughout these years. I am deeply grateful for the valuable scientific guidance and personal advice he provided. I especially appreciate the opportunity to pursue my research independently, while always being able to rely on his guidance and support whenever needed. I am thankful for the scientific discussion we had, and even more for the time and effort he dedicated to teaching me how to effectively communicate scientific results and hold presentations in a clear and engaging manner. Furthermore, I greatly appreciate the opportunities he offered me through collaborations, conference participation, and research placements, as well as the trust he placed in me throughout my PhD.

I would also like to sincerely thank the Studienstiftung des deutschen Volkes e.V., without whose financial support this PhD would not have been possible. I am equally grateful for the numerous educational opportunities they provided, including seminars, lectures, and language courses, which greatly enriched my academic and personal development.

I extend my thanks to Prof. Athina Anastasaki from ETH Zurich and Prof. Laura Gasque from UNAM for the outstanding and fruitful collaboration. In addition, I am grateful to Prof. Miquel Costas from the University of Girona for hosting me in his group during my research stay. I would further like to thank Dr. Christian Würtele for performing the crystal measurements and solving the crystal structures, and Prof. Dr. Richard Göttlich for serving as the second reviewer for this thesis.

In general, I would like to thank all my colleagues for the very pleasant working atmosphere and for the support they gave me both professionally and personally.

"The only impossible journey is the one you never begin."

− Anthony Robbins −

Abstract

Copper enzymes efficiently promote dioxygen reduction and catalyze the oxidation of small molecules. As a result, significant efforts have been directed toward the development of synthetic model systems that mimic the active sites of metalloproteins. Inspired by the efficiency of copper proteins and aiming to gain a deeper understanding of enzymatic processes involving copper-dioxygen adducts, this work focuses on the synthesis of bioinspired copper complexes featuring tetradentate tripodal ligands and on the investigation of the factors governing their stability and reactivity toward external substrates.

Chapter 3.1 presents the first part of this research and focuses on the unusual stability of a copper(II)−(*end-on*)superoxido ($\mathbf{S^E}$) complex observed under atom transfer radical polymerization (ATRP) conditions. A mechanistic study was performed to investigate the persistence of this species under ambient conditions, focusing on the roles of the ligand and the solvent. The detection of the $\mathbf{S^E}$ species for several hours after oxygenation was attributed to the establishment of a catalytic cycle that enables the accumulation of both the $\mathbf{S^E}$ intermediate and the dicopper(II)−(*end-on*)peroxido ($\mathbf{P^S}$) complex. A copper(II)−hydroxido species was also identified as a key intermediate in this process. Both the Me_6tren ligand and the DMSO solvent were found to play crucial roles in sustaining this cycle, as they can act as reducing agents and promote regeneration of the copper(I) precursor. These findings highlight the importance of ligand and solvent in the accumulation of reactive $\mathbf{S^E}$ intermediates and demonstrate that such species can also be accessed under ambient conditions. This work provides a basis for the development of new copper-based oxidation systems operating under mild conditions and contributes to bridging the gap between synthetic models and enzymatic active sites.

Chapter 3.2 presents the second part of this research, which investigates the formation of $\mathbf{S^E}$, copper(II)–hydroperoxido ($\mathbf{P^H}$), and copper(II)–alkylperoxido ($\mathbf{P^R}$) complexes supported by new tren-based ligand systems and explores their reactivity. First, the reaction of copper(I) and copper(II) species toward dioxygen, hydrogen peroxide, and cumene hydroperoxide was evaluated, demonstrating that minor variations in ligand steric and electronic properties have a significant influence on the formation and stabilization of oxygenated adducts. The reaction between the copper(I) precursors and dioxygen was monitored using stopped-flow techniques, and the conversion from $\mathbf{S^E}$ to $\mathbf{P^H}$ species could be observed. The reactivity of $\mathbf{P^R}$ and $\mathbf{P^H}$ species toward various substrates was then examined. Both systems exhibited nucleophilic reactivity toward benzoyl chloride, whereas only $\mathbf{P^R}$ intermediates promoted aldehyde deformylation, representing one of the few examples of mononuclear peroxido species capable of this process. Overall, this study provides new insight into the factors regulating the formation and reactivity of oxygenated adducts, contributing to laying the foundation for the design of future ligands for selective oxidation processes and providing valuable insight into the catalytic mechanism of enzymes, such as lytic polysaccharide monooxygenases.

Zusammenfassung

Kupferenzyme katalysieren die Reduktion von molekularem Sauerstoff und die Oxidation kleiner Moleküle. Daher wurden erhebliche Anstrengungen unternommen synthetische Modellsysteme zu entwickeln, welche die aktiven Zentren von Metalloproteinen nachahmen. Inspiriert von der hohen Effizienz kupferhaltiger Proteine und mit dem Ziel, ein besseres Verständnis enzymatischer Prozesse unter Beteiligung von Kupfer-Sauerstoff-Addukten zu gewinnen, konzentriert sich die vorliegende Arbeit auf die Synthese bioinspirierter Kupferkomplexe mit tetradentaten tripodalen Liganden sowie auf die Untersuchung, welche Faktoren Stabilität und Reaktivität gegenüber externen Substraten bestimmen.

Kapitel 3.1 stellt den ersten Teil dieser Arbeit dar und befasst sich mit der ungewöhnlichen Stabilität eines unter Bedingungen der Atomtransfer-Radikalpolymerisation (ATRP) beobachteten Kupfer(II)−(*end-on*)superoxid ($\mathbf{S^E}$) Komplexes. Zur Untersuchung der Persistenz dieser Spezies wurde eine mechanistische Studie durchgeführt, wobei insbesondere die Rolle des Liganden und des Lösungsmittels analysiert wurde. Die Detektion der $\mathbf{S^E}$ Spezies über mehrere Stunden nach der Oxygenierung wurde auf die Etablierung eines katalytischen Zyklus zurückgeführt, der die Akkumulation sowohl der $\mathbf{S^E}$ Intermediate als auch des Dikupfer(II)−(*end-on*)peroxido ($\mathbf{P^S}$) Komplexes ermöglicht. Darüber hinaus wurde eine Kupfer(II)−hydroxido Spezies als zentrales Zwischenprodukt dieses Prozesses identifiziert. Sowohl der Me$_6$tren-Ligand als auch das Lösungsmittel DMSO erwiesen sich als entscheidend für die Aufrechterhaltung dieses Zyklus, da beide als Reduktionsmittel wirken und die Regeneration des Kupfer(I)-Vorläufers fördern. Diese Ergebnisse unterstreichen die Bedeutung von Liganden und Lösungsmitteln für die Akkumulation reaktiver $\mathbf{S^E}$ Intermediate und zeigen zugleich, dass derartige Spezies auch unter Umgebungsbedingungen zugänglich sind. Die vorliegende Arbeit liefert damit eine Grundlage für die Entwicklung neuer kupferbasierter Oxidationssysteme unter milden Bedingungen und trägt dazu bei, die Lücke zwischen synthetischen Modellsystemen und enzymatischen aktiven Zentren zu schließen.

Kapitel 3.2 beschreibt den zweiten Teil dieser Arbeit, der die Bildung von $\mathbf{S^E}$, Kupfer(II)−Hydroperoxido ($\mathbf{P^H}$) und Kupfer(II)–Alkylperoxido ($\mathbf{P^R}$) Komplexen untersucht, die durch neue tren-basierte Ligandensysteme stabilisiert werden, sowie deren Reaktivität analysiert. Zunächst wurde die Reaktion dieser Spezies mit molekularem Sauerstoff, Wasserstoffperoxid und Cumylperoxid untersucht. Dabei konnte gezeigt werden, dass bereits geringe Variationen der sterischen und elektronischen Eigenschaften der Liganden einen signifikanten Einfluss auf die Bildung und Stabilisierung oxygenierter Addukte haben. Die Reaktion von Kupfer(I)-Vorläufern mit molekularem Sauerstoff wurde mittels „Stopped-Flow"-Technik analysiert und die Umwandlung von $\mathbf{S^E}$ zu $\mathbf{P^H}$ Spezies wurde beobachtet. Anschließend wurde die Reaktivität von $\mathbf{P^R}$ und $\mathbf{P^H}$ Spezies gegenüber verschiedenen Substraten untersucht. Beide Systeme zeigten nukleophile Reaktivität gegenüber Benzoylchlorid, während ausschließlich $\mathbf{P^R}$ Intermediate die Deformylierung von Aldehyden katalysierten, was eines der wenigen Beispiele mononuklearer Peroxido-Spezies darstellt, die diesen Prozess katalysieren. Insgesamt liefert diese Studie neue Erkenntnisse über die Faktoren, welche die Bildung und Reaktivität oxygenierter Addukte steuern. Dadurch wird eine Grundlage für das Design zukünftiger Liganden für selektive Oxidationsprozesse ermöglicht sowie ein wertvoller Beitrag zum Verständnis des katalytischen Mechanismus von Enzymen wie der lytischen Polysaccharid-Monooxygenase geleistet.

Table of Contents

Selbstständigkeitserklärung III
Acknowledgements V
Abstract VIII
Zusammenfassung IX
1. Introduction 1
1.1 Metalloproteins 1
1.1.1 Biological Role of Copper Complexes 1
1.1.1.1 Type-1 Copper Proteins 3
1.1.1.2 Type-2 Copper Proteins 3
1.1.1.3 Type-3 Copper Proteins 6
1.2 Bioinspired Model Complexes 7
1.2.1 Characterization of Copper-Dioxygen Adducts 9
1.2.2 Mononuclear Copper-Dioxygen Complexes 10
1.2.2.1 Structure and Characterization 10
1.2.2.2 Reactivity of Copper(II) *End-on* Superoxido Complexes 12
1.2.3 Copper Hydroperoxido and Alkylperoxido Complexes 15
1.2.3.1 Synthesis and Characterization 15
1.2.3.2 Reactivity of Copper(II) Hydroperoxido and Cumylperoxido Complexes 18
2. Research Goals 23
3. Published Research Articles 25
3.1 Unusual Stability of an *End-on* Superoxido Copper(II) Complex under Ambient Conditions 25
3.2 Copper Complexes with Arylated Triethylenetetramine Ligands: Reactivity Toward Dioxygen and Peroxides 31
3.3 Additional Published Research Articles 46
4. References 47

1. Introduction

1.1 Metalloproteins

Metalloproteins are a broad class of proteins that contain one or more metal ions in their active site, which influence both their structure and biological function.[1,2] Common metal ions include iron, zinc, copper, manganese, nickel, and magnesium, which are typically coordinated by specific amino acid residues such as histidine, cysteine, aspartate, glutamate, and occasionally by external ligands.[3–5] By tailoring the local coordination environment, such as geometry, ligand structure, polarity, and flexibility, the key properties of the metal center, including redox potential, Lewis acidity, spin state, and substrate specificity, can be finely tuned, enabling metalloproteins to carry out chemical reactions efficiently and selectively.[6–8] As a result, metalloproteins are involved in a multitude of essential biological processes, such as electron transfer (e.g., cytochromes and iron-sulfur proteins), small-molecule activation and transport (e.g., hemoglobin, myoglobin, nitrogenase), catalysis (e.g., carbonic anhydrase, superoxide dismutase, DNA polymerase), and regulation and signaling (e.g., zinc-finger transcription factors, copper- and heme-based sensors).[2,6,9]

1.1.1 Biological Role of Copper Complexes

In this context, particular attention has been directed toward copper-based metalloproteins. Copper has been identified in the active sites of numerous enzymes in humans, animals, plants, and microorganisms, where it is most commonly found in the +I and +II oxidation states, and occasionally as +III in some intermediates.[10] Based on the facile interconversion between copper(I) and copper(II) species, copper centers are able to act as intermediates in a wide range of biological catalytic processes. For instance, copper centers enable reversible binding and activation of molecular dioxygen (O_2), support one- or two-electron redox processes, and catalyze oxygen insertion into organic substrates. Accordingly, copper enzymes are mainly involved in electron transfer processes (e.g., plastocyanin), oxygen transport and storage (e.g., hemocyanin), oxidation and oxygenation reactions (e.g., cytochrome *c* oxidase and dopamine β-monooxygenase), and superoxide dismutation (e.g., superoxide dismutase; Figure 1).[11–13]

Copper is present in the human body as a trace element in approximately 150 mg and is essential for the development of connective tissue, bone, and nerve, as well as for the regulation of numerous redox processes.[14–16] The physiological significance of copper proteins is highlighted by the existence of severe diseases, such as Wilson's and Menkes diseases, which result from disrupted copper metabolism.[17,18] In addition to a classification according to their function (e.g., as oxidases or oxygenases), copper proteins are categorized according to their structural and spectroscopic characteristics, including the number of copper ions in the active site, coordination geometry, and distinctive UV–vis and electron paramagnetic resonance (EPR) features. Although numerous classes of copper proteins have been identified, the majority are grouped into type-1, type-2, and type-3 categories (Figure 2).[19–21]

Copper proteins that do not fit into this classification are referred to as non-classical copper proteins and can be further divided into distinct categories, namely type-4, CuA, CuB, and CuZ.[20,25] Type-4 proteins are found in enzymes such as laccase and ascorbate oxidase, and their

active site consists of a trinuclear cluster of type-2 and type-3 copper centers, which catalyze the oxidation of phenols and arylamines.[26–28] Mixed-valent binuclear CuA centers, mononuclear CuB sites, and tetranuclear CuZ clusters are found in metalloenzymes such as cytochrome *c* oxidase and nitrous oxide reductase.[29,30] In these systems, CuA and CuB centers participate in long-range intramolecular electron transfer processes and enable the reduction of O_2 to water in the respiratory chain, whereas the CuZ cluster catalyzes the two-electron reduction of N_2O to N_2.

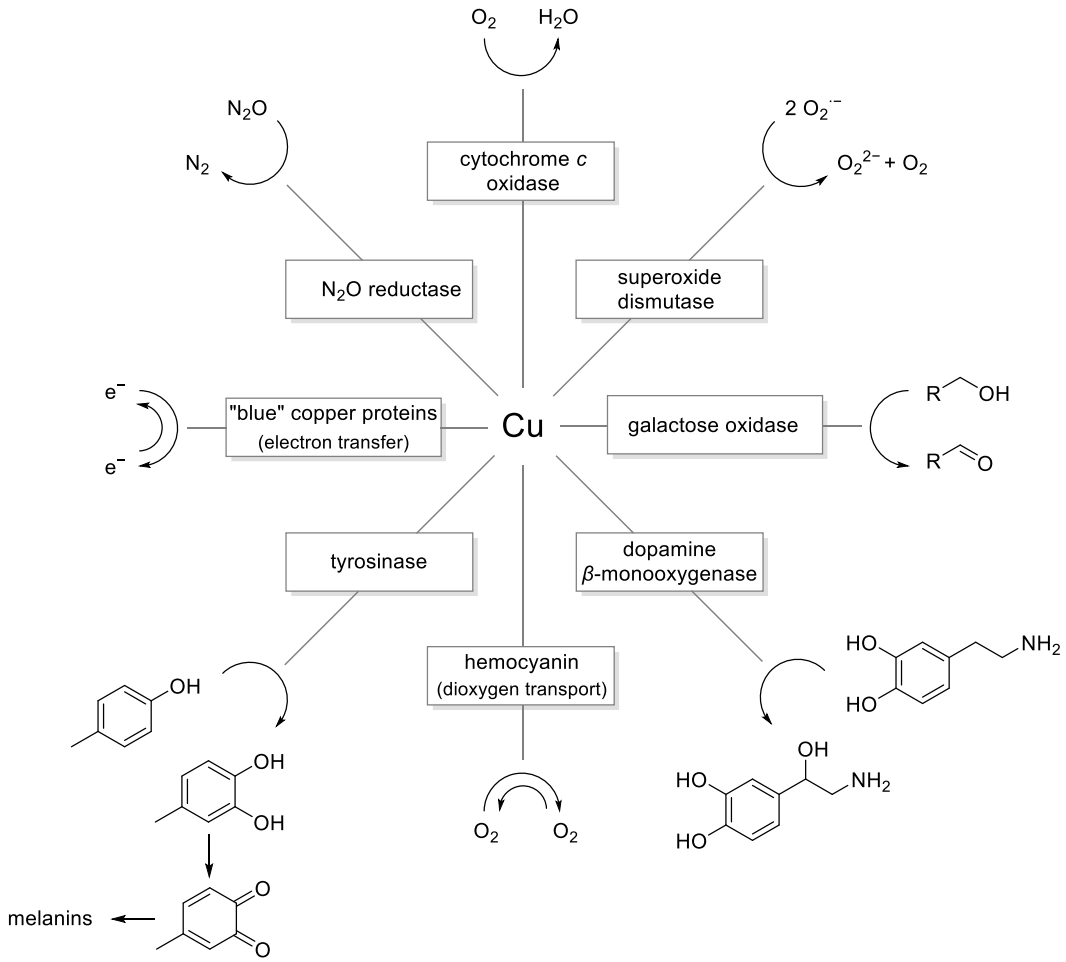


Figure 1: Examples of metabolic functions performed by copper-containing proteins.[11]

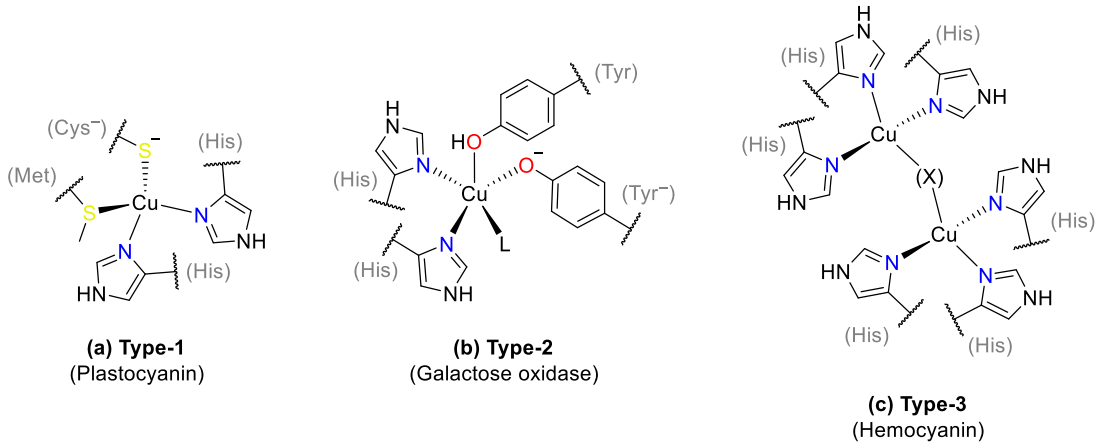


Figure 2: Active center of (**a**) type-1 (plastocyanin), (**b**) type-2 (galactose oxidase), and (**c**) type-3 (hemocyanin) copper proteins.[22–24]

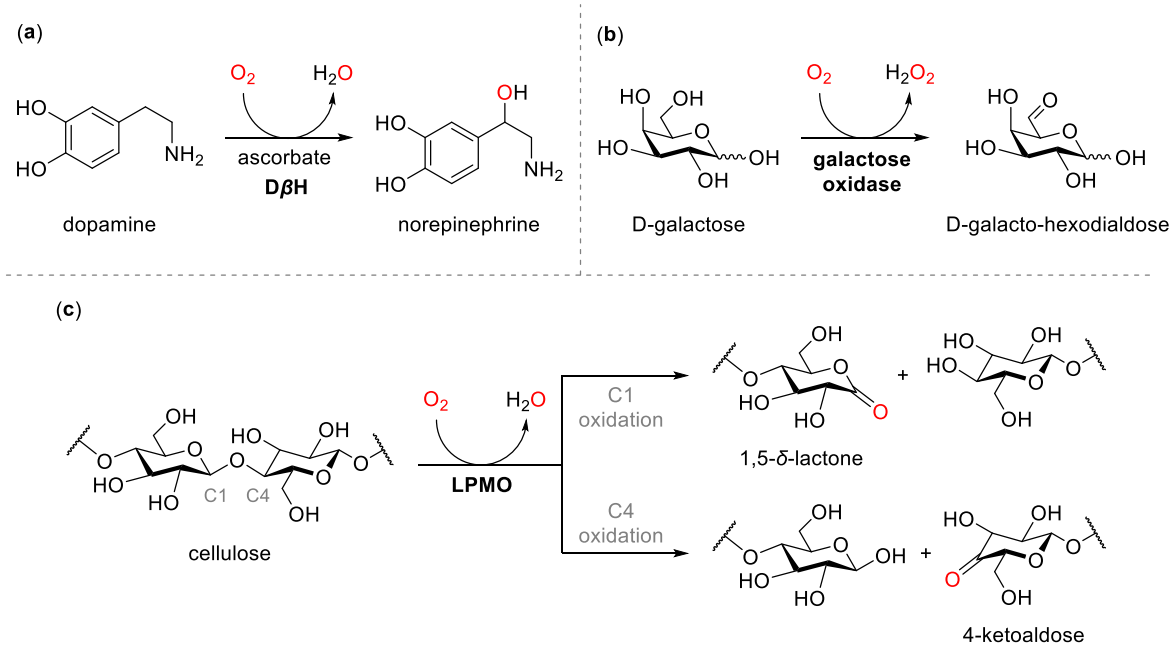
1.1.1.1 Type-1 Copper Proteins

Type-1 copper proteins (T1Cu), also referred to as cupredoxins, are primarily involved in electron transfer processes. Their active sites contain a single copper ion coordinated by one cysteine residue through a sulfur donor atom, two histidine residues, bound to the metal center through nitrogen donor atoms, and one or more variable axial ligands. Based on the number and nature of the axial ligands, T1Cu proteins are further divided into three subclasses. Both class I and class II T1Cu centers are bound to one axial ligand and adopt a distorted tetrahedral geometry. Class I T1Cu proteins, such as plastocyanin, display a methionine residue in the axial position (Figure 2a), whereas class II proteins, such as umecyanin, feature a non-methionine amino acid as the axial ligand.[22] In contrast, class III T1Cu proteins, such as azurin, contain two axial ligands, with the copper center coordinated by one methionine and one glycine residue.[2,19,20]

The coordination geometry of type-1 copper centers is generally described as distorted tetrahedral, which represents a compromise between the tetrahedral arrangement preferred by copper(I) and the square-planar coordination commonly adopted by copper(II) complexes.[31] This geometry facilitates rapid electron transfer between the two oxidation states, enabling T1Cu proteins to function efficiently as single-electron transfer agents.[22] An exception is azurin, which contains an additional weakly bound fifth ligand, resulting in a distorted trigonal bipyramidal coordination geometry. Type-1 copper proteins typically exhibit positive reduction potentials (exceeding 0.25 V) and display an intense blue color in their oxidized state. For this reason, they are often referred to as "*blue copper proteins*." This color arises from a strong absorption band near 600 nm, which is attributed to a ligand-to-metal charge-transfer (LMCT) from the sulfur of the cysteine to the copper(II) center.[32] Representative examples of type-1 copper proteins include plastocyanin and azurin, which act as electron carriers in plant and bacterial photosynthesis.[22,31]

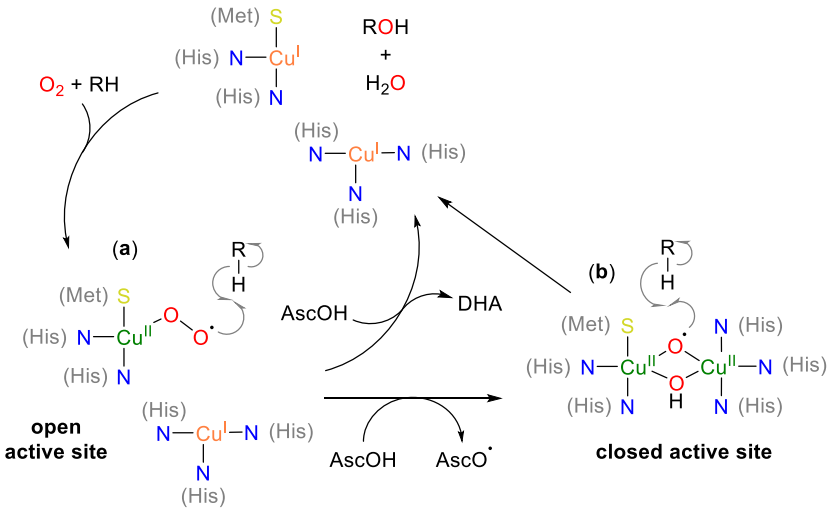
1.1.1.2 Type-2 Copper Proteins

Type-2 copper proteins (T2Cu) are primarily involved in catalytic processes. Their active sites contain a copper ion coordinated by four nitrogen and/or oxygen donor atoms, which typically originate from two histidine or tyrosine residues. In contrast to T1Cu proteins, the axial coordination site in T2Cu proteins may be vacant or occupied by labile external ligands, such as water molecules, enabling catalytic activity (Figure 2b). The copper center displays a square-planar or distorted tetrahedral geometry and exhibits electron paramagnetic resonance (EPR) features characteristic of copper(II) complexes.[2,20,33] Since no sulfur-based ligands are coordinated to the copper center, type-2 copper centers do not display intense absorption bands in the UV–vis region and are therefore commonly referred to as "*non-blue copper centers*." However, in their oxidized state, they also exhibit a slightly weak blue color, which results from symmetry-forbidden *d–d* electronic transitions. T2Cu proteins are commonly found in oxidases, oxygenases, and superoxide dismutases. Representative examples include dopamine *β*-hydroxylase (D*β*H), which catalyzes the side-chain hydroxylation of dopamine to norepinephrine (Scheme 1a); galactose oxidase, which catalyzes the two-electron oxidation of primary alcohols to the corresponding aldehydes (Scheme 1b); lytic polysaccharide monooxygenases (LPMOs), which catalyze oxidative cleavage of glycosidic bonds (Scheme 1c); and Cu/Zn superoxide dismutase, which catalyzes the disproportionation of superoxide anion radicals into molecular oxygen and hydrogen peroxide (H_2O_2).[13,23,34,35]



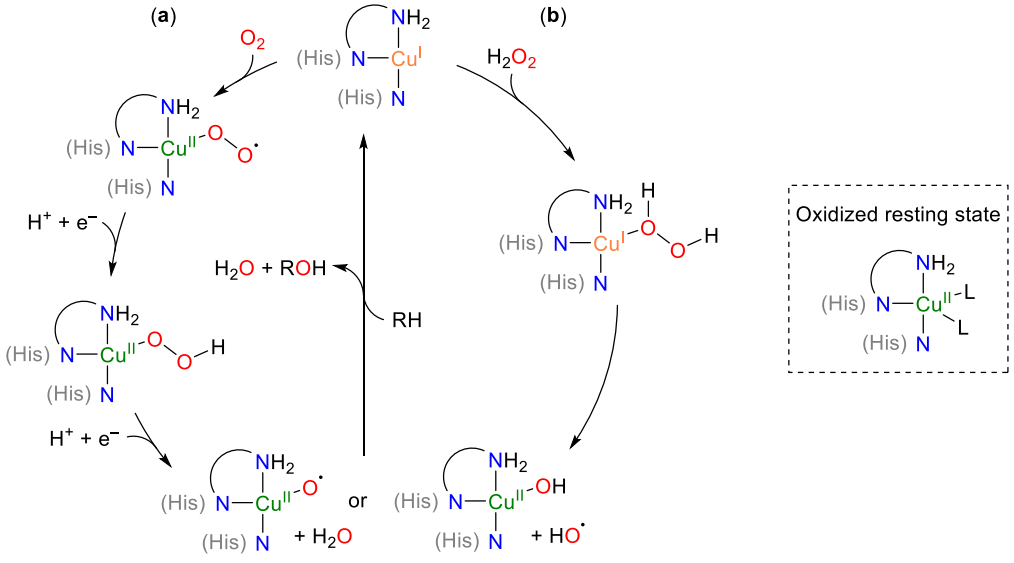
Scheme 1: Reaction catalyzed by (**a**) dopamine *β*-monooxygenase, (**b**) galactose oxidase, and (**c**) lytic polysaccharide monooxygenases.[36–38]

D*β*H is a copper-dependent monooxygenase that catalyzes the stereospecific hydroxylation of dopamine to norepinephrine in the presence of O_2 and ascorbate (Scheme 1a). The enzyme is essential for the biosynthesis and regulation of neurotransmitters and hormones, and plays a central role in maintaining the physiological balance between dopamine and norepinephrine, preventing neurological, physiological, and psychiatric disorders.[39] The catalytic core of D*β*H consists of two uncoupled copper ions, Cu_H and Cu_M, which are separated by approximately 11 Å in the resting state. The Cu_M site is coordinated by one methionine and two histidine residues, whereas the Cu_H site is coordinated by three histidine residues. Dioxygen activation and substrate hydroxylation occur at the Cu_M center, while the Cu_H serves as the ascorbate-binding site and mediates long-range electron transfer.[36] Although the structures of the resting enzyme states are known, the detailed mechanism of hydroxylation and the timing of electron transfer remain unclear. The prevailing mechanistic hypothesis proposes that O_2 binds at the Cu_M site, leading to the formation of a copper(II)−superoxido intermediate, which is supposed to be the active species responsible for hydrogen atom transfer (HAT) from the substrate (Scheme 2a). The subsequent hydroxylation of dopamine is driven by the oxidation of two equivalents of ascorbate under the release of a water molecule. However, alternative intermediates, including Cu(II)–hydroperoxido and Cu(III)–oxo species, have also been proposed to participate in substrate activation, and the precise nature of the reactive intermediate remains under investigation.[34,40–42] Moreover, recent crystal structures of human D*β*H have revealed significant structural flexibility, with the enzyme adopting both an open conformation, in which the copper centers are separated by approximately 14 Å, and a closed conformation, in which the Cu–Cu distance is reduced to 4-5 Å, suggesting the possible formation of a coupled binuclear copper site during catalysis (Scheme 2b). Together with complementary computational studies, these findings are prompting a reevaluation of the classification of D*β*H as a type-2 copper oxygenase.[43,44]



Scheme 2: Proposed mechanisms for DβH involving an HAT by: (**a**) superoxido intermediate and (**b**) η-oxyl dicopper intermediate. Abbreviation: AscOH for ascorbic acid; DHA for dehydroascorbic acid.[36]

Lytic polysaccharide monooxygenases (LPMOs) are mononuclear copper enzymes that catalyze the oxidative cleavage of polysaccharides through hydroxylation at the C1 or C4 carbon, thereby facilitating subsequent cleavage of the glycosidic bond (Scheme 1c). Since their discovery in the early 2010s[45], LPMOs have attracted considerable attention due to their crucial role in the degradation of recalcitrant polysaccharides, including cellulose and chitin, which are of paramount commercial interest for the production of advanced biofuels and bio-based chemicals.[46] These enzymes are classified as auxiliary activity enzymes and are categorized into eight families based on substrate specificity and organism of origin.[47] Despite their diversity, LPMOs share similar active sites in which the copper ion is coordinated by three nitrogen donor atoms. Specifically, the metal center is bound by two histidine residues, one of which acts as a chelating bidentate ligand in the characteristic histidine brace motif. In the oxidized state, additional ligands, such as water molecules, have also been observed coordinated at the copper center.[36,42,48] LPMOs exhibit catalytic activity in the presence of either O_2 or H_2O_2 (Scheme 3).



Scheme 3: Proposed mechanism for LPMO-catalyzed hydroxylation via (**a**) monooxygenase pathway and (**b**) peroxygenase pathway.[36] The oxidized resting state of the LMPOs active center is shown on the right.

Initially, these enzymes were classified as monooxygenases, with O_2 proposed as the primary co-substrate. However, more recent studies suggest that LPMOs may operate predominantly as peroxygenases, involving H_2O_2 as the co-substrate. Despite extensive investigation, the exact nature of the oxygenated co-substrate and the reactive copper-dioxygen intermediate involved in polysaccharide hydroxylation remains debated. Although a recent study by Schröder and coworkers reported a cryo-trapped structure of an activated dioxygen intermediate displaying features consistent with a mixture of superoxido and hydroperoxido states, alternative reactive intermediates, including Cu(II)–oxyl species and hydroxyl radicals, have also been proposed within the catalytic cycle.[49–51]

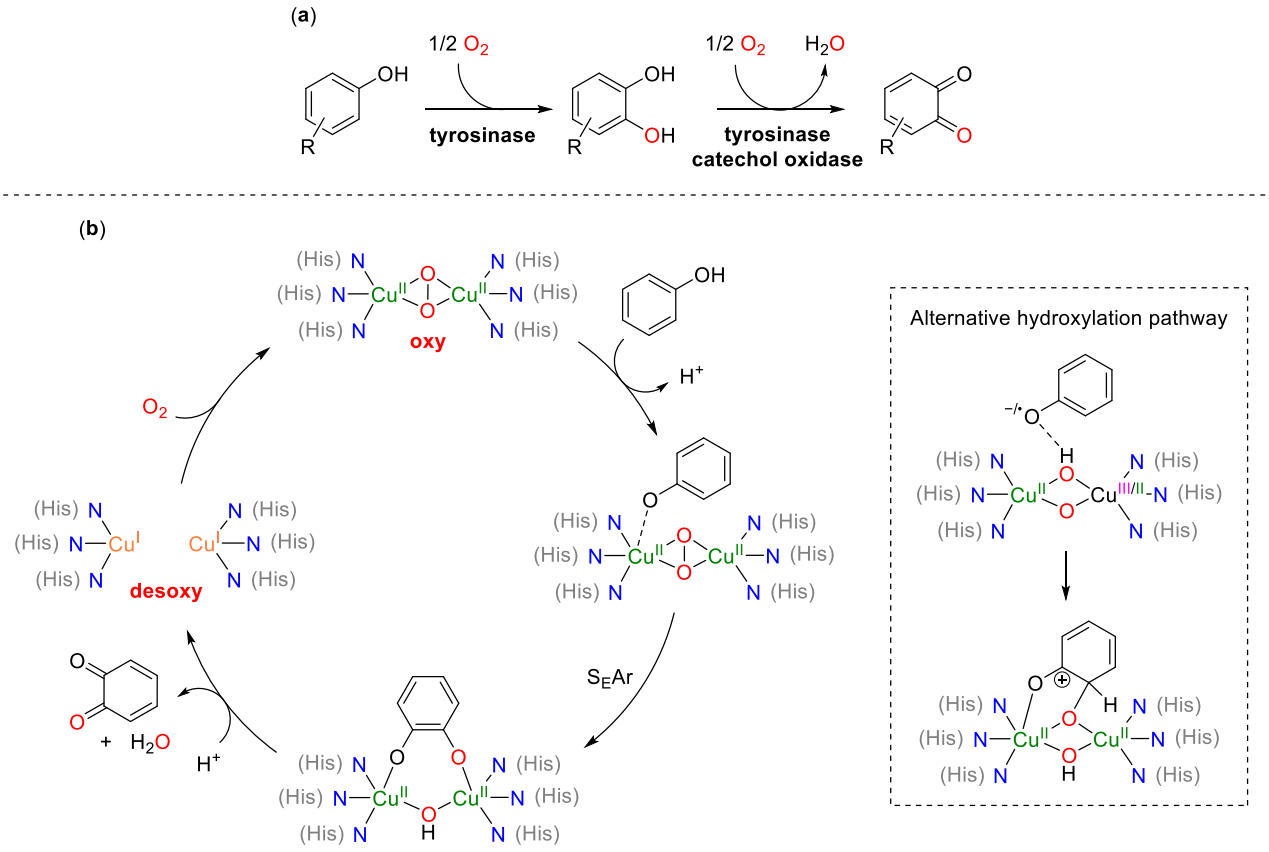
1.1.1.3 Type-3 Copper Proteins

In contrast to T1Cu and T2Cu copper proteins, type-3 copper proteins (T3Cu) contain a binuclear copper center consisting of two antiferromagnetically coupled ions, each coordinated by three histidine residues (Figure 2c). These proteins are able to reversibly bind O_2 between the two copper ions and activate it under ambient conditions.[20] While in the absence of O_2 the metal centers exhibit trigonal planar coordination geometry, the binding of O_2 induces a change toward a trigonal bipyramidal geometry due to the close proximity of the copper atoms.[21] In their oxy form, O_2 is coordinated as a *side-on* peroxido ligand to the metal centers, giving rise to two characteristic absorption bands at approximately 350 nm and 600 nm. Additionally, T3Cu proteins appear EPR-silent in their oxidized state because of the strong antiferromagnetic coupling between the two paramagnetic copper ions.[52] T3Cu proteins are mainly involved in oxidation reactions, functioning either as oxidases (e.g., catechol oxidase), oxygenases (e.g., tyrosinase), or in dioxygen transport (e.g., hemocyanin).[53–55] Tyrosinase and catechol oxidase catalyze the hydroxylation of phenolic substrates and oxidation of catechols to *ortho*-quinones, respectively, whereas hemocyanin serves as the oxygen carrier in many arthropods and mollusks and is responsible for the characteristic blue color of their blood.

Tyrosinases are enzymes that widely occur in prokaryotic and eukaryotic organisms, including plants, fungi, arthropods, and mammals, and are involved in several biological processes such as tissue pigmentation, wound healing, radiation protection, and primary immune responses.[36] They exhibit both monooxygenase and oxidase activity, which arise from the binding of O_2 between the two copper centers of the dinuclear active site. Phenolic substrates undergo *ortho*-hydroxylation to form catechols (e.g., conversion of tyrosine to L-DOPA (3,4-dihydroxy-L-phenylalanine)), whereas catechols undergo further two-electron oxidation to the corresponding *ortho*-quinones (e.g., oxidation of L-DOPA to L-dopaquinone, Scheme 4a).[12,48]

The catalytic cycle is initiated by the binding of O_2 between the two copper ions, resulting in the formation of the "oxy" state (Scheme 4b). A phenolic substrate subsequently coordinates to one of the copper centers in an axial position and undergoes monooxygenation to yield the corresponding catechol. Although tyrosinase has been extensively investigated, the detailed mechanism of this step remains under debate.[36,56] The majority of the studies support that the hydroxylation reaction proceeds through electrophilic aromatic substitution (S_EAr) of the phenolate substrate coordinated to the bis(μ-oxido) core.[52,57–59] However, more recent studies by Solomon and coworkers proposed an alternative pathway involving an initial hydrogen

transfer from the phenol to the bis(μ-oxido) moiety, resulting in O−O bond cleavage, followed by the coordination of the phenolate to one copper site and the concomitant C−O bond formation (Scheme 4b).[60,61] In the final step, the resulting catechol, bound to the dicopper center in a bidentate fashion, is oxidized to the corresponding *ortho*-quinone, thereby regenerating the "desoxy" form of the enzyme.[52]

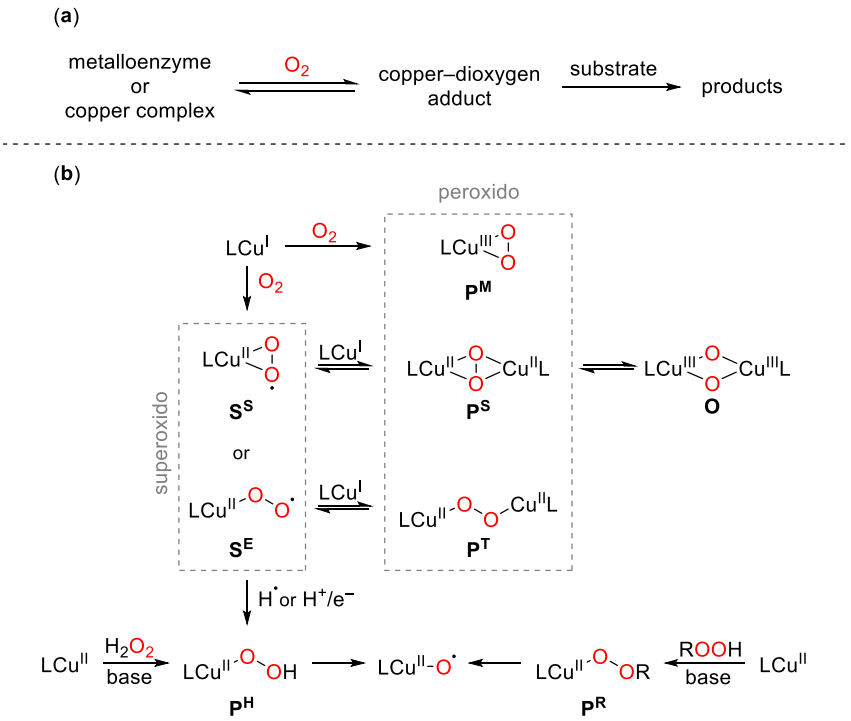


Scheme 4: (**a**) Reactions catalyzed by tyrosinase; (**b**) proposed catalytic cycle of tyrosinase (left). Hydroxylation pathway proposed by Solomon and coworkers (right). Abbreviation: S_EAr for electrophilic aromatic substitution.[52,61]

1.2 Bioinspired Model Complexes

Since copper enzymes efficiently promote O_2 reduction and catalyze the oxidation of small molecules, significant effort has been directed toward the development of model systems that mimic the active sites of metalloproteins. Such studies provide insight into the structure and reactivity of the active species and contribute to the design of catalytic systems for mild and selective oxidation reactions.[12,62–64] In many biological redox processes, dioxygen activation represents a key step in which the copper center binds O_2 prior to performing substrate oxidation (Scheme 5a). Therefore, particular attention has been directed toward the investigation of copper-dioxygen adducts.[36,63,65,66] As all these intermediates are highly reactive, low temperatures (typically below 200 K), aprotic solvents (e.g., dichloromethane, tetrahydrofuran, acetone), and weakly coordinating anions (e.g., perchlorate, triflate, and tetraphenylborate) are commonly employed in reactions between copper(I) complexes and O_2. In particular, low reaction temperatures are often required to enhance the lifetime of the copper-dioxygen adducts by reducing

the entropic cost of formation and suppressing subsequent reactions.[65] This approach enabled the characterization of different types of highly reactive oxygenated species, typically in a 1 : 1 or 2 : 1 Cu/O_2 stoichiometries (Scheme 5b). Some of these species are analogous to the active intermediates observed in copper proteins (Chapter 1.1.1), whereas others have not yet been observed in biological systems. However, the application of these reaction conditions does not always allow detection of oxygenated intermediate, as most copper(I) complexes react with O_2 via outer sphere oxidation to the corresponding copper(II) species, without any measurable accumulation of intermediates.[65]



Scheme 5: (**a**) Copper-dioxygen adducts as active species for substrate oxidation and (**b**) their possible formation pathways.[64,67]

Upon binding of O_2 to a copper(I) complex, mononuclear copper-dioxygen adducts, such as copper(II)−(*end-on*)superoxido ($\mathbf{S^E}$), copper(II)−(*side-on*)superoxido ($\mathbf{S^S}$), and copper(III)−(*side-on*)peroxido ($\mathbf{P^M}$) complexes, are formed in solution. As the nature of the resulting intermediate is strongly influenced by the properties of the ligand (L), careful ligand design can be used to selectively promote the formation of a specific intermediate species (Chapter 1.2.2.1).[64,65]

In many cases, due to their lability, these mononuclear species readily react with an additional equivalent of the copper(I) precursor to form μ-peroxido dicopper(II) complexes, which can adopt either *side-on* ($\mathbf{P^S}$) or *end-on* ($\mathbf{P^T}$) coordination modes. Depending on the ligand features, these μ-peroxido dicopper(II) species can undergo further reaction to yield bis(μ-oxido) dicopper(III) complexes (**O**). This process involves O–O bond cleavage induced by electron transfer from the copper centers to the peroxide unit.[64] In systems supported by less sterically demanding bidentate ligands, the resulting **O** core can further react with an additional copper(I) complex to generate mixed-valent trinuclear species containing copper in the +II and +III oxidation states. The various copper-dioxygen species can generally be considered to exist in

equilibrium, as only minor structural changes are formally required for their interconversion. Mononuclear copper(II)−hydroperoxido ($\mathbf{P^H}$) complexes can be generated from $\mathbf{S^E}$ intermediates through hydrogen-atom abstraction or proton-coupled electron transfer. However, only a few examples of such reactivity have been reported to date (Chapter 1.2.2.2 and Chapter 3.2). More commonly, $\mathbf{P^H}$ and copper(II)–alkylperoxido ($\mathbf{P^R}$) complexes are accessed via the reaction of copper(II) precursors with H_2O_2 or alkyl hydroperoxides (ROOH, typically with R = *tert*-butyl or cumyl) in the presence of a base (typically triethylamine, Chapter 1.2.3.1). Homolytic cleavage of the O–O bond in $\mathbf{P^H}$ and $\mathbf{P^R}$ species has been proposed to generate highly reactive copper-oxyl intermediates ($\mathbf{Cu^{II}}$–$\mathbf{O^{\cdot}}$). However, such $\mathbf{Cu^{II}}$–$\mathbf{O^{\cdot}}$ species have not yet been directly observed, neither in synthetic model systems nor in enzymatic studies.[64]

1.2.1 Characterization of Copper-Dioxygen Adducts

As these oxygenated copper intermediates are highly reactive and thermally sensitive, their isolation and structural characterization by X–ray diffraction (XRD) remain challenging. Consequently, their identification and the elucidation of their structural and electronic properties rely primarily on spectroscopic techniques. In this context, UV–vis and resonance Raman spectroscopy (rR), as well as cold-spray ionization mass spectrometry (CSI–MS), are particularly valuable, as they enable measurements in solution at low temperatures. UV–vis spectroscopy provides information on the electronic structure of the copper center and the geometry of copper-dioxygen intermediates. The oxygenated species typically exhibit intense ligand-to-metal charge transfer (LMCT) bands arising from oxygen-to-copper charge transfer, indicative of highly covalent Cu–O bonds.[65] When combined with stopped-flow techniques, UV–vis spectroscopy also enables detection of short-lived intermediates (e.g., copper(II)−superoxido species) by recording absorption spectra within milliseconds after mixing the dioxygen-free copper(I) solutions with the dioxygen-saturated solutions.[68] Resonance Raman spectroscopy offers complementary structural insight through characteristic Cu–O and O–O vibrational modes. These modes can be selectively enhanced, and their assignment can be further supported by isotopic labeling with $^{18}O_2$, which induces a predictable down-shift ($\Delta \approx 50$ cm^{-1}) in the vibrational frequencies of Cu–O and O–O bonds.[69] Similarly, $^{18}O_2$ labeling is widely applied in CSI–MS analysis, where the coordination of labeled O_2 to the copper center leads to a characteristic 4-unit shift in the mass-to-charge ratio of the complexes. CSI–MS is a low-temperature variant of electrospray ionization mass spectrometry and is therefore well suited for detecting the exact mass of labile copper-dioxygen species while minimizing thermal decomposition.[70] Further structural and electronic information can be obtained by X–ray absorption spectroscopy (XAS) and extended X–ray absorption fine structure (EXAFS), which provide insight into the oxidation states of the oxygenated intermediate and provide structural parameters such as Cu···Cu, Cu–O, and Cu–N distances in both solution and solid state.[65]

1.2.2 Mononuclear Copper-Dioxygen Complexes

1.2.2.1 Structure and Characterization

The development of model systems able to stabilize mononuclear copper-dioxygen species has proven challenging, as these systems preferentially form the corresponding dinuclear intermediates, which are thermodynamically more stable. This limitation was mainly addressed through ligand design, employing sterically demanding and strongly electron-donating ligands to suppress dimerization and enable access to mononuclear species.[64]

Early contributions by Kitajima and coworkers demonstrated that the monoanionic hydrotris(pyrazolyl)borate ligand **L1** (Figure 3) was able to stabilize the dinuclear $\mathbf{P^S}$ copper complex, leading to the first structural characterization of this intermediate in 1989.[71] Based on these findings, the same group increased the steric hindrance of the ligand through the substitution of one *iso*-propyl residue with a *tert*-butyl group per arm, affording ligand **L2** (Figure 3). The use of this ligand enabled the first crystallographic characterization of a copper(II)−superoxido intermediate, identified as an $\mathbf{S^S}$ species.[72] Although this modification shifted the equilibrium from the $\mathbf{P^S}$ to the $\mathbf{S^S}$ species, partial dimerization of the $\mathbf{S^S}$ complex could still be observed in solution.[65] To suppress this process, the steric hindrance was further increased by replacing the *tert*-butyl moieties with adamantyl groups (**L3**, Figure 3), which completely prevented the formation of the $\mathbf{P^S}$ intermediate, allowing exclusive detection of the $\mathbf{S^S}$ species in solution.[73] Spectroscopically, the $\mathbf{S^S}$ intermediates exhibit a singlet ground state (S = 1), arising from ferromagnetic coupling between the copper(II) center and the superoxide radical.[36,73] Additionally, they are characterized by O–O vibration frequencies in the range of 950 cm^{-1} to 1100 cm^{-1}, which slightly shift depending on the steric and electronic properties of the ligands.[36]

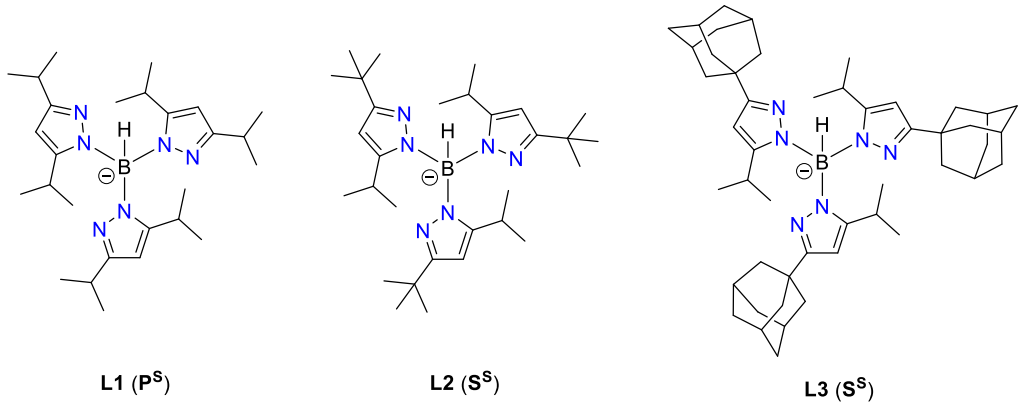


Figure 3: Selection of ligands employed for spectroscopic and structural characterization of $\mathbf{P^S}$ to the $\mathbf{S^S}$ species.

In 2002, Tolman and coworkers reported a related *side-on* copper-dioxygen complex supported by a sterically hindered *β*-diketiminate ligand (**L4**, Figure 4).[74] In this system, the electronic configuration indicated that the copper center adopts the +III oxidation state, enabling the first crystallographic characterization of the $\mathbf{P^M}$ oxygenated species.[74,75] The stabilization of this complex is attributed to the strong electron-donating ability of the monoanionic bidentate ligand, which supports the higher oxidation state of the copper(III) center and favors a square-planar geometry around the metal ion. The $\mathbf{P^M}$ species was also observed in equilibrium with the corresponding $\mathbf{S^E}$ adduct by Itoh and coworkers using the bulky $TIPT_3tren$ ligand (**L5**,

Figure 4).[76] Oxygenation of the copper(I) complex at low temperature resulted in the coexistence of both binding modes, which could be identified by UV–vis as well as resonance Raman spectroscopy and was also supported by Density Functional Theory (DFT) computations. In fact, whereas both $\mathbf{S^E}$ and $\mathbf{P^M}$ species adopt a paramagnetic ground state, they exhibit different characteristic spectroscopic features. In particular, $\mathbf{P^M}$ species display an intense charge-transfer band around 380 nm and a weaker absorption band at approximately 600 nm, as well as diagnostic peaks in the resonance Raman spectrum in the range of 910 cm^{-1} to 1000 cm^{-1}, assigned to the O–O stretching vibrations.[63,74,76] Otherwise, the $\mathbf{S^E}$ species exhibit UV–vis spectra characterized by an intense charge-transfer band at around 410 nm, along with two weaker absorptions at approximately 600 nm and 750 nm, which can slightly change in accordance with the nature of the ligand.[36,65] Resonance Raman spectroscopy further provides characteristic vibrational modes at around 1120 cm^{-1} and approximately 470 cm^{-1}, corresponding to the O–O and Cu–O stretches, respectively.[63]

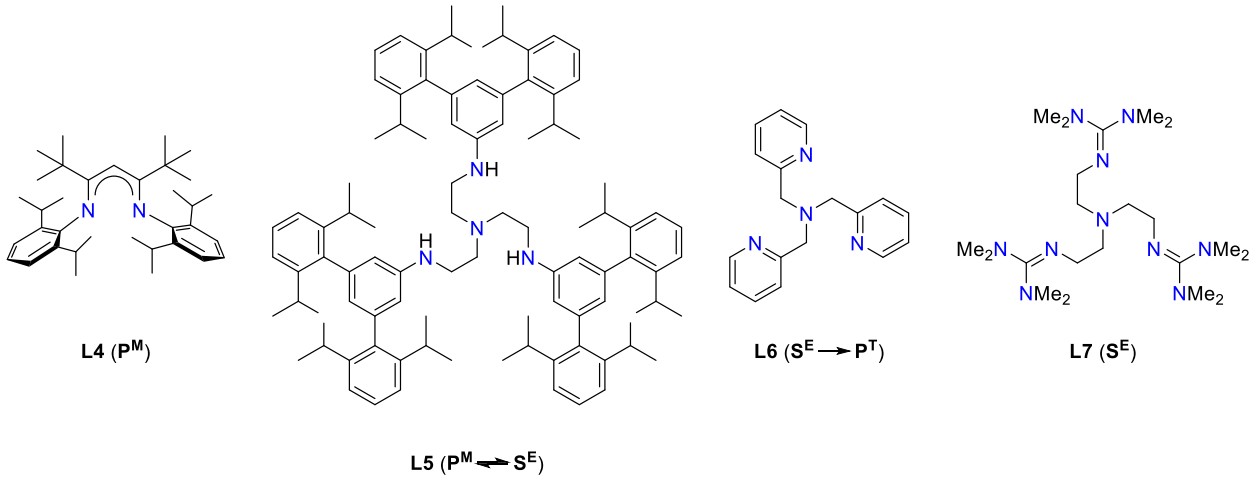
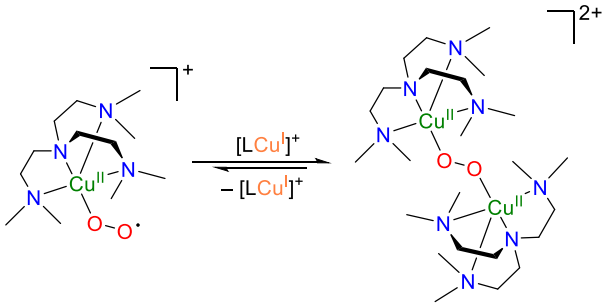


Figure 4: Selection of ligands employed for spectroscopic and structural characterization of $\mathbf{P^M}$ to the $\mathbf{S^E}$ species.

The first spectroscopic evidence for the transient formation of an $\mathbf{S^E}$ species using copper model complexes was reported in 1991 upon exposure of the copper(I) complex supported by ligand **L6** (Figure 4) to O_2, followed by a detailed kinetic study of the same system in 1993.[77,78] Structural insights into $\mathbf{S^E}$ intermediates were later obtained in 2004 with the crystal structure of peptidylglycine α-hydroxylating monooxygenase (PHM), which revealed an $\mathbf{S^E}$ species at its active site, providing the first direct structural evidence that superoxide intermediates participate in dioxygen activation in copper enzymes.[79] Over the years, $\mathbf{S^E}$ intermediates have been extensively investigated in solution using a variety of ligand systems designed to stabilize the *end-on* superoxido motif at low temperature. Finally, in 2006, Würtele *et al.* reported the first structurally characterized $\mathbf{S^E}$ complex using a tetradentate tripodal ligand based on tris(2-aminoethyl)amine (tren) functionalized with tetramethylguanidine substituents (**L7**, Figure 4).[80,81] This complex displayed a geometry consistent with that reported for the PHM active site, confirming that the $\mathbf{S^E}$ species is the primary adduct formed upon O_2 binding to copper(I) complexes and highlighting its central role in catalytic oxidation reactions.[79]

1.2.2.2 Reactivity of Copper(II) *End-on* Superoxido Complexes

The reactivity of copper-dioxygen adducts has been extensively investigated over the past four decades, with superoxido species identified as both competent oxidants toward external substrates and key intermediates in oxidative transformations.[36,63,82–84] Nevertheless, the dimerization of *end-on* superoxido complexes remains the most frequent reaction observed for this class of compounds. As mentioned in Chapter 1.2, in the absence of sufficient steric hindrance, $\mathbf{S^E}$ species readily react with excess copper(I) precursors to form dinuclear peroxido complexes, such as $\mathbf{P^S}$ and $\mathbf{P^T}$, while direct conversion to **O** species is only rarely reported.[85] Although increasing the steric bulk and tuning the electronic properties of the ligand can reduce dimerization reactions (e.g., **L5**[81], **L7**[76], Figure 4), this pathway remains prevalent in many systems. A representative example is provided by the copper complex based on the Me_6tren system (Scheme 6).[86] In this case, methylation of the amine donors increases the lifetime of the superoxido intermediate sufficiently to allow its detection and spectroscopic characterization at cryogenic temperatures in propionitrile. Nevertheless, subsequent conversion to the *end-on* peroxido species still occurs within minutes, and the transition from $\mathbf{S^E}$ to $\mathbf{P^T}$ complex could be followed spectroscopically only using stopped-flow techniques.

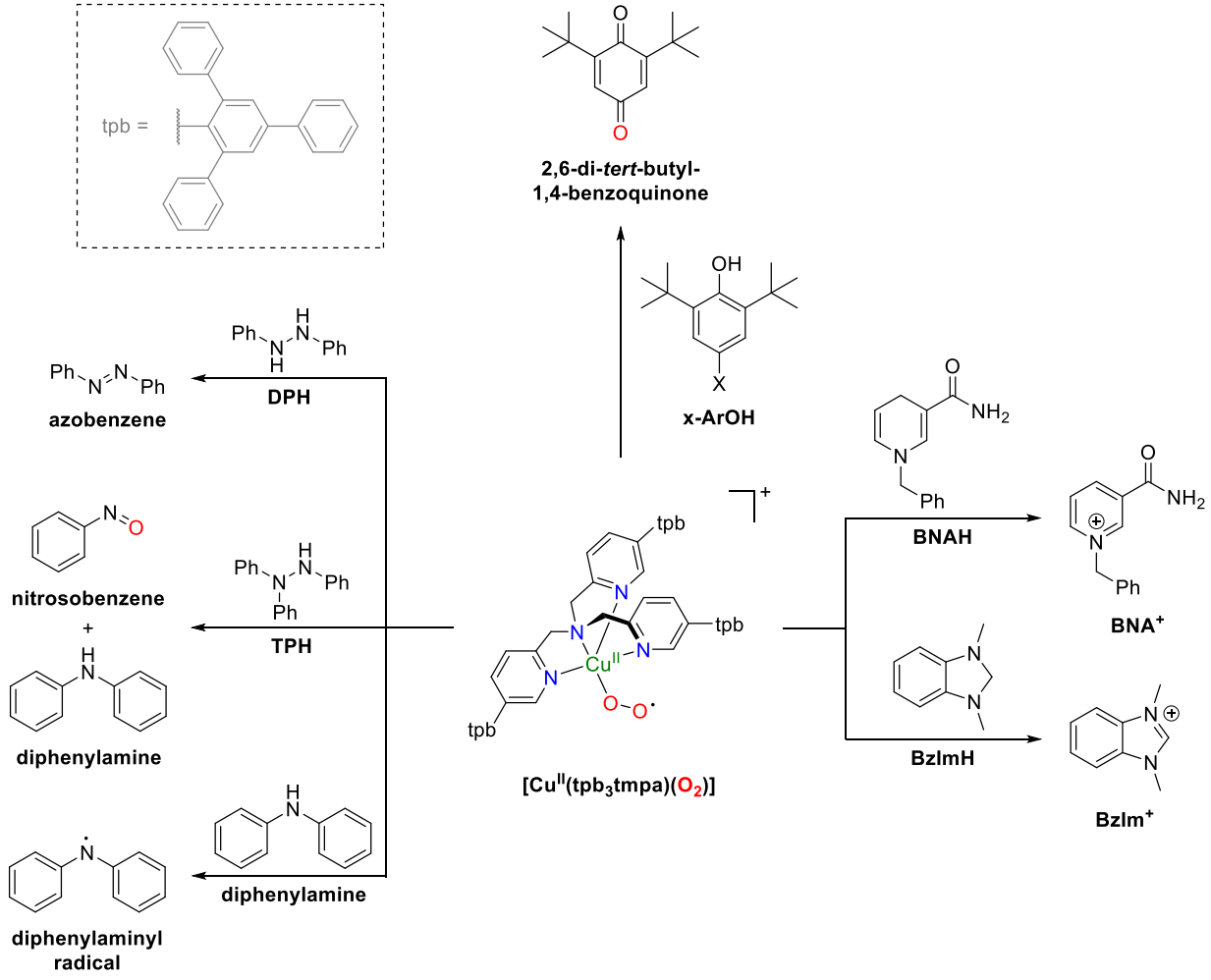


Scheme 6: Equilibrium between $\mathbf{S^E}$ and $\mathbf{P^T}$ species in copper(II) complex supported by Me_6tren ligand in propionitrile. Nonbinding anions and solvent molecules are omitted for clarity.

Besides their tendency to undergo dimerization, some $\mathbf{S^E}$ species exhibit hydrogen atom abstraction (HAA) reactivity toward O–H, N–H, and C–H bonds, which leads to the formation of the corresponding Cu–OOH species ($\mathbf{P^H}$, Chapter 1.2.3.1) and radical products.[36,62,63] To investigate this reactivity in more detail, England and coworkers developed sterically demanding tmpa-derived ligands bearing aryl substituents in the 3-position of the pyridine moieties, which enabled the stabilization of the superoxido complexes up to −20 °C.[87] This increased stability allowed systematic studies of their reactivity toward a broad range of substrates (Scheme 7), including 4-substituted 2,6-di-*tert*-butylphenols (x-ArOH, x = OMe, MPPO, OCH_2CF_3, Me, Et, ^{t}Bu; MPPO = 2-methyl-1-phenylpropan-2-yloxy), 1,2-diphenylhydrazine (DPH), and 1-benzyl-1,4-dihydronicotinamide (BNAH).[87] The HAA reactivity of $\mathbf{S^E}$ species was shown to be strongly dependent on the ligand environment. In particular, the incorporation of thioether donor and hydrogen-bonding substituents was found to enhance the oxidizing power of the superoxido adduct.[88–90] Karlin and coworkers demonstrated this effect using a series of tmpa-based ligands with different hydrogen-bonding ability. The increase of both the number and strength of hydrogen-bonding interactions promoted the suppression of dinuclear species in favor of mononuclear $\mathbf{S^E}$ complexes and enhanced their electrophilic reactivity toward HAA.[90]

In addition to HAA reactivity, some $\mathbf{S^E}$ species, based on tridentate nitrogen-donor ligands, also exhibit nucleophilic behavior. These intermediates are proposed to promote aldehyde

deformylation reactions and induce aldol reaction between carbonyl substrates and the solvent molecules, such as acetone, leading to the corresponding *β*-hydroxy ketones.[91,92] Whereas the $\mathbf{S^E}$ species is widely accepted as the active intermediate in the aldol-type reactivity, more recent investigations by Tolman and coworkers suggest that the deformylation reaction may instead be promoted by the decay product $[LCu^{II}OH]^-$ rather than by the $\mathbf{S^E}$ species itself.[93] Based on this study, the copper hydroxide species is proposed to be the actual reactive intermediate responsible for the activation of the aldehyde substrate and the formation of a copper(II) enolate complex, which subsequently undergoes aerobic oxidation upon workup to yield acetophenone. Accordingly, the $\mathbf{S^E}$ species is supposed to act as a base rather than as a nucleophile.[93] Overall, this reactivity remains under investigation, and further studies are required to fully elucidate the underlying mechanism.



Scheme 7: Summary of the reactivity of the $\mathbf{S^E}$ complex based on tpb_3tmpa ligand. Abbreviations: DPH for 1,2-diphenylhydrazine; TPH for 1,1,2-triphenylhydrazine; BNAH for 1-benzyl-1,4-dihydronicotinamide; BzImH for 1,3-dimethyl-2,3-dihydrobenzimidazole; x-ArOH for 4-substituted 2,6-di-tert-butylphenols (x = OMe, MPPO, OCH_2CF_3, Me, Et, ^{t}Bu; MPPO = 2-methyl-1-phenylpropan-2-yloxy).[87]

Finally, in the absence of external substrates, some $\mathbf{S^E}$ species have also been observed to undergo conversion into the corresponding $\mathbf{P^H}$ complexes via PCET or HAA from the ligand backbone (Figure 5a). Masuda and coworkers first reported this behavior using the H_2BPPA ligand system (**L8**, Figure 5b), where the $\mathbf{P^H}$ complex was generated through the reaction between the initial $\mathbf{S^E}$ species and the remaining unreacted copper(I) complex.[94] This process afforded approximately

50% of the $\mathbf{P^H}$ complex, along with 50% of a copper(II) species featuring a deprotonated ligand. A similar reactivity was subsequently observed by Schindler and coworkers using tren-based ligands such as $^{i}Pr_3$tren (**L9**, Figure 5b) and Ph_3tren derivatives (**L10**, Figure 5b, Chapter 3.2).[95,96] Otherwise, Itoh and coworkers reported that the $\mathbf{S^E}$ species supported by the tridentate ligand **L11** (Figure 5b) undergoes intramolecular ligand hydroxylation rather than react with an additional equivalent of the copper(I) complex, closely mimicking DβM and PHM biochemistry.[97] In this case, the $\mathbf{S^E}$ species first undergoes hydrogen atom transfer from the ligand scaffold to generate the $\mathbf{P^H}$ intermediate, which subsequently rebounds its proximal oxygen atom to afford the Cu(II)−alkoxide product and eventually promote benzylic C–H bond hydroxylation of the ligand.

The conversion of $\mathbf{S^E}$ species into $\mathbf{P^H}$ complex was also recently achieved by Karlin and coworkers through a novel approach involving cryoreduction of an $\mathbf{S^E}$ precursor supported by a tetradentate tmpa-based ligand **L12** (Figure 5b), followed by annealing.[98] In this procedure, the frozen sample was irradiated with γ-ray at 77 K (using a ^{60}Co source), and the temperature was subsequently increased stepwise to monitor the formation of new intermediates, which were stabilized with intermittent cooling to allow their characterization. Specifically, the reduction of the $\mathbf{S^E}$ complex led to the formation of a metastable copper(I) superoxido species, $[LCu^{I}(O_2^{\bullet-})]^{+}$, which, upon annealing, underwent internal electron transfer (IET) to generate an *end-on* copper(II)−peroxido species, $[LCu^{II}(O_2^{2-})]$. Eventually, protonation of this intermediate afforded the corresponding $\mathbf{P^H}$ species.

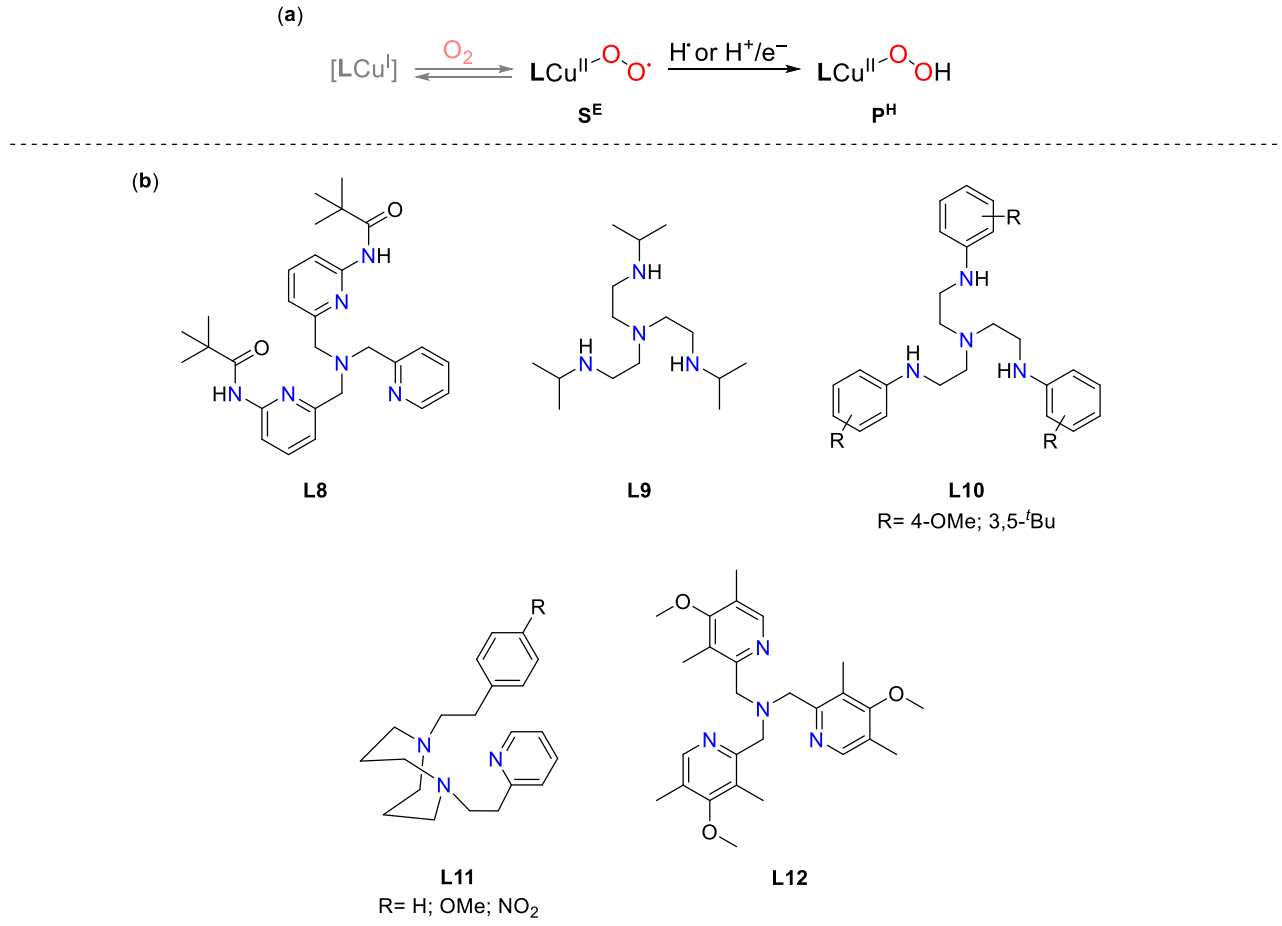


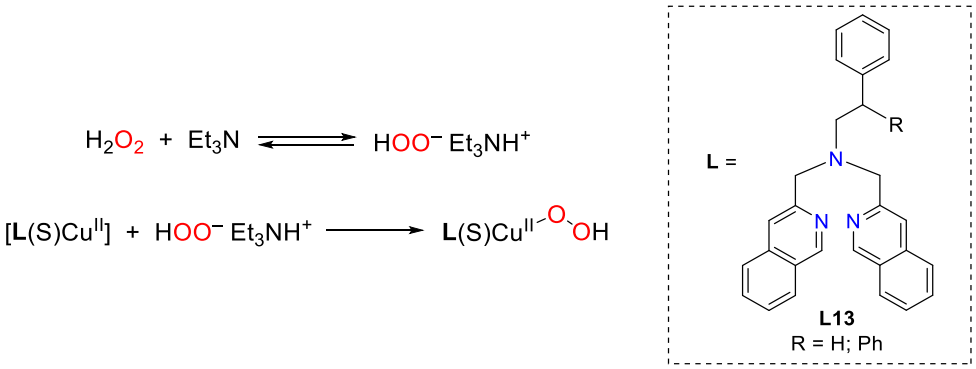
Figure 5: (**a**) General scheme for the conversion of $\mathbf{S^E}$ intermediate into $\mathbf{P^H}$ species (charge of the complex and nonbinding anions are omitted for clarity); (**b**) Ligand systems that support the conversion between $\mathbf{S^E}$ and $\mathbf{P^H}$ species.

1.2.3 Copper Hydroperoxido and Alkylperoxido Complexes

1.2.3.1 Synthesis and Characterization

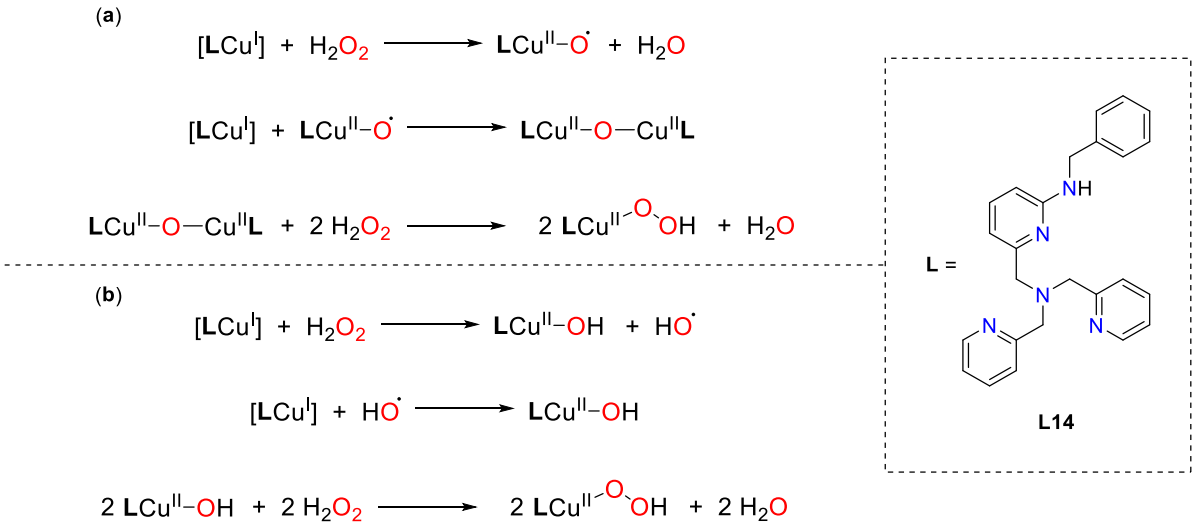
As discussed in Chapter 1.1.1.2, copper(II)−hydroperoxido species have been postulated as key intermediates in copper monooxygenases such as DβH and LPMOs. Therefore, a detailed investigation of their structure, spectroscopic features, and reactivity is crucial for advancing the understanding of biological oxidation processes and for the development of efficient and sustainable catalytic systems for selective oxidation reactions. Synthetic access to $\mathbf{P^H}$ complexes can be achieved through several pathways, including HAA or PCET from a superoxido precursor, as well as by treatment of copper(I) or copper(II) complexes with H_2O_2, either in the presence or absence of base.[63,87,89,94,96,99–104] Although this first synthetic route closely mimics the proposed formation pathway of hydroperoxido species in biological systems, direct synthesis of $\mathbf{P^H}$ complexes from $\mathbf{S^E}$ intermediates remains rarely reported, and the most relevant examples have already been discussed in Chapter 1.2.2.2. In contrast, several examples of $\mathbf{P^H}$ complexes have been prepared using alternative synthetic approaches based on the use of H_2O_2.

Most commonly, synthetic $\mathbf{P^H}$ complexes are generated by treating copper(II) precursors with H_2O_2 in the presence of a base. This approach is particularly convenient, as it allows reactions to be performed under ambient conditions without the need for glovebox or Schlenk techniques, which are typically required when working with copper(I) precursors. Thanks to this approach, the first $\mathbf{P^H}$ complex was spectroscopically characterized and isolated by Wada *et al.* in 1998, employing H_2BPPA as a supporting ligand (**L8**, Figure 5b), establishing an important benchmark for subsequent structural and spectroscopic studies.[105] In 2005, Itoh and coworkers provided the first mechanistic insight into $\mathbf{P^H}$ complex formation through kinetics studies combined with DFT-based computations, using a copper(II) complex supported by tridentate ligand **L13** as a model system.[106] The results indicated that H_2O_2 undergoes an initial rapid deprotonation prior to coordination to the copper center, eventually leading to the formation of the $\mathbf{P^H}$ intermediate (Scheme 8). This study complements an earlier work by the same group, in which analogous kinetic behavior was observed for less sterically demanding ligands in which the quinoline groups of **L13** were replaced by pyridine moieties.[107] However, in those systems, no appropriate characterization of the $\mathbf{P^H}$ product could be achieved due to its rapid conversion into a dimeric peroxido $\mathbf{P^S}$ species.



Scheme 8: Proposed mechanism for the generation of $\mathbf{P^H}$ complexes from copper(II) precursor supported by ligand **L13**.[106] The charge of the complex and the nonbinding anions are omitted for clarity. S = solvent molecule (CH_3CN or CH_3COCH_3).

A less common route for the synthesis of $\mathbf{P^H}$ complexes involves the use of copper(I) precursors in combination with H_2O_2 and in the absence of base. In 2012, Karlin and coworkers first reported the formation of a $\mathbf{P^H}$ species upon the reaction of a copper(I) complex supported by ligand **L14** with 1.5 equivalents of H_2O_2 at −90 °C in acetone.[103] The resulting intermediate was stabilized by intramolecular hydrogen bonding, which enabled its spectroscopic characterization. This synthetic approach represents the first example of $\mathbf{P^H}$ complexes formation via hydrogen peroxide oxidation of the copper(I) precursor. Although such reactivity is unusual for copper systems, it is relatively common in iron chemistry, where the iron(II) complexes react with H_2O_2 to generate Fe(III)–OOH species.[108,109] By analogy, two possible pathways were proposed to rationalize the reactivity of the copper complex, based on a Fenton-like mechanism. One involves the initial formation of a copper-oxyl species, $\mathbf{Cu^{II}–O^{\cdot}}$, which is trapped by the copper(I) precursor to form a (μ-oxo)dicopper(II) intermediate that eventually reacts with H_2O_2 to yield the $\mathbf{P^H}$ product (Scheme 9a). Alternatively, following a more classic pathway, the initial complex is proposed to react directly with H_2O_2 to generate a hydroxyl radical and a copper(II)−hydroxido complex, which further reacts with H_2O_2 to afford the final $\mathbf{P^H}$ complex (Scheme 9b). Although the exact mechanism remains unclear, this unconventional synthetic route is of particular interest, as it mimics the pathway proposed for the formation of the initial oxygenated intermediates in LPMO enzymes (Chapter 1.1.1.2).



Scheme 9: Proposed mechanisms for the generation of $\mathbf{P^H}$ complexes from H_2O_2 and the copper(I) precursor supported by ligand **L14**.[103] The charge of the complex and nonbinding anions are omitted for clarity.

Due to their thermal instability, most $\mathbf{P^H}$ complexes have been characterized only in solution at cryogenic temperatures, typically stabilized by tridentate or tetradentate nitrogen-donor ligands.[63] These species generally adopt an η^1 coordination mode and display a diagnostic UV–vis feature around 350 nm, assigned to peroxide-to-copper LMCT transition. $\mathbf{P^H}$ complexes exhibit EPR signatures characteristic of copper(II) species, and their resonance Raman spectra are characterized by two specific bands at approximately 850 cm^{-1} and 550 cm^{-1}, corresponding to the O−O and Cu−O stretching modes, respectively. Despite the large number of $\mathbf{P^H}$ complexes that have been spectroscopically investigated over the years, only a limited number have been isolated and structurally characterized by X-ray diffraction, often requiring hydrogen-bonding ligand frameworks to improve their stability (e.g., **L8**, Figure 5b).[102,105]

Similarly, copper(II)–alkylperoxido complexes ($\mathbf{P^R}$) are difficult to isolate and structurally characterize. To date, besides the first structure reported by Kitajima and coworkers in 1993 based on ligand **L1**, only one additional $\mathbf{P^R}$ complex has been structurally characterized, featuring **L15** as ligand (Figure 6).[110,111] As for $\mathbf{P^H}$ complexes, these species are typically investigated in solution at low temperature and are supported by tridentate or tetradentate nitrogen-donor ligands.[63] The spectroscopic features of $\mathbf{P^R}$ complexes closely resemble those of $\mathbf{P^H}$ species. In particular, the resonance Raman peaks associated with the O–O and Cu–O stretching modes are observed at ca. 860 cm^{-1} and 600 cm^{-1}, respectively, with additional features at approximately 540 cm^{-1}, attributed to C–C–C and O–C–C vibrational modes. The EPR signals are characteristic of copper(II) complexes, and the UV–vis spectra display diagnostic peroxide-to-copper LMCT bands in the range of 350-600 nm, depending on the coordination geometry and the nature of the ligand.[63] Despite the limited number of structurally characterized examples, $\mathbf{P^R}$ species have been widely investigated to gain insight into copper-dioxygen reactivity and are commonly regarded as functional models for lipid peroxidation as well as potential precursors to highly reactive copper-dioxygen intermediates.[36,112,113]

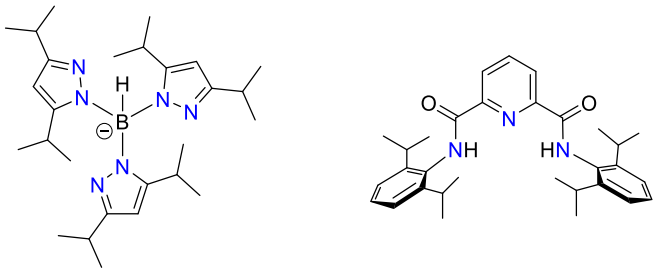
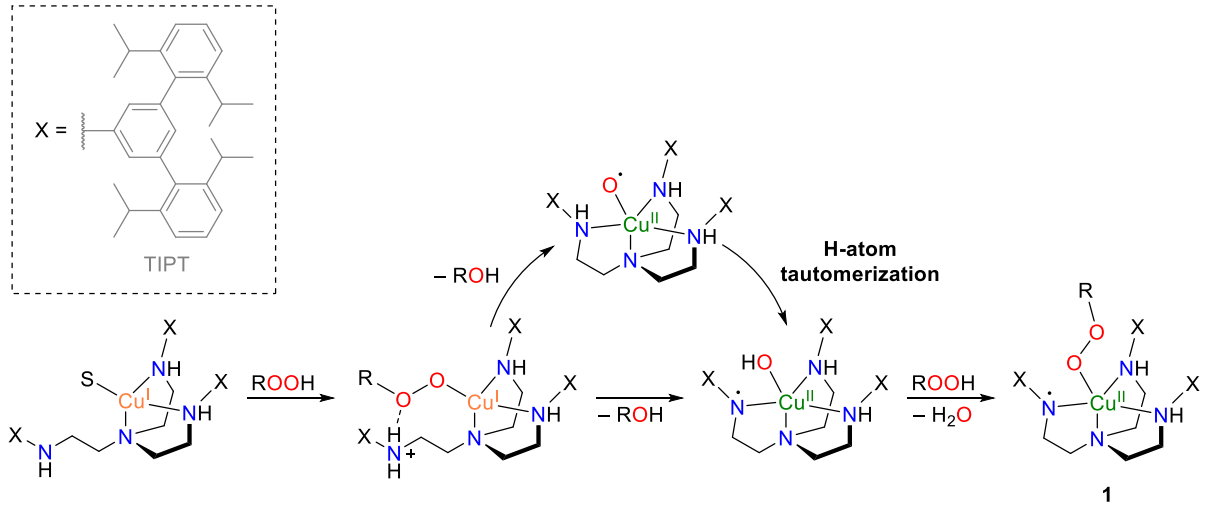


Figure 6: Ligands employed for structural characterization of $\mathbf{P^R}$ species.

Synthetic access to $\mathbf{P^R}$ complexes is achieved by treatment of copper(I) or copper(II) precursors with organic ROOH, either in the presence or absence of base.[113–119] Most commonly, $\mathbf{P^R}$ complexes are generated starting from copper(II) precursors in the presence of ROOH and triethylamine. This approach is particularly convenient, as copper(II) starting materials can be handled under ambient conditions without undergoing parallel reactions with O_2 and are generally more stable in solution than the corresponding copper(I) species, which often undergo disproportionation.[86,120,121] The presence of base is typically required when copper(II) complexes are employed, as it promotes deprotonation of the hydroperoxide, facilitating its coordination to the metal center (in a similar mechanism as proposed for the formation of $\mathbf{P^H}$ species in Scheme 8).

Formation of $\mathbf{P^R}$ intermediates from copper(I) precursors is less common. However, a representative example was reported by Itoh and coworkers using the highly sterically hindered tren-based ligan **L5** (Figure 4) at −60 °C in dichloromethane under anaerobic conditions.[114] Based on kinetic experiments and spectroscopic evidence, a Fenton-type mechanism was proposed for the formation of the $\mathbf{P^R}$ complex **1** (Scheme 10). The addition of cumene hydroperoxide to the metal precursor leads to the formation of an initial copper(I) peroxide adduct, [$LCu^{I}OOR$], stabilized by an intramolecular hydrogen-bonding. Subsequent heterolytic O−O bond cleavage, associated with the release of ROH, generates a copper(II)−hydroxido intermediate ($(L\cdot)Cu^{II}OH$). The authors proposed that this step may occur either in a concerted manner or a stepwise pathway involving the transient formation of a copper–oxyl species ($\mathbf{Cu^{II}–O\cdot}$), which rapidly

undergoes hydrogen atom tautomerization. Finally, the substitution of the hydroxide moiety on the copper center by a second equivalent of cumene hydroperoxide affords the final $\mathbf{P^R}$ complex **1**. Notably, complex **1** featured not only the peroxide moiety $[CuOOR]^+$ but also an anilino radical ligand. This mechanistic hypothesis is significant as it provides insight into possible pathways relevant to copper-mediated oxidation reactions and might help to understand analogous processes occurring in enzymatic systems.

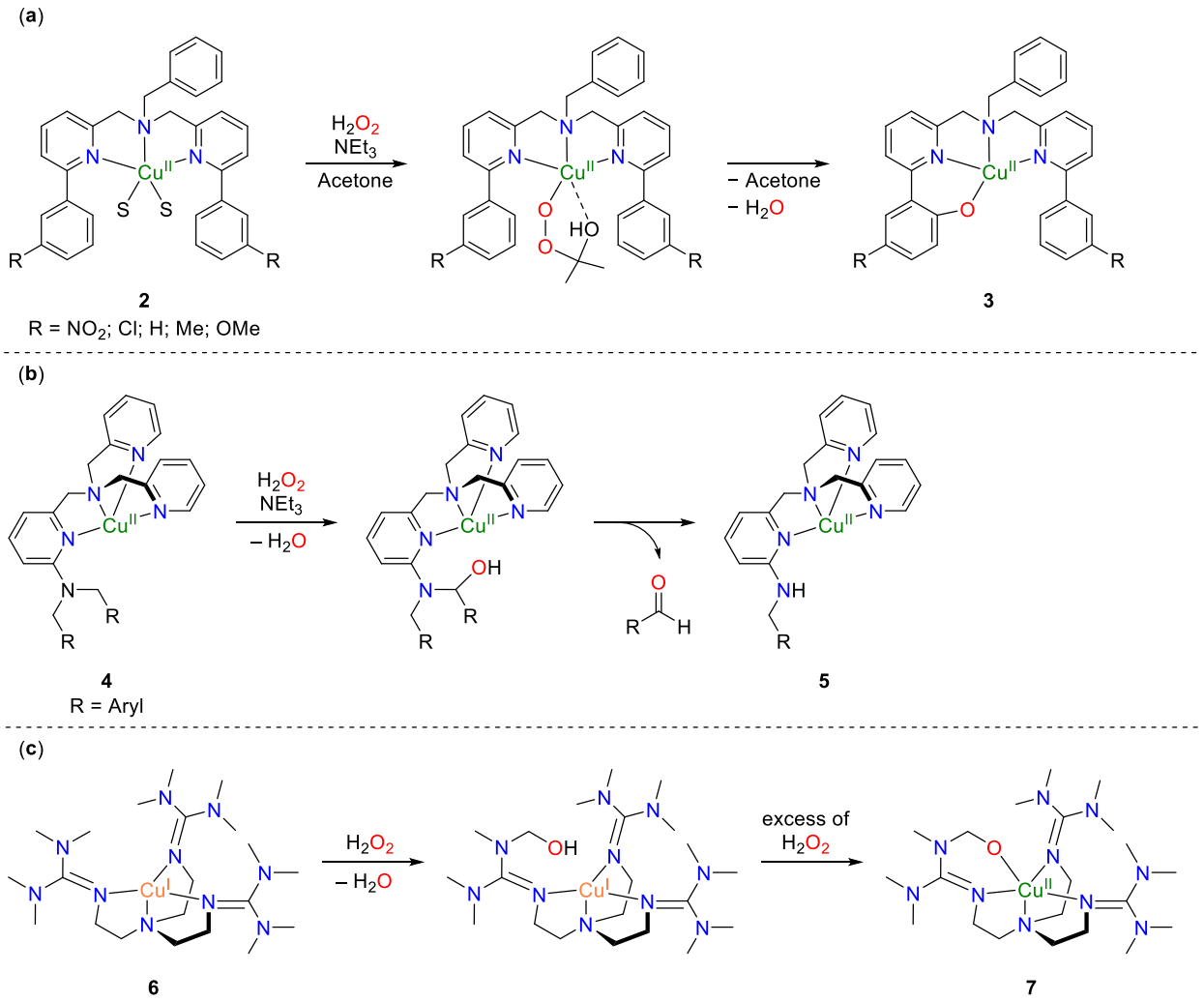


Scheme 10: Proposed mechanism for the formation of $\mathbf{P^R}$ complex **1** supported by ligand **L5**.[114] S = solvent molecule (CH_3CN). The charge of the complex and the nonbinding anions are omitted for clarity.

1.2.3.2 Reactivity of Copper(II) Hydroperoxido and Cumylperoxido Complexes

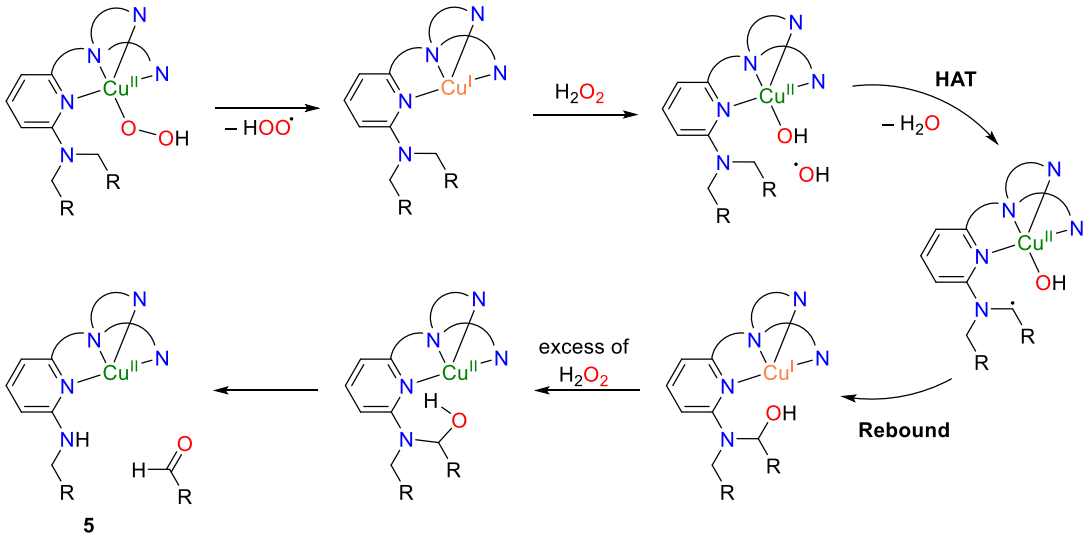
As mentioned in Chapter 1.1.1.2, $\mathbf{P^H}$ species are considered key intermediates in enzymes such as DβH and LPMOs and are therefore widely investigated as active species in catalytic oxidation reactions, along with $\mathbf{P^R}$ species. Their reactivity is influenced by the ligand environment, as well as by hydrogen-bonding interactions involving the proximal or distal oxygen atoms.[102] In particular, hydrogen bonding to the proximal oxygen weakens the Cu–O bond while strengthening the O–O bond, resulting in decreased reactivity of the intermediate. In contrast, hydrogen bonding to the distal oxygen destabilizes the intermediate, leading to increased reactivity and faster decomposition. Moreover, Cho and coworkers demonstrated that the reactivity of alkylperoxido species is also strongly affected by the solvent.[122] Specifically, non-polar solvents were found to enhance reactivity toward external C–H bonds, as they facilitate O–O homolytic cleavage and promote more efficient HAA reactions. Despite these effects, $\mathbf{P^H}$ and $\mathbf{P^R}$ species generally exhibit limited reactivity toward external substrates and are often considered as precursors for more reactive intermediates, such as copper–oxyl ($\mathbf{Cu^{II}–O^{\cdot}}$) and alkoxyl radicals ($RO^{\cdot}$), generated by O–O bond homolysis.[36]

Intramolecular ligand hydroxylation has been observed upon decay of several $\mathbf{P^H}$ complexes.[63,123-129] For instance, aryl groups hydroxylation of the ligand was observed by Itoh and coworkers upon reaction of the copper(II) complex **2** with H_2O_2 in acetone and in the presence of triethylamine as base (Scheme 11a).[123,130] The final product was identified as the corresponding phenoxide complex **3**, which was isolated and characterized by X-ray diffraction. Subsequent demetalation of the complex using aqueous ammonia also afforded the free hydroxylated ligand.



Scheme 11: (**a**) Intramolecular aryl hydroxylation of complex **2** via $\mathbf{P^H}$ intermediate. S = solvent molecule (CH_3CN or H_2O);[130] (**b**) and (**c**) intramolecular oxidation of pendant *N*-alkyl amine groups of complexes **4** and **6** via $\mathbf{P^H}$ intermediate.[127,128] The charge of the complex and the nonbinding anions are omitted for clarity. Abbreviation: NEt_3 for triethylamine.

$\mathbf{P^H}$ species are also known to undergo intramolecular oxidation of pendant *N*-alkyl amine groups, including *N*-dealkylations, mimicking the reactivity of PHM, D*β*M, and LPMOs enzymes. A representative example was reported by Karlin and coworkers using complex **4** based on tmpa-derived ligands (Scheme 11b).[125,127,131] The initial $\mathbf{P^H}$ complexes were generated from the corresponding copper(II) precursor **4** with an excess of H_2O_2 in the presence of base at −90 °C. Subsequent warming triggered intramolecular oxidation, which was investigated in detail and provided valuable mechanistic insight (Scheme 12). Combined experimental and DFT-based computations indicated that the oxidation proceeds via a Fenton-like pathway, initiated by the homolytic cleavage of the Cu–O bond of the $\mathbf{P^H}$ species to yield a copper(I) complex and hydroperoxyl radical. The copper(I) species subsequently reacts with an additional equivalent of H_2O_2 to form a Cu(II)–hydroxido species and hydroxyl radical, which then abstracts a hydrogen atom from the ligand backbone. The resulting alkyl radical undergoes so-called rebound with the hydroxide moiety to generate a copper(I) carbinolamine intermediate, which ultimately undergoes oxidation of the metal center and N-dealkylation of the ligand arm to form complex **5**, releasing benzaldehyde.

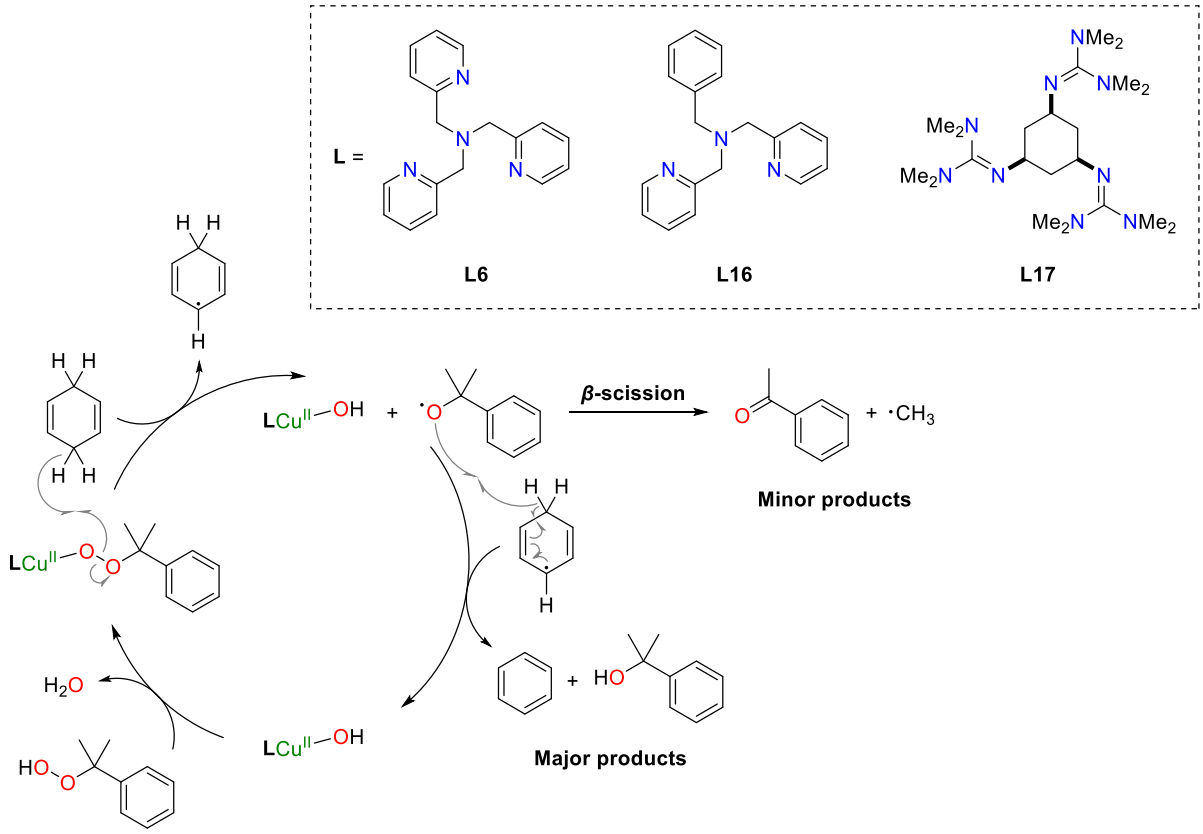


Scheme 12: Proposed mechanism for N-dealkylation of complex **4** (R = Aryl group).[127] Only one arm of the ligand is shown for clarity. The charge of the complex and the nonbinding anions are omitted for clarity. Abbreviation: HAT for hydrogen atom transfer.

A related behavior was also observed for the copper(I) complex **6** supported by TMG_3tren ligand (**L7**, Figure 4), where the intramolecular ligand oxidation likewise proceeds via the formation of copper(II)−hydroxido species and hydroxyl radical, which initiates HAT, generating the hydroxylated ligand (Scheme 11c).[128] The resulting carbinolamine complex is stabilized at low temperature and undergoes further oxidation in the presence of an excess of H_2O_2 to yield the corresponding phenoxide product **7**. *N*-dealkylation of the ligand is only observed as a side reaction under highly oxidative conditions.

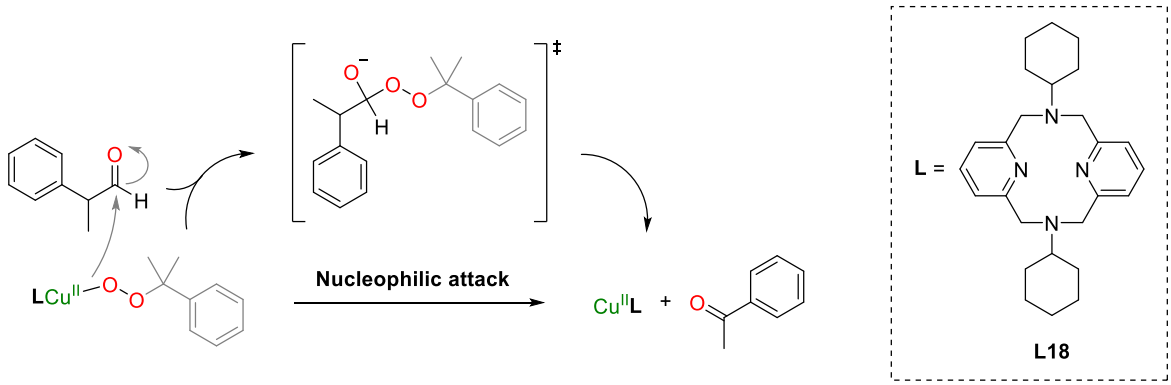
Beyond intramolecular reactivity, $\mathbf{P^H}$ and $\mathbf{P^R}$ species are also capable of oxidizing a wide range of external substrates. For instance, the $\mathbf{P^H}$ complex based on bis(benzimidazole)amine ligand is reported to promote the oxidative degradation of cellulose,[132] while the alkylperoxide/anilino radical complex **1** mentioned in Chapter 1.2.3.1 catalyzes the oxidation of para-substituted benzyl compounds, likely via a mechanism analogous to that of galactose oxidase.[114] Some $\mathbf{P^R}$ species exhibit oxygen atom transfer reactivity toward phosphines, dimethyl sulfide, and thioanisole,[113,129,133] whereas specifically designed $\mathbf{P^H}$ species are even able to promote hydroxylation of aromatic substrates such as benzene and toluene, as reported by Mayilmurugan and Ghosh.[134,135] Moreover, several $\mathbf{P^H}$ and $\mathbf{P^R}$ species have been reported to promote C−H bond activation of 1,4-cyclohexadiene (CHD), typically involving O−O bond homolysis.[113,116,118,119,129,136] Investigation of this reactivity is important for gaining a deeper understanding of biological C–H bond activation and for the development of efficient oxidation catalysts for industrial applications. Accordingly, mechanistic insight into this process has been obtained for tmpa (**L6**), bpa (**L16**), and TMG_3tach (**L17**) systems through product analysis, kinetic studies, and DFT-based computations (Scheme 13).[118,136] The studies indicate that the reaction proceeds via a concerted pathway, in which O–O bond homolysis and hydrogen atom abstraction occur simultaneously, generating copper(II)−hydroxido species, CHD radical, and cumyloxyl radical (CmO·). The resulting CmO· species mainly undergoes hydrogen atom abstraction from the CHD radical intermediate to ultimately yield cumyl alcohol and benzene as

products. However, minor pathways that involve *β*-scission to form acetophenone and a methyl radical have also been observed. Finally, the catalytic cycle closes when the Cu(II)–hydroxido species reacts with an additional equivalent of cumene hydroperoxide to regenerate the initial $\mathbf{P^R}$ species.



Scheme 13: Proposed mechanism for C–H bond activation of CHD, promoted by $\mathbf{P^R}$ species featuring **L6**, **L16,** and **L17** ligands.[118,136]

In addition to the electrophilic reactivity discussed above, $\mathbf{P^H}$ and $\mathbf{P^R}$ species have recently attracted attention for their ability to react with benzoyl chlorides and aldehydes, such as 2-phenylpropionaldehyde (2-PPA) and cyclohexylcarboxaldehyde (CCA), yielding oxidation products including benzoic acid, acetophenone, and cyclohexene.[100,113,119] Reactivity toward benzoyl chlorides and aldehydes was first reported by Cho and coworkers in 2017 using mononuclear $\mathbf{P^R}$ complexes supported by the CHDAP ligand (**L18**, Scheme 14) and was attributed to a nucleophilic attack of the alkylperoxido ligand on the carbonyl group.[119] The deformylation of 2-PPA was investigated in detail through kinetic analysis, which revealed a negative activation entropy and second-order kinetics, consistent with a bimolecular pathway. Accordingly, the reaction was proposed to proceed via an initial nucleophilic attack of the alkylperoxido group on the aldehyde carbonyl, forming a putative peroxyhemiacetal-like intermediate that subsequently undergoes O−O bond cleavage to yield acetophenone and regenerate the initial copper(II) species (Scheme 14). Similar mechanistic features were reported by Oh *et al.* for the oxidation of CCA using a $\mathbf{P^R}$ complex based on a tetradentate ligand containing a bis(2-picolyl)amine backbone and a pendant ethoxyethanol side chain.[113]



Scheme 14: Proposed pathway for nucleophilic oxidation of 2-PPA.[119] Additional products are not reported in the scheme as they are not mentioned in the original publication.

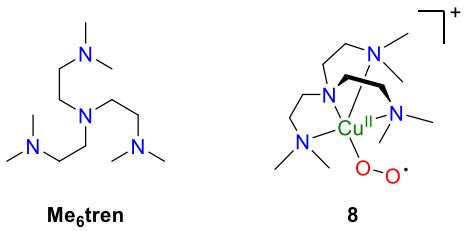
Subsequent studies by Cho and coworkers on a $\mathbf{P^H}$ complex supported by the $^{i}Pr_3$tren ligand **L9** demonstrated that $\mathbf{P^H}$ intermediates are also capable of nucleophilic reactivity toward acyl chlorides and aldehydes.[100] Analogously to the $\mathbf{P^R}$ species based on ligand **L18**, a bimolecular mechanism was suggested for aldehyde deformylation. However, no evidence could be obtained to establish whether the initial nucleophilic attack occurs at the proximal or distal oxygen atom. Although the detailed mechanism remains to be fully elucidated, these findings revealed a new reactivity for $\mathbf{P^H}$ and $\mathbf{P^R}$ species that will need to be further explored to better define their potential applications and biological relevance.

2. Research Goals

As described in Chapter 1.2, copper-dioxygen adducts are highly reactive and are prone to rapid decomposition, even at low temperatures. This intrinsic instability hampers the investigation of their reactivity toward external substrates and limits their potential application in selective oxidation catalysis. Over the past decades, a wide range of tridentate and tetradentate ligands has been developed to generate and stabilize mononuclear oxygenated copper intermediates. Among these, *end-on* superoxido species ($\mathbf{S^E}$) have attracted particular attention, as they are generally considered as the primary adducts formed upon reaction of copper(I) complexes with O_2 and have been identified as key intermediates in oxidative transformations (Chapter 1.2.2.2).

Despite their significance, these species have almost exclusively been generated and characterized under cryogenic conditions. A notable exception was reported in 2023 by the group of Anastasaki, in collaboration with Schindler and coworkers, describing the formation of an $\mathbf{S^E}$ complex supported by the tren-based ligand Me_6tren (**8**, Figure 7) in DMSO at room temperature.[137] Remarkably, this species was generated under aerobic conditions in atom transfer radical polymerization (ATRP) and was found to significantly accelerate the polymerization rate during the initial stages. Copper(I) complexes are widely employed in living radical polymerization as initiators in radical processes for the synthesis of well-defined polymeric materials, such as styrene/methyl acrylate copolymer and methyl methacrylate/*n*-butyl acrylate copolymer.[138–140] However, these processes are typically highly sensitive toward O_2, which can act both as a radical scavenger for the polymeric chain and as an oxidant for the catalyst, leading to deactivation of the polymerization. Therefore, the detection of a persistent $\mathbf{S^E}$ species under ambient polymerization conditions represents an unusual finding that prompted further investigation.

Accordingly, the first part of my research focused on elucidating the factors underlying the stability and persistence of the $\mathbf{S^E}$ species **8** at room temperature. In particular, the roles of ligand and solvent in the stabilization of the $\mathbf{S^E}$ intermediate were systematically investigated, and a catalytic cycle involving copper(II) *end-on* peroxido and hydroxido species was proposed to rationalize its unusual persistence in solution. For this purpose, the formation of **8**, along with the subsequent oxygenated intermediates, was examined using stopped-flow techniques and Raman spectroscopy. In addition, the roles of the ligand and the solvent as reducing agents were assessed using UV–vis spectroscopy and GC–MS analysis of the reaction products. Details of this study are presented in Chapter 3.1.



Me$_6$tren **8**

Figure 7: Structure of ligand Me_6tren and the corresponding $\mathbf{S^E}$ complex **8**.

In addition to $\mathbf{S^E}$ species, copper(II) hydroperoxido and alkylperoxido complexes, $\mathbf{P^H}$ and $\mathbf{P^R}$, have attracted considerable attention as putative intermediates in enzymes such as DβH and LPMOs, as well as in catalytic oxidation processes. However, despite their mechanistic relevance, their direct formation from copper(I) and $\mathbf{S^E}$ precursors has rarely been observed and remains poorly understood. Furthermore, studies on their reactivity are still limited, especially concerning their nucleophilic behavior toward acyl derivatives and aldehydes. Overall, these limitations hinder a comprehensive understanding of the role of $\mathbf{P^H}$ and $\mathbf{P^R}$ species in copper-mediated dioxygen activation processes.

Accordingly, the second part of my research focuses on investigating the conversion between $\mathbf{S^E}$ and $\mathbf{P^H}$ species and exploring the reactivity of $\mathbf{P^R}$ intermediates supported by new tripodal tetradentate ligands (**L19-L25**, Figure 8). These systems were designed to provide steric and electronic properties intermediate between ^{i}Pr$_3$tren (**L9**, Figure 5) and TIPT$_3$tren (**L5**, Figure 4), with the goal of promoting the stabilization of both $\mathbf{S^E}$ and $\mathbf{P^H}$ intermediates within the same system. This approach allows systematic evaluation of the influence of the ligand environment on the $\mathbf{S^E}$ to $\mathbf{P^H}$ species conversion and on the properties of the resulting oxygenated species.

$\mathbf{P^H}$ and $\mathbf{P^R}$ complexes were generated via multiple synthetic routes, including the reaction of copper(I) precursors with O_2 and hydroperoxides, as well as the more conventional treatment of copper(II) complexes with H_2O_2 or cumene hydroperoxide in the presence of a base. The resulting copper-dioxygen intermediates were characterized and investigated using low-temperature stopped-flow techniques. In addition, their reactivity toward external substrates was evaluated in both hydrogen atom abstraction and nucleophilic oxidation reactions. The results of this study provide new insight into the formation and reactivity of copper(II)−alkylperoxido species and are discussed in detail in Chapter 3.2.

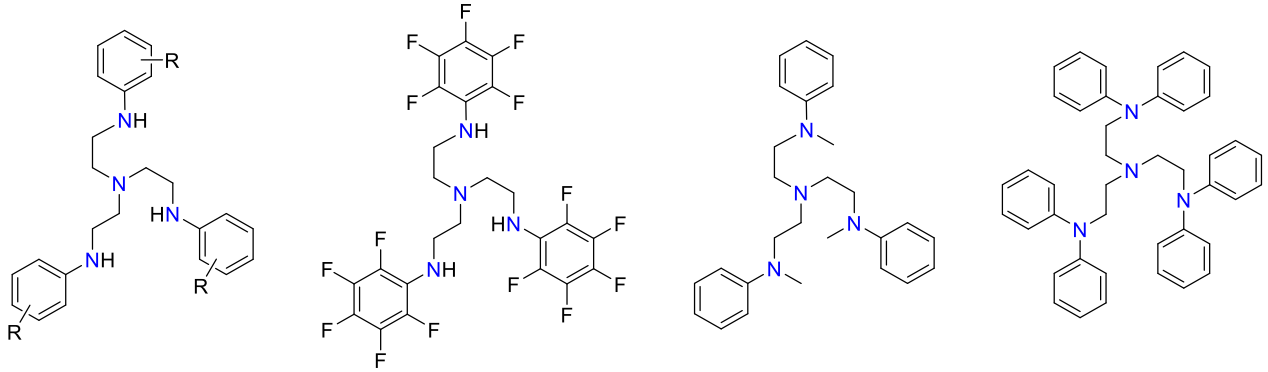


Figure 8: Tripodal tetradentate ligands employed in the second part of my research project.

3. Published Research Articles

3.1 Unusual Stability of an *End-on* Superoxido Copper(II) Complex under Ambient Conditions

This article has been published in Chemistry – A European Journal

Chiara Eleonora Campi, Dr. Kostas Parkatzidis, Prof. Dr. Athina Anastasaki, Prof. Dr. Siegfried Schindler

Chem. Eur. J. **2024**, *41*, e202401634

DOI: https://doi.org/10.1002/chem.202401634

Copyright © 2024 The Authors. Chemistry - A European Journal published by Wiley-VCH GmbH.

Reproduced under the terms of the CC BY-NC 4.0 license

(https://creativecommons.org/licenses/by-nc/4.0/).

Check for updates

Chemistry–A European Journal

Research Article
doi.org/10.1002/chem.202401634

Chemistry Europe
European Chemical Societies Publishing

www.chemeurj.org

Unusual Stability of an *End-on* Superoxido Copper(II) Complex under Ambient Conditions

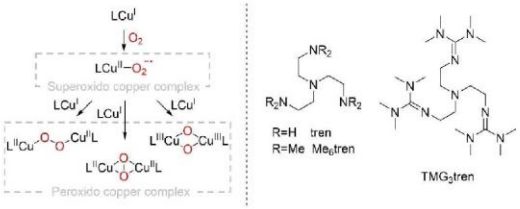
Chiara Eleonora Campi,[a] Kostas Parkatzidis,[b] Athina Anastasaki,[b] and Siegfried Schindler*[a]

Superoxido copper complexes play an important role as usually short-lived intermediates in biology and chemistry. The unusual stability of an *end-on* superoxido copper complex observed in an oxygen-enhanced atom transfer radical polymerization (ATRP) led to a detailed mechanistic investigation of the formation of $[Cu^{II}(Me_6tren)(O_2^{\bullet-})]^+$ (Me_6tren = tris(2-dimethylaminoethyl)amine) under ambient conditions. The persistence of the superoxido copper complex could be explained by a reaction cycle including the peroxido complex $[(Me_6tren)_2Cu^{II}_2(O_2)]^{2+}$ together with $[Cu^{I}(Me_6tren)(DMSO)]^+$ and $[Cu^{II}(Me_6tren)(OH)]^+$ in the overall reaction.

Introduction

The superoxide radical anion plays a significant role across various fields of chemistry, including biochemistry/medicine (superoxide belongs to the group of reactive oxygen species – ROS), the development of lithium-dioxygen batteries, and catalysis.[1,2] Superoxido transition metal complexes, e.g., well-known oxyhemoglobin (which can be formally described as Fe^{III}–O_2), can be obtained in the first step of the reactions with dioxygen.[3–5] Furthermore, these species are recognized as crucial reactive intermediates in selective hydroxylation reactions catalyzed by mononuclear copper monooxygenase enzymes, including peptidylglycine α-hydroxylating monooxygenase (PHM) and dopamine β-monooxygenase (DβM).[6,7] However, end-on superoxido metal complexes are often formed as short-lived intermediates preceding fast consecutive reactions into dinuclear "oxygen adduct" complexes, according to Scheme 1.[3,8,9]

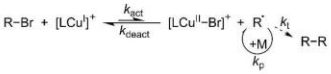
The use of ligand Tris[2-(N-tetramethylguanidyl)ethyl]amine (TMG_3tren, Scheme 1), derived from tris(2-aminoethyl)amine (tren), facilitated the stabilization of an *end-on* superoxido copper(II) complex to such an extent that enabled its structural characterization at low temperatures.[10,11] In contrast, the use of the fully methylated tren ligand Me_6tren (Scheme 1) only allowed brief spectroscopic observation of the corresponding superoxido copper(II) complex at low temperatures before its fast parallel reaction to the dinuclear peroxido copper(II) complex (Scheme 1).[12] In this context, detecting a persistent *end-on* superoxido copper(II) complex using the ligand Me_6tren under ambient conditions in an atom transfer radical polymerization (ATRP) was notably unexpected.[13,14]



Scheme 1. Possible pathways of dioxygen binding to copper complexes (left, charges omitted for clarity); tren-derived ligands (right).

ATRP is one of the most prevalent techniques in reversible deactivation radical polymerization (RDRP).[15–18] It relies on the dynamic equilibrium between active and dormant states of polymers. The metal complex in a low oxidation state, typically a copper(I) complex (LCu^{I}, L = Me_6tren had turned out to be beneficial for ATRP),[19] abstracts the halogen from the initiator, usually an alkyl halide (R–X), to give a carbon-centered radical and a metal complex in a higher oxidative state. While the radical species induce the propagation of the polymeric chain, the copper(II) complex (LCu^{II}–Br) promotes its fast deactivation, minimizing termination reactions and shifting the equilibrium towards the dormant state (Scheme 2).[18]

The observation of the formation of an unusual persistent *end-on* superoxido copper complex under these conditions led



Scheme 2. General ATRP mechanism.

[a] C. E. Campi, Prof. Dr. S. Schindler
Institute of Inorganic and Analytical Chemistry
Justus Liebig University Giessen
Giessen, Hessen 35392, Germany
E-mail: siegfried.schindler@chemie.uni-giessen.de

[b] Dr. K. Parkatzidis, Prof. Dr. A. Anastasaki
Laboratory of Polymeric Materials, Department of Materials
ETH Zurich
Zurich 8093, Switzerland

Supporting information for this article is available on the WWW under https://doi.org/10.1002/chem.202401634

© 2024 The Authors. Chemistry - A European Journal published by Wiley-VCH GmbH. This is an open access article under the terms of the Creative Commons Attribution Non-Commercial License, which permits use, distribution and reproduction in any medium, provided the original work is properly cited and is not used for commercial purposes.

© 2024 The Authors. Chemistry - A European Journal published by Wiley-VCH GmbH

15213765, 2024, 41, Downloaded from https://chemistry-europe.onlinelibrary.wiley.com/doi/10.1002/chem.202401634, Wiley Online Library on [14/05/2026]. See the Terms and Conditions (https://onlinelibrary.wiley.com/terms-and-conditions) on Wiley Online Library for rules of use; OA articles are governed by the applicable Creative Commons License

us to investigate in detail the mechanism behind the stabilization of this otherwise extremely reactive intermediate.

Results and Discussion

To gain a better understanding of the persistence of the *end-on* superoxido copper(II) complex, we first examined the early stages of the oxidation of [Cu^{I}(Me$_6$tren)(Br)] (**1**) under aerobic conditions. Stopped-flow UV-vis measurements (Figure 1) were performed by mixing a deoxygenated solution of **1** in DMSO with a saturated O_2 solution of pure solvent at 25.0 °C. The rapid formation of the *end-on* superoxido copper complex [Cu^{II}(Me$_6$tren)($O_2^{\bullet-}$)]$^+$ (**3**) was detected by the characteristic absorption band at $\lambda = 418$ nm.[12,20] Concurrently, the absorbance maxima at $\lambda = 560$ and 633 nm indicated the formation of the dinuclear *end-on* peroxido copper complex [(Me$_6$tren)Cu^{II}-O-O-Cu^{II}(Me$_6$tren)]$^{2+}$ (**4**), in accordance with previous results.[12,20] Notably, the measurements showed a fast decrease in spectral absorption over the first 0.075 seconds, indicating the decomposition of species **3** and **4**. This finding confirmed the high reactivity of the oxygenated complexes at room temperature, as reported in other solvents.[12,20–22] However, it contradicted our previous findings, as the Raman measurements ($\lambda_{Laser} =$ 402 nm) had provided evidence that the superoxido complex persisted over hours after the oxygenation.[13]

To clarify this point, the measurement time was extended to 350 seconds. Notably, a gradual band increase at $\lambda = 418$ nm was detected, reaching its maximum after 80 seconds (Figure S1). This behavior suggested the involvement of the oxygenated species in a cycle that leads to the regeneration and slight accumulation of **3** in solution over time. Moreover, this finding explained the remarkable and unusual persistence of the oxygenated intermediate at room temperature, which can still be detected over minutes.

Raman measurements were performed anew to support further the assignments postulated by UV-vis spectroscopy. As shown in Figure 2, the peaks at 1128 cm^{-1} and 809 cm^{-1} appeared upon oxygenation of **1** in DMSO. These peaks are characteristic of the vibrational frequency of the ^{16}O–^{16}O unit and can be attributed to complexes **3** and **4**, respectively.[11,12,22,23] Once again, the peaks were visible both immediately after the oxygenation and over several minutes after mixing, supporting the involvement of species **3** and **4** in a catalytic cycle.

To elucidate the pathway that leads to the reformation of the superoxido copper(II) complex **3** and the nature of the species involved, the spectral changes were monitored over 10 minutes in a range of $\lambda = 300$–1000 nm. The analysis was conducted at 25.0 °C immediately after exposing the deoxygenated solution of **1** to air. The solution of **1**, which appeared slightly yellow under inert conditions (see below), rapidly turned its color to dark green upon oxygenation and ultimately became dark yellow (Figure S2). The UV-vis measurements revealed the prompt rise of two bands at $\lambda = 673$ and 847 nm, which undergo a fast decrease over 5 minutes, concurrently with an increase of the absorption band at $\lambda = 443$ nm (Figure 3).

The presence of bands at $\lambda = 673$ and 847 nm is associated with the formation of the species [Cu^{II}(Me$_6$tren)(OH)]Br **5**. The nature of the copper(II) intermediate was confirmed through comparison with the UV-vis spectrum of the isolated [Cu^{II}(Me$_6$tren)(OH)](ClO$_4$) complex (Figure S3).[24] The formation of **5** was additionally proved by detecting an ion peak at m/z of 310.1782 in the electrospray ionization spectrum (ESI-MS) of the solution of **1** upon oxygenation. The observed mass and isotope distribution pattern corresponded to [Cu^{II}(Me$_6$tren)(OH)]$^+$ (calculated m/z of 310.1783).

The band assignment at 443 nm proved more challenging. Initially, we had attributed it to the formation of the *end-on* superoxido copper(II) complex **3**, in accordance with the absorption of the corresponding complex [Cu^{II}(TMG$_6$tren)($O_2^{\bullet-}$)]$^+$ at 442 nm, and the resonance Raman

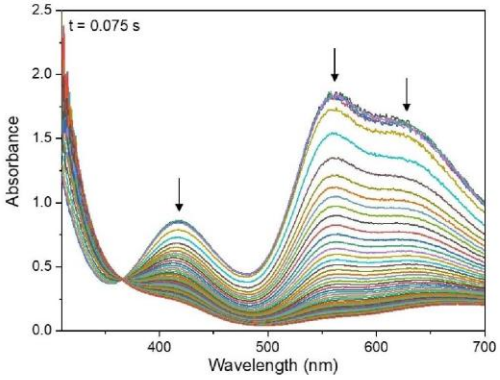


Figure 1. Time-dependent UV-vis spectra, recorded by stopped-flow measurements in the first 0.075 seconds of the reaction between **1** and oxygen-saturated DMSO. [CuBr] = 0.002 mol/L, [Me$_6$tren] = 0.014 mol/L (before mixing), T = 25.0 °C.

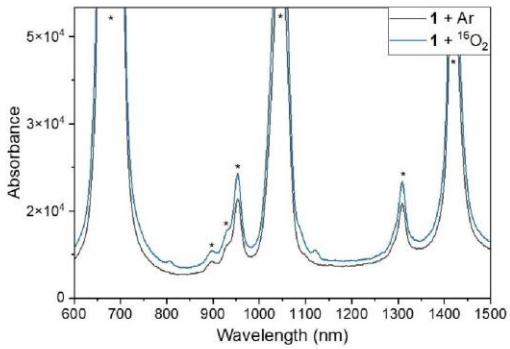


Figure 2. Resonance Raman spectra of compound **1** in DMSO before its reaction with dioxygen (black line) and after its reaction with $^{16}O_2$ (blue line). All the peaks denoted with stars belonged to the solvent. [CuBr] = 0.001 mol/L, [Me$_6$tren] = 0.007 mol/L, T = 25.0 °C.

© 2024 The Authors. Chemistry - A European Journal published by Wiley-VCH GmbH

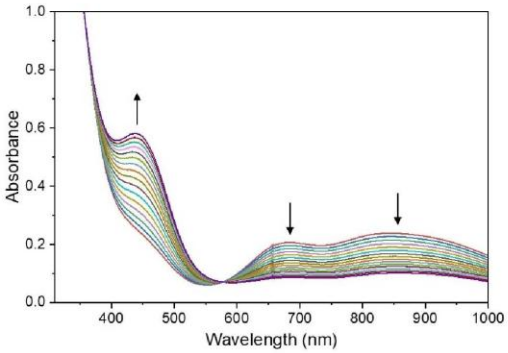


Figure 3. Time-dependent UV-vis spectra were recorded in the first 350 s of the reaction between **1** and air in DMSO. [CuBr] = 0.001 mol/L, [Me_6tren] = 0.007 mol/L, T = 25.0 °C.

measurements.[11,13] We first attributed the shift from 418 nm, previously observed for complex **3** in different solvents, to 443 nm using DMSO as solvent.[12] However, as demonstrated above with the results of the stopped-flow measurements, the absorbance at 443 nm cannot be associated with the formation of **3**. To identify the nature of the species responsible for this absorption, the reactivity of **1** in DMSO was investigated under inert conditions. The colorless solution turned to a pale yellow color when argon was bubbled through it over a period of 40 minutes (Figure S2). An increase in the band at $\lambda = 443$ nm was detected over time (Figure 4, blue solid line) and was attributed to the slow formation of the DMSO adduct [Cu^{I}-(Me_6tren)(DMSO)]Br (**2**).

DMSO is widely recognized as a strong coordinating solvent that competes with other ligands to bind to copper ions.[25–28] Thus, it is likely that an equilibrium between species **1** and **2** exists in solution. To validate this idea, [$Cu^{I}(CH_3CN)_4$](OTf) was applied as an initial copper source. A more significant increase in the absorption band at $\lambda = 443$ nm was observed over 40 minutes (Figure 4, red solid line). This finding can be attributed to the less coordinating nature of the triflate counterion compared to bromide, thereby favoring the coordination of DMSO to the copper center.

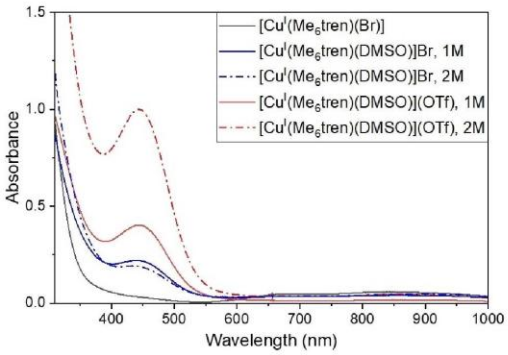
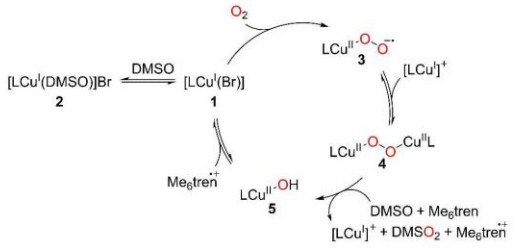


Figure 4. Uv-vis spectra of compounds **1** and **2** in DMSO under inert conditions at room temperature: **1**, immediately after mixing (black line); [Cu^{I}(Me_6tren)(DMSO)]Br **2**, after 40 minutes under an argon stream (blue line: 1 mol/L solid line, 2 mol/L dotted line); [Cu^{I}(Me_6tren)(DMSO)](OTf) after 40 minutes under argon stream (red line: 1 mol/L solid line, 2 mol/L dotted line).

Additionally, different amounts of copper(I) complex **1**, as well as [Cu^{I}(Me_6tren](OTf), were used to investigate the effect of the concentration on the equilibrium. When the concentration of copper(I) was increased from 1 mol/L to 2 mol/L, the solutions of **1** and [Cu^{I}(Me_6tren](OTf) exhibited marked differences in the absorption features (Figure 4). Specifically, the absorption at $\lambda = 443$ nm increased proportionally to the concentration of [$Cu^{I}(CH_3CN)_4$](OTf), while no discernible variation in the absorption bands was detected at different concentrations of CuBr. These results confirmed that the formation of complex [Cu^{I}(Me_6tren)(DMSO)](OTf) increases with the amount of copper(I) salt in solution. On the contrary, the formation of complex **2** is enhanced by the use of a higher concentration of DMSO and hampered by the increase in the concentration of bromide ion, thus resulting in similar absorption at $\lambda = 443$ nm in both the 1 mol/L and 2 mol/L solutions. Additionally, our hypothesis was further confirmed as no absorption at $\lambda = 443$ nm was observed when DMSO was replaced with different solvents such as methanol, acetonitrile, and toluene. However, similar behavior was observed in DMF, thus indicating that the absorbance could be attributed to an MLCT from copper to oxygen. Under the conditions previously applied, the absorbance of **2** at 443 nm overlaid the absorbance of **3** at 418 nm, which caused our wrong assignment of this band.[13]

Based on the overall results presented above, a mechanism that explains the persistence of the superoxido complex can be postulated according to Scheme 3.

The copper(I) complex **1** first reacts with dioxygen to form the superoxido and peroxide complexes **3** and **4**. We further propose that the formation of complex **5** occurs by the homolytic cleavage of the peroxide O–O bond of the intermediate **4**. The cleavage is facilitated by the presence of DMSO, which is oxidized to the corresponding sulfone, $DMSO_2$, and results in the reformation of **1**. The copper(I) complex that is thus generated *in-situ* can further react fast with the dioxygen dissolved in solution and start the cycle again, which leads to



Scheme 3. Proposed mechanism for the cyclic formation of the superoxido copper(II) complex **3** (L = Me_6tren).

© 2024 The Authors. Chemistry - A European Journal published by Wiley-VCH GmbH

15213765, 2024, 41, Downloaded from https://chemistry-europe.onlinelibrary.wiley.com/doi/10.1002/chem.202401634, Wiley Online Library on [14/05/2026]. See the Terms and Conditions (https://onlinelibrary.wiley.com/terms-and-conditions) on Wiley Online Library for rules of use; OA articles are governed by the applicable Creative Commons License

15213765, 2024, 41, Downloaded from https://chemistry-europe.onlinelibrary.wiley.com/doi/10.1002/chem.202401634, Wiley Online Library on [14/05/2026]. See the Terms and Conditions (https://onlinelibrary.wiley.com/terms-and-conditions) on Wiley Online Library for rules of use; OA articles are governed by the applicable Creative Commons License

the formation and accumulation of the **3** and **4**. This hypothesis is supported by detecting the sulfone $DMSO_2$ exclusively upon oxygenation, as confirmed by GC-MS analysis (Figure S8).

Concurrently, the excess of ligand Me_6tren promotes the formation of the hydroxido complex **5** through hydrogen atom abstraction (HAA). The formation of complex **5** is found to be promoted by the presence of trace amounts of water and atmospheric moisture, which can act as an additional hydrogen source. A significant enhancement of the absorption bands at $\lambda = 673$ and 847 nm can indeed be observed upon adding water to the solution of complex **1** in dry DMSO (Figure S4). Nevertheless, it's important to note that the water content should not exceed a threshold of 5% (v/v) in dry-DMSO to prevent the promotion of competitive reaction pathways, which can hinder the overall cycle. Although water can contribute to the formation of complex **5**, it is important to notice that it is insufficient to sustain the cycle of reformation of **3** on its own.

The rapid decrease in the absorption bands at $\lambda = 673$ and 847 nm (Figure 3) indicates the fast consumption of species **5** over 5 minutes. Since a consistent reduction of the bands was observed only upon oxygenation of the solution of complex **1** containing an excess of ligand, we assumed that the excess of Me_6tren plays a central role in the reductive step. To test this hypothesis, 6 fold excess of ligand was added to a DMSO solution of complex **5** and the spectral changes were monitored over 30 min. Notably, no reduction of the copper(II) intermediate was detected (Figure S5). Therefore, we assumed that the reduction of complex **5** is promoted by the radical cation $Me_6tren^{+\bullet}$, previously generated *in-situ* from Me_6tren *via* HAA (Scheme 3). Whether the exact mechanism of the reductive step is yet to be clarified, the detection of by-products such as N^1-(2-aminoethyl)ethane-1,2-diamine and N^2-[2-(dimethylamino)-ethylidene]-N^1,N^1-dimethyl-1,2-ethanediamine that are consistent with ligand modifications upon oxygenation (Figure S9), strongly suggest the formation of the radical-cation on the Me_6tren and its involvement in the reduction of the hydroxido intermediate. Furthermore, it is important to point out that other ligands, such as e.g., tris(2-methylpyridyl)amine (tmpa), were tested and did not show the same reactivity. No superoxido copper complexes could be detected with these ligands and demonstrated the particular properties of Me_6tren to form a radical cation.

To prove the ability of complex **5** to follow a radical-based reductive pathway under our working conditions, TEMPO–H was added to a solution of $[Cu^{II}(Me_6tren)(OH)]Br$ in DMSO and the reaction was monitored via UV-Vis spectroscopy.[29] The measurements revealed a consistent decrease of the absorption bands at $\lambda = 673$ and 887 nm within 20 minutes (Figure S6), thus confirming the reduction of the copper(II) hydroxido species. To further prove the process's radical nature and confirm the system's catalytic application, we tested the phenol derivative 2,6-di-tert-butylphenol (DTBP). A solution of 5 mol% of complex **1**, 20 mol% of Me_6tren, and DTBP in DMSO was prepared under inert conditions and oxygenated for 2 minutes. After 12 hours of stirring, DTBP was converted into a mixture of 2,6-di-tert-butyl-1,4-benzoquinone (DTBQ, 1%) and 3,5,3′,5′-tetra-tert-butyl-4,4′-diphenoquinone (TTDBQ, 45%). The formation of the main product TTDBQ is coherent with a radical coupling reaction promoted by HAA.[30–33]

Finally, being aware that the reduction of certain Cu(II) complexes can be enhanced by UV irradiation in the presence of excess ligand, we examined the effect of UV light on our DMSO solution of complex **1** and Me_6tren ($[Cu^{I}(Me_6tren)]:[Me_6tren] = 1:6$).[34,35] The UV-Vis measurements performed after oxygenation revealed a significant acceleration in the reduction rate of complex **5** to complex **1**, as evidenced by the faster decrease in the absorption bands at $\lambda = 673$ and 847 nm upon UV irradiation (Figure S7). These data support the hypothesis of a radical-based mechanism, and they also are in line with the findings of Anastasaki and co-workers, who observed a strong increase in polymerization rates under similar irradiation conditions.[14] Although the overall results confirmed the formation of persistent reactive oxygenated species, namely complex **3**, **4**, and **5**, under conditions analogous to ATRP, further work should be carried out to completely elucidate the role of this catalytic system in the polymerization process.

Conclusions

End-on superoxido copper complexes form in the first step when copper(I) complexes are reacted with dioxygen. These reactive species are often difficult to catch, and sometimes temperatures as low as −140 °C are needed to observe their formation at least spectroscopically.[35] In so far, the very unusual persistence of an *end-on* superoxido copper complex under ambient conditions applied in oxygen-enhanced atom transfer radical polymerization (ATRP) has been quite puzzling. However, it was possible to explain this finding by identifying additional copper complexes as intermediates in a reaction cycle. Furthermore, the importance of the solvent and the special properties of the tripodal ligand Me_6tren (that need to be applied in excess) could be clarified. A dinuclear peroxido copper complex, in equilibrium with the superoxido copper complex is responsible for hydrogen abstraction of the Me_6tren ligand. Hydrogen abstraction, applying a related dinuclear peroxido complex (with the ligand tmpa), had been demonstrated previously for the selective oxygenation of toluene to benzaldehyde.[36]

These findings should interest not only ATRP scientists but also researchers working on superoxide interaction in other research areas. Keeping a superoxido/peroxido copper complex persistent under ambient conditions for some time makes the overall system quite interesting for more testing in stoichiometric or catalytic oxygenation reactions. Furthermore, as pointed out in the introduction, alkali/air batteries can have problems with the formation of superoxide, and our results might help with finding a solution to overcome these. Additionally, superoxide as ROS (reactive oxygen species) plays an important role in biology and medicine. DMSO is a common solvent used in some of these studies and could influence the fate of the superoxide, as observed in our work.

© 2024 The Authors. Chemistry - A European Journal published by Wiley-VCH GmbH

Supporting Information

The data supporting this study's findings are available in the article's Supporting Information, which includes additional references cited by the Authors.[20,24,37,38]

Acknowledgements

We acknowledge the German Academic Scholarship Foundation (Studienstiftung des deutschen Volkes) for financial support. We thank Prof. Dr. Peter J. Klar and Dr. Limei Chen for their assistance with Raman measurements. We also acknowledge Friedemann Dreßler and Alexander Petrillo for their scientific discussions and valuable suggestions. Open Access funding enabled and organized by Projekt DEAL.

Conflict of Interests

The authors declare no conflict of interest.

Data Availability Statement

The data that support the findings of this study are available from the corresponding author upon reasonable request.

Keywords: Copper · Superoxido complex · Polymerisation · Mechanism · Dioxygen Activation

[1] M. Hayyan, M. A. Hashim, I. M. Al Nashef, *Chem. Rev.* **2016**, *116*, 3029–3085.
[2] C. Wang, Z. Zhang, W. Liu, Q. Zhang, X. Wang, Z. Xie, Z. Zhou, *Angew. Chem. Int. Ed.* **2020**, *59*, 17856–17863.
[3] S. Schindler, *Eur. J. Inorg. Chem.* **2000**, *11*, 2311–2326.
[4] S. Itoh, *Acc. Chem. Res.* **2015**, *48*, 2066–2074.
[5] H. Kim, P. J. Rogler, S. K. Sharma, A. W. Schaefer, E. I. Solomon, K. D. Karlin, *J. Am. Chem. Soc.* **2020**, *142*, 3104–3116.
[6] J. M. Bollinger, C. Krebs, *Curr. Opin. Chem. Biol.* **2007**, *11*, 151–158.
[7] J. P. Klinman, *J. Biol. Chem.* **2006**, *281*, 3013–3016.
[8] A. Brinkmeier, R. A. Schulz, M. Buchhorn, C.-J. Spyra, S. Dechert, S. Demeshko, V. Krewald, F. Meyer, *J. Am. Chem. Soc.* **2021**, *143*, 10361–10366.
[9] T. Hoppe, S. Schaub, J. Becker, C. Würtele, S. Schindler, *Angew. Chem. Int. Ed.* **2013**, *52*, 870–873.
[10] C. Würtele, E. Gaoutchenova, K. Harms, M. C. Holthausen, J. Sundermeyer, S. Schindler, *Angew. Chem. Int. Ed.* **2006**, *45*, 3867–3869.
[11] M. Schatz, V. Raab, S. P. Foxon, G. Brehm, S. Schneider, M. Reiher, M. C. Holthausen, J. Sundermeyer, S. Schindler, *Angew. Chem. Int. Ed.* **2004**, *43*, 4360–4363.
[12] M. Becker, F. W. Heinemann, S. Schindler, *Chem. Eur. J.* **1999**, *5*, 3124–3129.
[13] K. Parkatzidis, N. P. Truong, R. Whitfield, C. E. Campi, B. Grimm-Lebsanft, S. Buchenau, M. A. Rübhausen, S. Harrisson, D. Konkolewicz, S. Schindler, A. Anastasaki, *J. Am. Chem. Soc.* **2023**, *145*, 1906–1915.
[14] S. D. Casa, K. Parkatzidis, N. P. Truong, A. Anastasaki, *J. Polym. Sci.* **2023**, pol.20230479.
[15] J.-S. Wang, K. Matyjaszewski, *J. Am. Chem. Soc.* **1995**, *117*, 5614–5615.
[16] K. Matyjaszewski, *Macromolecules* **2012**, *45*, 4015–4039.
[17] K. Matyjaszewski, *Adv. Mater.* **2018**, *30*, 1706441.
[18] F. Lorandi, M. Fantin, K. Matyjaszewski, *J. Am. Chem. Soc.* **2022**, *144*, 15413–15430.
[19] W. Tang, K. Matyjaszewski, *Macromolecules* **2006**, *39*, 4953–4959.
[20] M. Weitzer, S. Schindler, G. Brehm, S. Schneider, E. Hörmann, B. Jung, S. Kaderli, A. D. Zuberbühler, *Inorg. Chem.* **2003**, *42*, 1800–1806.
[21] S. Y. Quek, S. Debnath, S. Laxmi, M. Van Gastel, T. Krämer, J. England, *J. Am. Chem. Soc.* **2021**, *143*, 19731–19747.
[22] K. Komiyama, H. Furutachi, S. Nagatomo, A. Hashimoto, H. Hayashi, S. Fujinami, M. Suzuki, T. Kitagawa, *B. Chem. Soc. Jpn.* **2004**, *77*, 59–72.
[23] M. Bhadra, W. J. Transue, H. Lim, R. E. Cowley, J. Y. C. Lee, M. A. Siegler, P. Josephs, G. Henkel, M. Lerch, S. Schindler, A. Neuba, K. O. Hodgson, B. Hedman, E. I. Solomon, K. D. Karlin, *J. Am. Chem. Soc.* **2021**, *143*, 3707–3713.
[24] S. C. Lee, R. H. Holm, *J. Am. Chem. Soc.* **1993**, *115*, 11789–11798.
[25] S. Monge, V. Darcos, D. M. Haddleton, *J. Polym. Sci. Part A* **2004**, *42*, 6299–6308.
[26] R. D. Willett, G. Pon, C. Nagy, *Inorg. Chem.* **2001**, *40*, 4342–4352.
[27] S. Racioppi, L. Orian, C. Tubaro, A. Gennaro, A. A. Isse, *Catalysts* **2022**, *12*, 1656.
[28] T. J. Zerk, M. Martinez, P. V. Bernhardt, *Inorg. Chem.* **2016**, *55*, 9848–9857.
[29] M. C. Ryan, L. D. Whitmire, S. D. McCann, S. S. Stahl, *Inorg. Chem.* **2019**, *58*, 10194–10200.
[30] K. V. N. Esguerra, Y. Fall, L. Petitjean, J.-P. Lumb, *J. Am. Chem. Soc.* **2014**, *136*, 7662–7668.
[31] J. J. Liu, D. E. Diaz, D. A. Quist, K. D. Karlin, *Isr. J. Chem.* **2016**, *56*, 738–755.
[32] S. E. Allen, R. R. Walvoord, R. Padilla-Salinas, M. C. Kozlowski, *Chem. Rev.* **2014**, *114*, 899–899.
[33] T. Wu, S. N. MacMillan, K. Rajabimoghadam, M. A. Siegler, K. M. Lancaster, I. Garcia-Bosch, *J. Am. Chem. Soc.* **2020**, *142*, 12265–12276.
[34] T. G. Ribelli, D. Konkolewicz, S. Bernhard, K. Matyjaszewski, *J. Am. Chem. Soc.* **2014**, *136*, 13303–13312.
[35] A. Anastasaki, V. Nikolaou, Q. Zhang, J. Burns, S. R. Samanta, C. Waldron, A. J. Haddleton, R. McHale, D. Fox, V. Percec, P. Wilson, D. M. Haddleton, *J. Am. Chem. Soc.* **2014**, *136*, 1141–1149.
[36] M. Bhadra, W. J. Transue, H. Lim, R. E. Cowley, J. Y. C. Lee, M. A. Siegler, P. Josephs, G. Henkel, M. Lerch, S. Schindler, A. Neuba, K. O. Hodgson, B. Hedman, E. I. Solomon, K. D. Karlin, *J. Am. Chem. Soc.* **2021**, *143* (10), 3707–3713.
[37] C. Noß, R. Göttlich, S. Schindler, *Chem. Eur. J.* **2023**, *29*, e202301142.
[38] G. J. P. Britovsek, J. England, A. J. P. White, *Inorg. Chem.* **2005**, *44*, 8125–8134.
[39] S. Srivastava, A. Ali, A. Tyagi, R. Gupta, *Eur. J. Inorg. Chem.* **2014**, 2113–2123.

Manuscript received: May 8, 2024
Accepted manuscript online: May 8, 2024
Version of record online: June 24, 2024

© 2024 The Authors. Chemistry - A European Journal published by Wiley-VCH GmbH

15213765, 2024, 41, Downloaded from https://chemistry-europe.onlinelibrary.wiley.com/doi/10.1002/chem.202401634, Wiley Online Library on [14/05/2026]. See the Terms and Conditions (https://onlinelibrary.wiley.com/terms-and-conditions) on Wiley Online Library for rules of use; OA articles are governed by the applicable Creative Commons License

3.2 Copper Complexes with Arylated Triethylenetetramine Ligands: Reactivity Toward Dioxygen and Peroxides

This article has been published in European Journal of Inorganic Chemistry

Chiara Eleonora Campi, Dr. Christian Würtele, Prof. Dr. Siegfried Schindler

Eur. J. Inorg. Chem. **2026**, e70203

DOI: https://doi.org/10.1002/ejic.70203

Copyright © 2026 The Authors. European Journal of Inorganic Chemistry published by Wiley-VCH GmbH. Reproduced under the terms of the CC BY license (https://creativecommons.org/licenses/by/).

Check for updates

European Journal of Inorganic Chemistry

EurJIC
European Journal of Inorganic Chemistry

Chemistry Europe
European Chemical Societies Publishing

RESEARCH ARTICLE OPEN ACCESS

Copper Complexes with Arylated Triethylenetetramine Ligands: Reactivity Toward Dioxygen and Peroxides

Chiara Eleonora Campi | Christian Würtele | Siegfried Schindler

Institute of Inorganic and Analytical Chemistry, Justus Liebig University Giessen, Giessen, Germany

Correspondence: Siegfried Schindler (siegfried.schindler@anorg.chemie.uni-giessen.de)

Received: 11 February 2026 | **Revised:** 9 March 2026 | **Accepted:** 23 March 2026

Keywords: aldehyde deformylation | alkylperoxide complex | copper | dioxygen activation | hydrogen peroxide

ABSTRACT

Copper model complexes that mimic metalloenzyme active sites provide important insight into copper-mediated oxygen activation. Among the ligand frameworks explored, tripodal tetradentate nitrogen–donor ligands based on the tris(2-aminoethyl)amine (tren) scaffold proved particularly effective at stabilizing reactive copper–oxygen intermediates. Here, we report the synthesis and characterization of new arylated tren derivatives and their coordination to Cu(I) and Cu(II) centers. The reactivity of the resulting complexes toward dioxygen (O_2), hydrogen peroxide (H_2O_2), and cumene hydroperoxide was investigated, and transient copper–oxygen species were examined using low-temperature stopped-flow techniques. Superoxido intermediates were detected when electron-donating and sterically hindered ligands were employed. Hydroperoxido species were generated through reactions of the copper complexes with both O_2 and H_2O_2, while treatment with cumene hydroperoxide led to the formation of alkylperoxido species. The reactivity of the peroxide species was evaluated toward external substrates. All the complexes exhibited reactivity toward benzoyl chloride, whereas efficient aldehyde deformylation was observed exclusively for the cumylperoxido species.

1 | Introduction

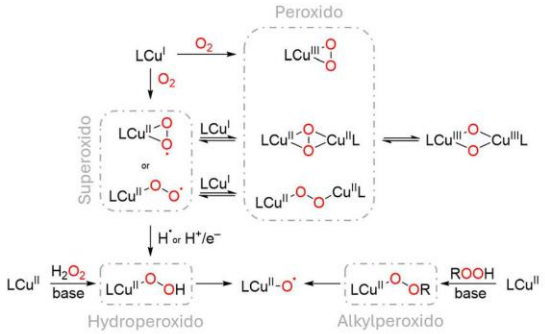
Copper is a key component of many metalloenzymes that activate molecular oxygen (O_2) to catalyze biologically essential transformations, including C–H hydroxylation, oxygen–atom insertion, and oxidative dehydrogenation [1–3]. In these systems, O_2 activation typically occurs at mononuclear or dinuclear Cu(I) centers, generating transient copper–oxygen intermediates. Among them, superoxido, peroxido, hydroperoxido, oxido/or oxyl radical copper complexes were proposed as key intermediates in the active site of copper monooxygenases and oxidases, including dopamine β-monooxygenase (DβM), peptidylglycine α-hydroxylating monooxygenase (PHM), lytic polysaccharide monooxygenases (LPMOs), and copper amine oxidases (Scheme 1) [1, 4].

Mononuclear *end–on* superoxido copper(II) complexes were widely investigated as the earliest intermediates formed upon O_2 binding to Cu(I) and were proposed as putative active oxidants in DβM and PHM [5–8]. However, their high reactivity makes these species short-lived and difficult to isolate or characterize. Their stabilization was achieved using tripodal tetradentate nitrogen–donor ligands, including tris(2-pyridylmethyl) amine (tmpa) and tris(2-aminoethyl)amine (tren) derivatives (Scheme 2) [9–13]. In particular, sterically demanding ligands such as $HIPT_3$tren (HIPT = 2,2″,4,4″,6,6″-hexaisopropyl-1,3′:5′,1″-terphenyl, Scheme 2) and $TIPT_2$aped (TIPT = 2,2″,6,6″-tetraisopropyl-1,3′:5′,1″-terphenyl, aped = *N*′-(2-aminoethyl)-*N*′-(pyridin-2-ylmethyl)ethane-1,2-diamine, Scheme 2) facilitated detailed spectroscopic studies, and strongly basic ligands such as TMG_3tren (TMG = 1,1,3,3-tetramethylguanidine, Scheme 2) stabilized *end–on* Cu(II)–superoxido complexes sufficiently to allow the first structural characterization at low temperatures by Würtele et al. [6, 14, 15].

Hydroperoxido copper(II) complexes represent another important class of copper–oxygen intermediates that were proposed as a key species in enzymatic catalysis [1, 16]. These complexes can arise in biological systems from superoxido copper(II) species

This is an open access article under the terms of the Creative Commons Attribution License, which permits use, distribution and reproduction in any medium, provided the original work is properly cited.

© 2026 The Author(s). *European Journal of Inorganic Chemistry* published by Wiley-VCH GmbH..

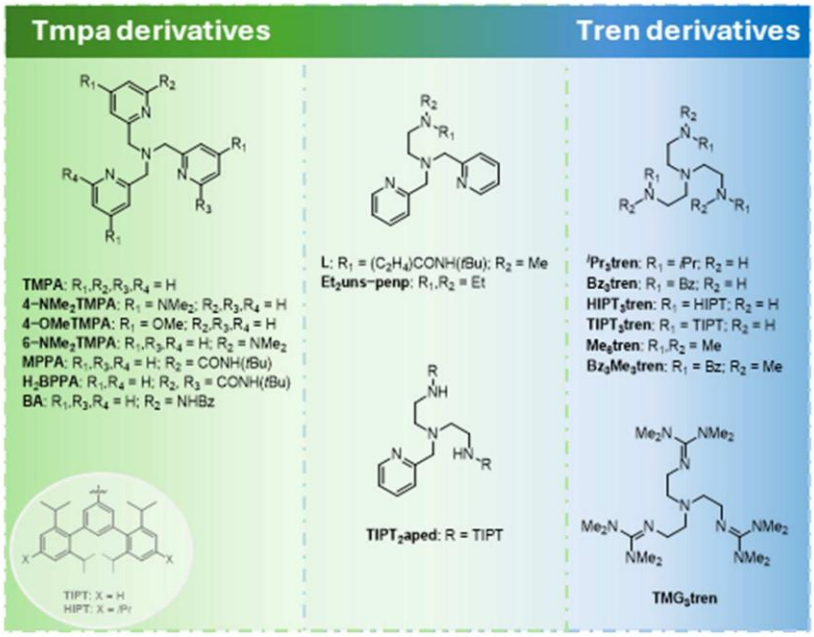


SCHEME 1 | Possible formation pathways of mononuclear and dinuclear copper–oxygen active species.

through hydrogen atom abstraction or proton-coupled electron transfer and are capable of O–O bond cleavage and substrate oxidation [17–21]. Despite its mechanistic relevance, direct formation of hydroperoxido species from superoxido complexes is scarcely reported, and synthetic hydroperoxido complexes are most commonly generated by treating Cu(II) precursors with hydrogen peroxide in the presence of base. Due to their thermal instability, most complexes were characterized only in solution at cryogenic temperatures, typically stabilized by tripodal tetradentate nitrogen–donor ligands. Only a few examples were isolated and structurally characterized, often requiring hydrogen-bonding ligand frameworks [22]. The first crystal structure of a hydroperoxido copper(II) complex was reported by Wada et al. using the H_2BPPA ligand (*N*-(2-pyridylmethyl)bis(6-pivalamido-2-pyridylmethyl)amine, Scheme 2) based on tmpa scaffold, establishing an important benchmark for subsequent structural and spectroscopic studies [23].

Closely related alkylperoxido copper(II) complexes were also investigated to provide further insight into copper–oxygen reactivity and were commonly regarded as functional models for lipid peroxidation as well as precursors to highly reactive copper–oxygen species [24, 25]. Since the first structurally characterized example reported by Kitajima and coworkers in 1993, extensive studies have elucidated their structural, spectroscopic, and reactive properties [26]. These complexes commonly undergo homolytic Cu–O or O–O bond cleavage, leading to electrophilic or radical reactivity and formation of Cu(II) oxyl or related intermediates [27–29]. Although electrophilic pathways predominate, recent work demonstrated that nucleophilic reactivity can also be accessed through appropriate ligand design, highlighting the versatility of copper–peroxide chemistry [30].

Overall, studies on Cu(II) superoxido, hydroperoxido, and alkylperoxido complexes provided critical insight into copper-mediated oxygen activation in both biological and synthetic systems, with tripodal tetradentate nitrogen–donor ligands based on the tren scaffold playing a key role in stabilizing these reactive intermediates. Here, we report the investigation of new Cu(I) and Cu(II) complexes supported by arylated tren ligands and their reactivity toward O_2, H_2O_2, and cumene hydroperoxide (cumyl–OOH). Some of these ligands, such as Ph_3tren (2,2′,2″-tris(phenylamino)triethylamine) and $(C_6F_5)_3$tren (2,2′,2″-tris (pentafluorophenylamino)triethylamine), were originally introduced by Kol et al. for dinitrogen activation at molybdenum centers [31] and were adapted here to explore their coordination chemistry and oxygen activation behavior at copper centers. The resulting transient copper–oxygen species were examined using low-temperature–stopped flow techniques, and systematic ligand modifications were employed to elucidate steric and electronic effects on oxygen activation.



SCHEME 2 | Selected list of tripodal tetradentate ligands able to stabilize reactive copper–oxygen species [1, 14].

10990682c, 0, Downloaded from https://chemistry-europe.onlinelibrary.wiley.com/doi/10.1002/ejic.70203, Wiley Online Library on [14/05/2026]. See the Terms and Conditions (https://onlinelibrary.wiley.com/terms-and-conditions) on Wiley Online Library for rules of use; OA articles are governed by the applicable Creative Commons License

2 | Results and Discussion

2.1 | Synthesis of Ligands L1–L7

The arylated triethylenetetramine ligands Ph_3tren (**L1**), $(CF_3Ph)_3$tren (2,2′,2″-tris(4-(trifluoromethyl)phenylamino) triethylamine, **L2**), $(tBu_2Ph)_3$tren (2,2′,2″-tris(3,5-(di-*tert*-butyl) phenylamino)triethylamine, **L4**), and Ph_6tren (2,2′,2″-tris(diphenylamino)triethylamine, **L5**) were synthesized via Buchwald–Hartwig coupling, according to Figure 1a. The synthesis of **L1** was reported previously by Kol et al. and was adapted in this work for the synthesis of the other ligands [31, 32]. The synthesis of ligands **L1**, **L2**, and **L4** involved the treatment of tren with the corresponding aryl bromides in the presence of $Pd_2(dba)_3$ (tris (dibenzylideneacetone)dipalladium(0), 5 mol%) and rac–BINAP ((±)–2,2′-bis(diphenylphosphino)–1,1′-binaphthalene), while the synthesis of **L5** required the use of $Pd_2(dba)_3$ (6 mol%) and X–Phos (2-dicyclohexylphosphino-2′,4′,6′-triisopropylbiphenyl) as the catalyst. The yields ranged from 33% for **L5** to 55% for **L2**. The N-methylated ligand Me_3Ph_3tren (2,2′,2″-tris(*N*-phenyl-*N*-methylamino)triethylamine, **L6**) was synthesized by reductive amination of ligand **L1**, in good yield (73%, Figure 1c). A different approach was used for $(C_6F_5)_3$tren (**L7**), which was obtained by nucleophilic attack of tren on the electron-deficient hexafluorobenzene in a yield of 71% (Figure 1b) [31].

The synthesis of ligand $(OMePh)_3$tren (2,2′,2″-tris(4-(methoxy) phenylamino)triethylamine, **L3**) proved particularly challenging. Initial attempts to obtain the ligand via Buchwald–Hartwig coupling only resulted in partial functionalization of the triamine, yielding mono- or di-substituted tren derivatives. Neither the increase in the amount of palladium catalyst and the use of different palladium ligands, nor the increase in temperature and reaction time led to the formation of the tri-substituted ligand. The attempt to synthesize **L3** through nucleophilic substitution of *p*-anisidine on tris(2-chloroethyl)amine hydrochloride led to the formation of the *N*-arylpiperazine derivative (**L3'**, ligand structure shown in supporting information), despite the use of a high excess of *p*-anisidine and low reaction temperature (Scheme S1).

Ultimately, **L3** was successfully synthesized in two steps involving the initial formation of a triamide from 2,2′,2″-nitrilotriacetic acid and *p*-anisidine in the presence of CDI (*N*, *N*'-carbonyldiimidazole), followed by reduction with $LiAlH_4$, as shown in Figure 1d [33]. All ligands were characterized by ESI–MS and NMR spectroscopy (Figures S36–S51 and S68–S74). The crystal structures of **L1** and **L5** are presented in Figure 1e.

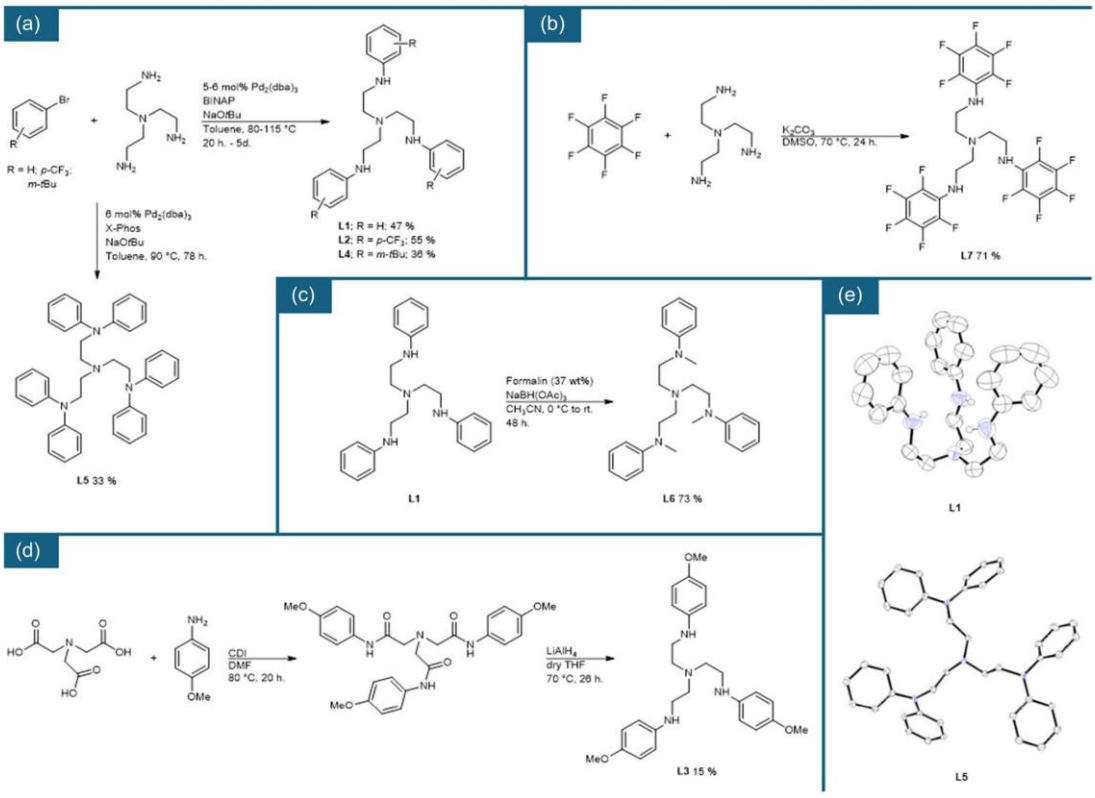


FIGURE 1 | (a) Synthesis of arylated triethylenetetramine ligands **L1**, **L2**, **L4**, **L5**, via Buchwald–Hartwig coupling; (b) Synthesis of **L7** via nucleophilic attack; (c) Synthesis of **L6** by reductive amination of ligand **L1**; (d) Two-step synthesis of **L3** involving initial amidation of nitrilotriacetic acid with CDI, followed by reduction with $LiAlH_4$; (e) ORTEP Plot of the molecular structure of ligands **L1** and **L5** with displacement ellipsoids drawn at the 50% probability level. Hydrogen atoms are omitted for clarity, except those on nitrogen if present.

10990682c, 0, Downloaded from https://chemistry-europe.onlinelibrary.wiley.com/doi/10.1002/ejic.70203, Wiley Online Library on [14/05/2026]. See the Terms and Conditions (https://onlinelibrary.wiley.com/terms-and-conditions) on Wiley Online Library for rules of use; OA articles are governed by the applicable Creative Commons License

2.2 | Synthesis and Characterization of Copper(II) Complexes

The monomeric copper(II) complexes were obtained as solids by reacting one equivalent of $Cu(ClO_4)_2{\cdot}6\,H_2O$ with the corresponding ligands in acetone under inert atmosphere and then removing the solvent under reduced pressure. Elemental analyses indicate that the isolated compounds contain either a coordinated water molecule or a hydroxide anion as an additional ligand, along with different amounts of lattice water. Accordingly, the complexes obtained in the solid state are formulated as $[Cu(\mathbf{L1})(H_2O)](ClO_4)_2$ (**1a-H_2O**), $[Cu(\mathbf{L2})(H_2O)](ClO_4)_2{\cdot}4\,H_2O$ (**2a-H_2O**), $[Cu(\mathbf{L3})(OH)](ClO_4){\cdot}2\,H_2O$ (**3a-OH**), $[Cu(\mathbf{L4})(OH)](ClO_4){\cdot}3\,H_2O$ (**4a-OH**), $[Cu(\mathbf{L6})(OH)](ClO_4){\cdot}3\,H_2O$ (**6a-OH**), and $[Cu(\mathbf{L7})(OH)](ClO_4){\cdot}3\,H_2O$ (**7a-OH**). The coordination of water or hydroxide anion as an additional ligand is consistent with previous findings reported by Holm and coworkers for the copper–Me_6tren (tris[2-(dimethylamino)ethyl]amine) system [34]. However, structurally characterized copper(II) complexes of this type are rare, as chloride is frequently introduced as an auxiliary ligand to facilitate crystallization. Another example of a structurally characterized copper(II) complex featuring water as an additional ligand is $[Cu(Bz_3tren)(H_2O)](ClO_4)_2$, which was previously reported by our group [35].

Green crystals suitable for X-ray diffraction were obtained for copper(II) complexes bearing ligands **L1** ($[Cu(\mathbf{L1})((CH_3)_2CO)](ClO_4)_2$, **1a-acetone**) and **L4** ($[Cu(\mathbf{L4})((CH_3)_2CO)](ClO_4)_2$ **4a-acetone**) and are presented in Figures 2 and S75. The τ parameter of **1a-acetone** was determined as $\tau_5 = 0.61$ ($\tau_5 = 0.69$ for **4a-acetone**), indicating a distorted geometry intermediate between trigonal bipyramidal (TBP) and square pyramidal (SP) [36]. The copper(II) centers exhibit a five-coordinate arrangement, with one molecule of acetone bound in the axial position. This labile coordination site suggests the presence of a potential binding pocket that could facilitate the activation of small molecules such as dioxygen and hydrogen peroxide. For **1a-acetone**, the bond length between the copper(II) center and the axial nitrogen was measured to 2.011 Å, while the bond lengths to the equatorial nitrogen atoms ranged from 2.156 to 2.114 Å.

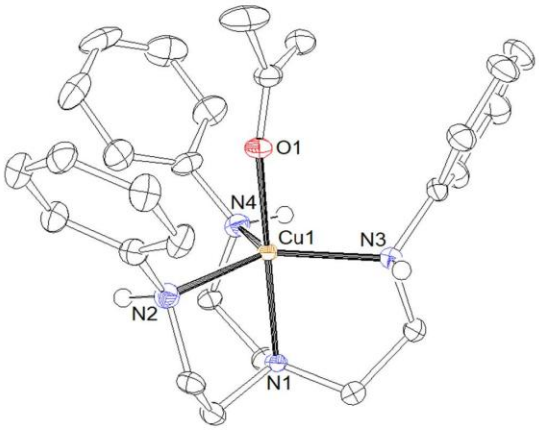


FIGURE 2 | ORTEP Plot of the molecular structure of **1a-acetone**. Nonbinding anions, solvent molecules, and carbon-bound hydrogen atoms are omitted for clarity. Ellipsoids are drawn at 50% probability.

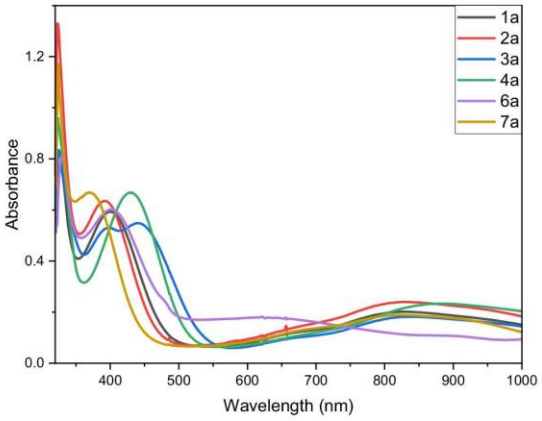


FIGURE 3 | UV–vis spectra of complexes **1a–7a** in acetone at −50°C.

UV–vis spectra of the copper(II) complexes (**1a–7a**) were obtained by mixing 1 equivalent of $Cu(ClO_4)_2{\cdot}6\,H_2O$ with the corresponding ligands in acetone under an inert atmosphere (Figure 3). The spectra of the intensively green-colored solutions presented similar features, characterized by an intense ligand-to-metal charge transfer (LMCT) band between 370 and 441 nm, and two broad d–d bands at around 680 and 840 nm, in line with data reported previously for the related copper(II) complex with the ligand $TIPT_2$aped by Itoh and coworkers [14]. The presence of two broad d–d bands indicates a TBP geometry of the complexes. However, the lack of a clear separation between these bands suggests a significant contribution of a SP arrangement, in accordance with the molecular structures of complexes **1a-acetone** and **4a-acetone** (Figures 2 and S75). Complexes with stronger electron-donating and sterically hindered ligands, such as **3a** and **4a**, exhibited red-shifted LMCT bands ($\lambda_{max} = 441$ and 432 nm) compared to **1a** ($\lambda_{max} = 403$ nm). In contrast, complexes containing electron-withdrawing ligands **L2** and **L7** showed a blueshift of the LMCT bands, as observed in complexes **2a** and **7a** ($\lambda_{max} = 392$ and 371 nm). Interestingly, complex **3a** showed two pronounced bands at 441 and 399 nm (blue line in Figure 3), whose intensity changes according to the pH. This indicates that for **3a**, in contrast to the other complexes, coordinated water is partially deprotonated to hydroxide, leading to two absorption maxima in the UV–vis spectrum. Whereas the band at 441 nm increases in the presence of perchloric acid ($HClO_4$), the one at 399 nm decreases drastically (Figure S1). This phenomenon can be attributed to reversible protonation of the coordinated hydroxide ion, which was previously reported for the copper(II) Me_6tren system and other copper(II) complexes [34, 37, 38]. The overall acid–base equilibria can be quite complex and were investigated in great detail by Itoh and coworkers for the copper–tmpa complex [39].

Finally, no formation of $[Cu(\mathbf{L5})](ClO_4)_2$ complex was observed. The solution of the ligand **L5** showed no color change upon addition of $Cu(ClO_4)_2{\cdot}6\,H_2O$, and the UV–vis spectrum displayed no significant variation in the absorption bands. Furthermore, attempts to obtain the complex only yielded the uncoordinated

10990682c, 0, Downloaded from https://chemistry-europe.onlinelibrary.wiley.com/doi/10.1002/ejic.70203, Wiley Online Library on [14/05/2026]. See the Terms and Conditions (https://onlinelibrary.wiley.com/terms-and-conditions) on Wiley Online Library for rules of use; OA articles are governed by the applicable Creative Commons License

crystalline ligand **L5** (Figure 1e). We hypothesize that the lack of coordination to the copper center is due to the substantial steric hindrance imposed by the six phenyl groups in close proximity to the nitrogen atoms.

2.3 | Synthesis and Characterization of Copper(I) Complexes

The copper(I) complexes [Cu(**L1**)](ClO_4) (**1b**), [Cu(**L2**)](ClO_4) (**2b**), [Cu(**L3**)](ClO_4) (**3b**), [Cu(**L4**)](ClO_4) (**4b**), [Cu(**L6**)](ClO_4) (**6b**), and [Cu(**L7**)](ClO_4) (**7b**) were synthesized by mixing 1 equivalent of [Cu($MeCN)_4$](ClO_4) with the corresponding ligand under inert atmosphere in a glovebox, affording colorless to pale yellow solutions. Despite numerous efforts, no crystals suitable for X-ray diffraction could be obtained, and disproportionation occurred in highly concentrated solutions as observed previously for copper complexes with tren-related ligands [40–43]. Therefore, the complexes were characterized by nuclear magnetic resonance (NMR) spectroscopy. The ^{1}H NMR spectra of ligand **L1** and complex **1b** are compared in Figure 4, while the corresponding data for the other systems are provided in the supplementary information (Figures S54–S67). The sharp NMR peaks are indicative of diamagnetic copper(I) complexes. The spectra of the complexes did not show coordination to acetonitrile and exhibited downfield shifts of the peaks compared to the free ligands. This shift is especially evident for protons adjacent to nitrogen donor atoms, and it is attributed to deshielding caused by the decrease of electron density upon coordination to the copper(I) center [44]. The fact that acetonitrile is not coordinated is in line with earlier investigations on related copper(I) complexes with tren-based ligands and is different in comparison with several complexes based on tmpa ligands [15, 43, 45, 46].

Attempts to synthesize the [Cu(**L5**)](ClO_4) complex were unsuccessful, as no coordination between ligand **L5** and [Cu($MeCN)_4$](ClO_4) was detected. The lack of coordination is evident from the complete overlap of the ^{1}H NMR spectra of ligand **L5** recorded both in the presence and absence of copper(I) source (Figure S2).

2.4 | Reactivity of Copper(I) Complexes with Dioxygen

Complexes **1b** and **2b** reacted with O_2 at low temperatures, leading to a color change of the solutions from pale yellow to dark green. Low–temperature–stopped flow UV–vis measurements revealed the gradual formation of absorption bands at around 370 nm (Figures S3 and S4), consistent with the formation of hydroperoxido complexes **1h** and **2h**, in excellent agreement with literature data for related systems [14, 20, 22, 43, 47].

In contrast, when **3b** reacted with dioxygen at −80°C, an absorption band at 419 nm was detected. The formation of this band occurred within the mixing time of the stopped-flow experiment,

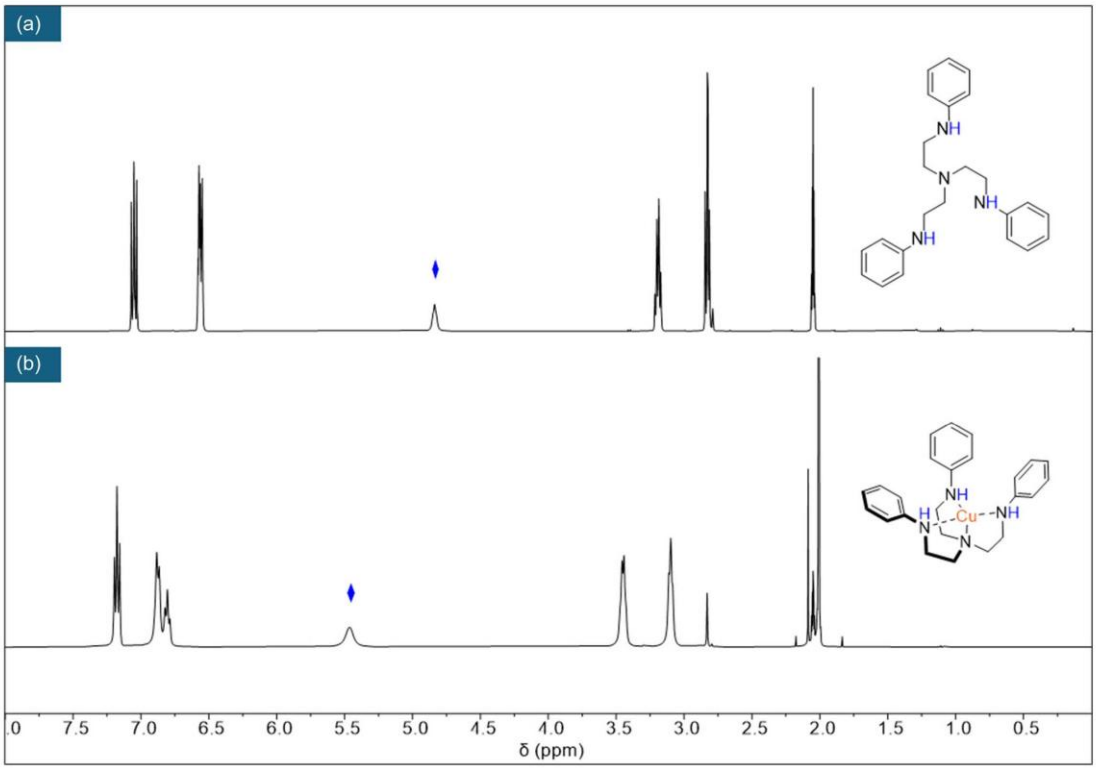


FIGURE 4 | ^{1}H NMR spectra of ligand **L1** (a) and complex **1b** (b) measured in $(CD_3)_2CO$ at room temperature. Charges and anions are omitted for clarity. The peak attributed to the N−H proton is highlighted with a blue diamond.

10990682c, 0, Downloaded from https://chemistry-europe.onlinelibrary.wiley.com/doi/10.1002/ejic.70203, Wiley Online Library on [14/05/2026]. See the Terms and Conditions (https://onlinelibrary.wiley.com/terms-and-conditions) on Wiley Online Library for rules of use; OA articles are governed by the applicable Creative Commons License

and its intensity decreased over time, while a simultaneous increase in absorbance at 387 nm was observed (Figures S5 and S6). According to our previous results and the reported literature data, the absorption at 419 nm was assigned to the *end-on* superoxido copper(II) complex **3s** (some representative examples are provided in the cited references) [10, 42, 48–52]. A detailed spectroscopic analysis of a related superoxido copper complex was previously reported by Solomon and coworkers [53]. Similarly, reaction of **4b** with dioxygen at −80°C led to the formation of an absorption band at 425 nm within the mixing time of the stopped-flow experiment, which was attributed to the *end-on* superoxido copper(II) complex **4s** (Figure 5a). In contrast to **3s**, the corresponding spectroscopic feature generated from **4b**, although lower in intensity, remained stable for approximately 10 s under the same conditions before undergoing further reactions. This difference is attributed to the steric influence of *tert*-butyl substituents, which restrict coordination at the metal center and better stabilize the transient intermediate **4s**.

The instability of the superoxido intermediates generated from **1b** and **2b** can be attributed to the electronic properties of the ligands. In particular, we assume that **L2** does not stabilize the radical moiety effectively due to the coordination of electron-deficient aniline groups to the copper center. Therefore, the superoxido intermediate rapidly converts to the hydroperoxido complex upon formation, and it cannot be detected spectroscopically. In contrast, ligands bearing strong electron-donating substituents in the *para*-position of the aromatic ring (**L3**) or sterically demanding moieties (**L4**) provide greater stabilization of the radical species, which can be detected through UV–vis measurements, as described above.

Analogous to the spectroscopic behavior observed for **3b**, the absorption band at 425 nm associated with **4s** decreased in intensity upon increasing the temperature to −60°C, while a new absorption band increased at 393 nm (Figure 5b). These observations are consistent with the rapid initial formation of the superoxido copper(II) intermediates **3s** and **4s**, followed by their subsequent conversion into the corresponding hydroperoxido complexes **3h** and **4h**. This assignment is supported by the similarity of their UV–vis spectra to those of related hydroperoxido complexes discussed above. All hydroperoxido intermediates undergo gradual decomposition over time, likely resulting from consecutive reactions and/or thermal instability.

The mechanism for these reactions can be described according to Scheme 3, in which the proton and electron required for the formation of the hydroperoxido copper(II) complex are provided either by the solvent or by a second equivalent of the copper(I) complex.

As mentioned in the introduction, Masuda and coworkers described the first crystal structure of a hydroperoxido copper(II) complex in 1998 [23]. In an excellent follow-up study, they proposed that, in accordance with the mechanism shown in Scheme 3, the hydroperoxido complex could be generated through the reaction between the initial superoxido copper(II) species and the remaining unreacted copper(I) complex [20]. This process results in approximately 50% yield of the hydroperoxido complex and 50% of a copper(II) complex featuring a deprotonated ligand. The reaction was proposed to proceed via coupled electron-transfer/proton-transfer steps or via a hydrogen atom abstraction pathway. Analogously, this mechanism represents the most plausible pathway for the formation of the hydroperoxido complexes in our system. In contrast to our complexes bearing ligands **L3** and **L4**, Masuda and coworkers did not observe the intermediate superoxido copper(II) complex using the H_2BPPA system (ligand structure in Scheme 1). This difference can be attributed to kinetic factors, while formation of the superoxido species is rate-determining, its consecutive reaction to the hydroperoxido complex proceeds significantly faster, thereby preventing its spectroscopic detection.

Unfortunately, a detailed kinetic analysis could not be performed because the formation and decay of the superoxido complexes occurred too rapidly, and the overall kinetics cannot be analyzed using simple kinetic models. In addition, the low stability of the superoxido intermediate prevented the collection of sufficient experimental data to perform a reliable global kinetic analysis.

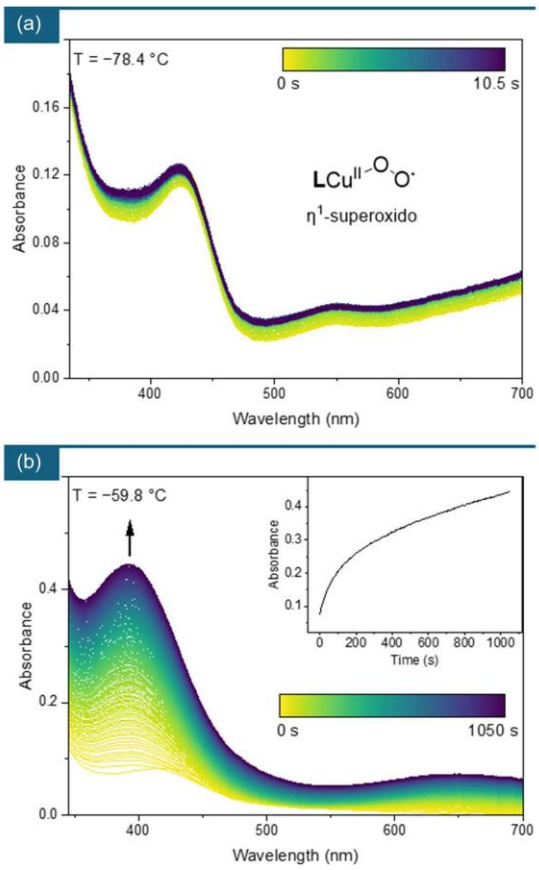
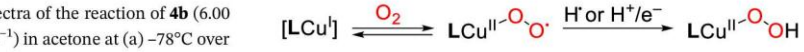


FIGURE 5 | Time-resolved UV–vis spectra of the reaction of **4b** (6.00×10^{-4} mol L^{-1}) with O_2 (5.72×10^{-3} mol L^{-1}) in acetone at (a) −78°C over a period of 10 s; (b) −60°C over a period of 1050s. The inset displays the time-dependent change in absorbance at 393 nm.



SCHEME 3 | Proposed mechanism for the formation of the hydroperoxido copper(II) complexes **1h**–**4h**.

10990682c, 0, Downloaded from https://chemistry-europe.onlinelibrary.wiley.com/doi/10.1002/ejic.70203, Wiley Online Library on [14/05/2026]. See the Terms and Conditions (https://onlinelibrary.wiley.com/terms-and-conditions) on Wiley Online Library for rules of use; OA articles are governed by the applicable Creative Commons License

In contrast, the use of the copper(I) complex supported by the $HIPT_3$tren ligand enabled Itoh and coworkers to determine both the rate constants and the equilibrium constant for the reversible formation of a superoxido complex, which are consistent with the mechanism proposed in Scheme 3 [15]. A summary of the reactivity of the copper(I) complexes toward O_2 reported in this work, together with selected examples from the literature, is presented in Table 1.

Hydroperoxido copper(II) complexes are commonly generated from copper(II) precursors using hydrogen peroxide in the presence of a base such as triethylamine (TEA) [23, 47, 52]. A notable exception previously reported by our group is the hydroperoxido copper(II) complex bearing the tren derivative $^{i}Pr_3$tren as a ligand, in which the consecutive reaction of the superoxido intermediate into the hydroperoxido complex could be clearly observed [43]. The corresponding hydroperoxido complex was also alternatively synthesized using H_2O_2 and TEA [52]. In addition, the use of external hydrogen atom donors such as TEMPO–H provides an alternative route to hydroperoxido copper(II) complexes via hydrogen atom abstraction (HAA) by a superoxido intermediate [14, 19, 54]. The investigation of those alternative synthetic approaches is particularly valuable for elucidating the formation of oxygenated copper(II) intermediates in biological systems, where hydroperoxido species are typically generated through HAA processes.

Finally, the reactivity of complexes **6b** and **7b** toward O_2 was examined in acetone at −80°C. Methylation of the amine moieties is often reported to enhance the stability of oxygenated intermediates, as observed in the Me_6tren and Bz_3Me_3tren (tris(*N*-benzyl-*N*-methylaminoethyl)amine) systems [50, 55]. Similarly, fluorination of ligands is also used to improve thermal and oxidative stability of organometallic complexes [56, 57]. Unfortunately, when O_2 was bubbled in the solutions, no color change occurred, and no oxygenated adducts could be detected using stopped-flow measurements. Only upon warming to 25°C, the solutions gradually turned green. The UV–vis monitoring of **6b** revealed a slow increase of a shoulder at 360 nm and the formation of a broad band at 689 nm over the course of 1 h (Figure S7). Comparison with the spectrum of the corresponding copper(II) complex suggested that the broad band arises from oxidation of the copper(I) center, while the shoulder at 360 nm likely reflects partial decomposition of the ligand. ESI–MS analysis of the oxygenated solution confirmed ligand degradation, showing the cleavage of one arm of the tripodal scaffold (m/z = 284.2135; calc m/z = 284.2127, Figure S34). Similarly, complex **7b** exhibited at room temperature the gradual formation of bands at 370 and 816 nm, which correspond to the UV–vis features of the copper(II) complex **7a**, indicating that the exposure to O_2 results exclusively in oxidation of the Cu(I) center (Figure S8).

2.5 | Reactivity of Copper(I) and Copper(II) Complexes with Hydrogen Peroxide

To verify the nature of the oxygenated intermediates, the corresponding hydroperoxido species were generated in situ by treatment of the copper(I) complexes with 2 equivalents of H_2O_2 (35% aq) in acetone at −30°C under inert atmosphere. In all the cases, the color of the solutions changed from pale yellow to dark green, and the resulting absorption spectra were superimposable with those previously described for **1h–4h**, confirming the formation of the analogous oxygenated species. The only notable difference concerned the stability of the intermediates, which were observed to be more stable under these conditions.

While the electronic properties of the ligands did not show a significant influence on the stability of the hydroperoxido species, the increase of steric hindrance enhanced its thermal stability, and the oxygenated intermediates could be detected up to room

TABLE 1 | Summary of the reactivity of the copper(I) complexes toward O_2.

Complex	UV–vis λ_{max}, nm	Reactivity toward dioxygen	Reference
1b	378	Formation of hydroperoxido (**1h**)	This work
2b	372	Formation of hydroperoxido (**2h**)	This work
3b	419, 387	Formation of *end-on* superoxido (**3s**), consecutive reaction to hydroperoxido (**3h**)	This work
4b	425, 393	Formation of *end-on* superoxido (**4s**), consecutive reaction to hydroperoxido (**4h**)	This work
6b	-	Oxidation to Cu(II) and ligand decomposition	This work
7b	370	Oxidation to Cu(II) (**7a**)	This work
$[Cu^{I}(Me_6tren)(EtCN)]^{+}$	412	Formation of *end-on* superoxido, consecutive reaction to *end-on* peroxido	[42]
$[Cu^{I}(Me_3Bz_3tren)]^{+}$	416	Formation of *end-on* superoxido	[50]
$[Cu^{I}(^{i}Pr_3\text{-tren})]^{+}$	414, 365	Formation of *end-on* superoxido, consecutive reaction to hydroperoxido	[43]
$[Cu^{I}(HIPT_3tren)]^{+}$	434	Formation of *end-on* superoxido	[15]
$[Cu^{I}(TMG_3tren)]^{+}$	442	Formation of *end-on* superoxido	[48]
$[Cu^{I}(TMPA)(MeCN)]^{+}$	420	Formation of *end-on* superoxido	[51]
$[Cu^{I}(H_2BPPA)]^{+}$	375	Formation of hydroperoxido	[20]

10990682c, 0, Downloaded from https://chemistry-europe.onlinelibrary.wiley.com/doi/10.1002/ejic.70203, Wiley Online Library on [14/05/2026]. See the Terms and Conditions (https://onlinelibrary.wiley.com/terms-and-conditions) on Wiley Online Library for rules of use; OA articles are governed by the applicable Creative Commons License

temperature. In contrast, the electronic effects played a small role in the formation rate of the hydroperoxido species. In particular, complex **3h**, characterized by a strongly electron-donating ligand, reached complete formation within 5 s, whereas complex **1h**, bearing the unsubstituted ligand **L1**, required 25 s, and complex **2h**, containing electron-deficient anilines, required 50 s for full formation (Figure S9–S11). Complex **4h** also required a longer time (150 s) to form due to steric hindrance imposed by the *tert*-butyl moieties (Figure S12).

Complexes **6b** and **7b** also reacted with H_2O_2 in acetone at −50°C and −30°C, respectively. When complex **7b** was treated with H_2O_2, a gradual increase in the shoulder at 350 nm was observed, together with the appearance of a broad band at 663 nm (Figure S14). The formation of hydroperoxido copper(II) complex **7h** is proposed based on the close similarity of these spectral features to those of the previously characterized oxygenated intermediates [1]. Upon treatment of **6b** with H_2O_2, the solution turned yellow. The UV–vis spectrum showed a broad increase in the absorption between 360 and 400 nm and a weak band near 700 nm (Figure S13). The absence of well-defined spectral features suggested the occurrence of consecutive reaction pathways rather than the formation of a stable intermediate. Notably, the final spectrum closely resembles that of alkoxide–copper(II) complex $[Cu^{II}(TMG_3trenO^-)]^+$, generated upon oxidation of $[Cu^{I}(TMG_3tren)]^+$ [58, 59]. Accordingly, it was hypothesized that an analogous pathway operated in this system, leading to the formation of the ligand-hydroxylated copper(II) alkoxide $[Cu(Me_3Ph_3trenO^-)]^+$. ESI–MS analysis supported this assignment, revealing a peak at m/z 494.2119 (calc m/z 494.2107) consistent with the formation of the alkoxide complex (Figure S35). Additional ESI–MS signals also indicated ligand oxygenation (m/z = 431.2823; calc m/z = 431.2811) and partial ligand degradation, consistent with cleavage of one arm of the tripodal scaffold (as previously observed upon addition of O_2, m/z = 284.2136; calc m/z = 284.2127). We propose that oxidation occurred at the N-methyl moieties, as such reactivity is not observed in analogous complexes lacking these methyl substituents.

All reactions with hydrogen peroxide investigated using stopped-flow methods exhibited complex kinetic behavior and were therefore not investigated in further detail. To date, no kinetic studies on these reactions have been reported in the literature. However, earlier work by Karlin and coworkers on a copper(I) complex bearing a tmpa-derived ligand (BA system) proposed a complex reaction mechanism involving Fenton-type chemistry [47]. Overall, the spectral data obtained for the reactions between complexes **1b**–**7b** and H_2O_2 are summarized in Table 2, together with selected examples from the literature.

The formation of the hydroperoxido complexes was also achieved by treating the corresponding Cu(II) precursors (**1a**–**7a**) with 2 equivalents of H_2O_2 (35% aq) and 1 equivalent of TEA in acetone at −30°C. Upon addition of the hydrogen peroxide, an intense absorption band between 350 and 396 nm (depending on the ligand structure) was detected in the UV–vis spectra, along with two weaker bands at around 650 and 840 nm, analogous to those reported above and attributed to hydroperoxido copper(II) complexes (**1h**–**4h** and **7h**). These spectral features are especially in close agreement with those described by Kim et al. and Choi et al. for Cu(II)–hydroperoxido complexes supported by the tren-derived ligands $^{i}Pr_3$-tren (tris[2-(isopropylamino)ethyl]amine) and Me_6-tren, respectively [52, 60]. The intense band is assigned to LMCT transitions from the hydroperoxide ligand to the copper center (HOO^-→Cu(II)), while the two weaker bands correspond to d–d transitions of the Cu(II) ion in a distorted trigonal–bipyramidal geometry [20]. The exact absorption maxima are summarized in Table 2, and the corresponding UV–vis spectra are provided in Figure 6.

2.6 | Reactivity of Copper(I) and Copper(II) Complexes with Cumene Hydroperoxide

The reaction of copper(I) complexes **1b**–**7b** with cumyl–OOH was investigated in acetone at −60°C under inert atmosphere. The corresponding cumylperoxido complexes were prepared in situ by the addition of 5 equivalents of cumyl–OOH to a solution of the copper(I) precursors, resulting in a gradual color change of the solution from light yellow to bright green. Low–temperature–stopped flow UV–vis measurements revealed similar features for complexes **1c**–**4c** and **7c**, showing two weak

TABLE 2 | Summary of the spectral data of Cu(II)–hydroperoxido and Cu(II)–cumylperoxido complexes.

Ligand	UV–vis LMCT (HOO^-→Cu(II)) λ_{max}, nm	UV–vis LMCT ($CumylOO^-$→Cu(II)) λ_{max}, nm	Reference
L1	378 (**1h**)	452, 675 (**1c**)	This work
L2	372 (**2h**)	456, 668 (**2c**)	This work
L3	387 (**3h**)	677 (**3c**)	This work
L4	393 (**4h**)	470, 662 (**4c**)	This work
L6	–	–	This work
L7	350 (**7h**)	461, 654 (**7c**)	This work
Me_6tren	375	440, 680, 787	[60]
$^{i}Pr_3$-tren	360	420, 670, 815	[52, 61]
$TIPT_3$tren		396, 465, 748	[62]
TMPA	379	430, 690, 790	[22, 63]
BA	393	–	[47]
H_2BPPA	380	–	[22]

10990682c, 0, Downloaded from https://chemistry-europe.onlinelibrary.wiley.com/doi/10.1002/ejic.70203, Wiley Online Library on [14/05/2026]. See the Terms and Conditions (https://onlinelibrary.wiley.com/terms-and-conditions) on Wiley Online Library for rules of use; OA articles are governed by the applicable Creative Commons License

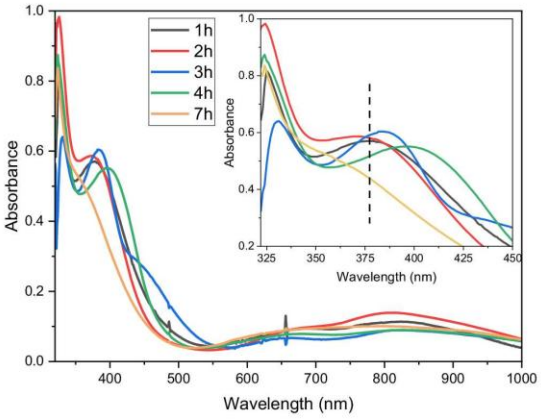


FIGURE 6 | UV–vis spectra of complexes **1h–4h** and **7h** in acetone at −30°C. The inset is focused on the 325–450 nm region to highlight the shifts in the absorption maxima of the complexes.

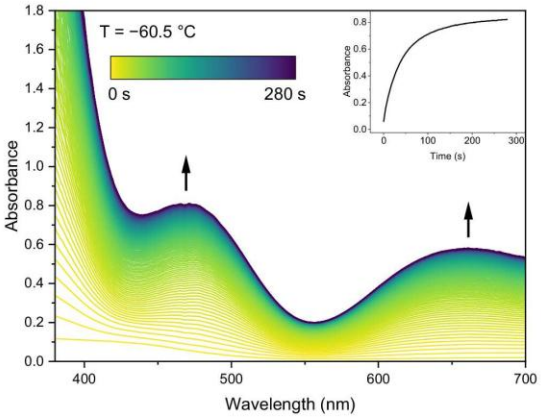


FIGURE 7 | Time-resolved UV–vis spectra of the reaction of **4b** (1.80 × 10^{-3} mol L^{-1}) with cumyl–OOH (9.00 × 10^{-3} mol L^{-1}) in acetone at −60°C over a period of 480 s. The inset displays the time-dependent change in absorbance at 470 nm.

absorption bands at around 460 and 660 nm, slightly shifted depending on the ligand structure (e.g., complex **4c** in Figure 7). Based on the close resemblance of these UV–vis features to those previously reported for Cu(II)–alkylperoxido complexes, the species generated in this reaction were assigned to cumylperoxido complexes [1, 60–63]. Accordingly, the absorption bands were assigned to the LMCT transitions from the alkylperoxide to the copper center (Cumyl–OO^{-}→Cu(II)). The exact absorption maxima are summarized in Table 2 together with selected examples from the literature, and the corresponding UV–vis spectra are provided in the supporting information (Figures S15–S19).

Unlike the hydroperoxido species, increased steric hindrance did not enhance the stability of the alkylperoxido complex. In contrast, electron-deficient ligands promoted their stabilization, as observed especially for complex **7c**, which remained stable for 100 s at 0°C before slowly decaying. All the other intermediates exhibited gradual decomposition at lower temperatures and underwent rapid decay upon warming to room temperature. Both steric and electronic properties of the ligands influenced the formation rates of the alkylperoxido species and induced slight variations in their absorption features. Whereas complex **1c** formed within 4 min, complexes bearing electron-deficient ligands, such as **2c** and **7c**, required longer formation times, up to 50 min at −60°C. When sterically demanding ligands were employed (L4), the increased hindrance around the copper center also slightly slowed the formation of the oxygenated intermediates to 8 min. In contrast, complex **3c**, featuring an electron-donating ligand, reached complete formation within only 40 s.

As described above for the formation of the hydroperoxido complexes, the kinetics of the reactions between the copper(I) species and cumene hydroperoxide are complex and were therefore not investigated in detail. However, Itoh and coworkers successfully obtained kinetic data for the reaction of the related complex $[Cu^{I}(TIPT_3tren)(CH_3CN)]ClO_4$ with cumene hydroperoxide, which allowed them to propose a mechanistic model involving Fenton-type chemistry [62]. Although those measurements were performed in dichloromethane, whereas our experiments were carried out in acetone, the overall reaction rates are comparable, and a similar reaction pathway is considered plausible in our systems. This mechanistic interpretation also explains why the use of simple kinetic models was not successful in describing the reaction behavior of our systems.

The formation of cumylperoxido complexes was also tested by treating the corresponding Cu(II) precursors (**1a**–**7a**) with 5 equivalents of cumyl–OOH and 1 equivalent of TEA in acetone at −60°C. When **1a**, **2a**, and **7a** were tested, the color of the solutions changed from green to bright green, and the resulting absorption spectra matched those previously described for **1c**, **2c**, and **7c**, confirming the formation of the analogous oxygenated species (Figure S20). However, the intermediates were found to be less stable under these conditions, as the absorption bands assigned to the alkylperoxido species gradually decayed at −60°C. In contrast, when complexes **3a** and **4a** were reacted with cumyl–OOH and TEA, no alkylperoxido species could be detected, and the spectra collected immediately after the addition of the cumylperoxido solution only showed decomposition of the intermediates.

2.7 | Reactivity of Copper(II) Hydroperoxido Complexes with External Substrates

Hydroperoxido copper(II) complexes often display limited reactivity toward external substrates. In most cases, they are either unreactive, as observed for systems bearing Me_6tren or BA ligands, or they undergo rapid intramolecular ligand hydroxylation, as reported for the TMG_3tren system (ligands structure in Scheme 1) [47, 59, 60]. Nevertheless, examples of hydroperoxido copper(II) complexes capable of oxidizing external substrates have been described in the literature. For instance, bis(benzimidazole)amine-based systems proved to be reactive in the oxidative degradation of cellulose, serving as functional models for LPMOs [64]. Similarly, hydroperoxido complexes bearing the $^{i}Pr_3$tren ligand exhibit pronounced nucleophilic reactivity toward

10990682c, 0, Downloaded from https://chemistry-europe.onlinelibrary.wiley.com/doi/10.1002/ejic.70203, Wiley Online Library on [14/05/2026]. See the Terms and Conditions (https://onlinelibrary.wiley.com/terms-and-conditions) on Wiley Online Library for rules of use; OA articles are governed by the applicable Creative Commons License

substrates such as benzoyl chloride and 2-phenylpropionaldehyde (2-PPA) [52]. Therefore, complexes **1h–4h** and **7h** were investigated in electrophilic and nucleophilic oxidative reactions between −50°C and 0°C.

The electrophilic character of the hydroperoxido species was evaluated through the oxidation of thioanisole and cyclohexene [60]. However, upon addition of 100 equivalents of substrates to a solution of **1h–4h** and **7h** in acetone, no spectral changes were detected. The product analysis of the reaction mixtures confirmed the absence of oxidized products, indicating that these hydroperoxido complexes were not capable of electrophilic oxidative reactions under these conditions.

The nucleophilic character of complexes **1h–4h** and **7h** was evaluated through the oxidation of benzoyl chloride (PhCOCl) and the aldehyde deformylation of 2-PPA [52]. Similar to the $^{i}Pr_3$tren system, in which the addition of 100 equivalents of PhCOCl led to a first-order decay of the hydroperoxido-related absorption bands, the treatment of the **1h–4h** and **7h** in acetone with PhCOCl (100 equivalents) resulted in modifications of the characteristic absorption bands associated with the oxygenated intermediates (Figures 8a, S21–S24). Specifically, the absorption maxima shifted toward those of the corresponding copper(II) complexes, with partial decomposition occurring at higher temperatures. In all cases, the analysis of the products confirmed the formation of benzoic acid, consistent with a nucleophilic oxidation pathway. In contrast, the addition of 2-PPA to complexes **1h–4h** and **7h** resulted in no detectable spectral changes, and the intermediates remained intact in solution, demonstrating that the hydroperoxido complexes are capable of oxidative reactions but are unreactive in aldehyde deformylation under these conditions. A summary of the reactivity of the hydroperoxido copper(II) complexes reported in this work, together with selected examples from the literature, is presented in Table 3.

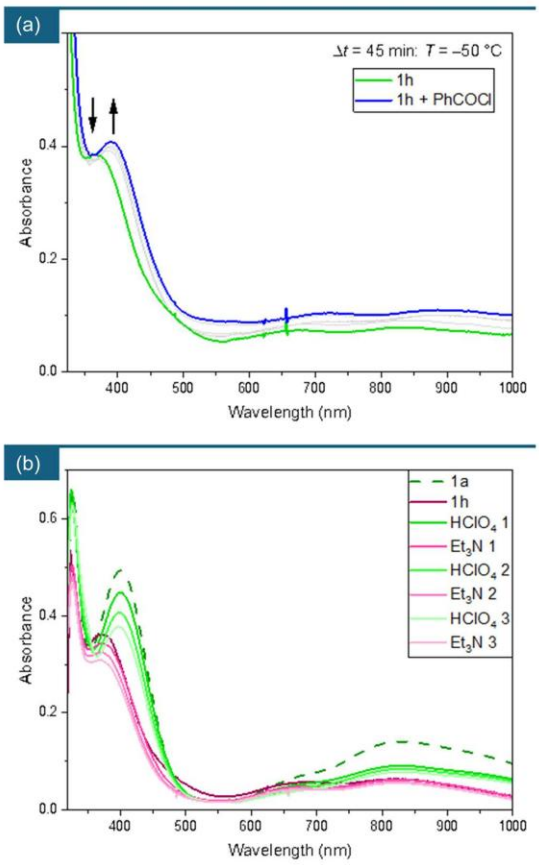


FIGURE 8 | (a) UV–vis spectra of the reaction of **1h** (2.00×10^{-4} mol L^{-1}) with PhCOCl (1.99×10^{-2} mol L^{-1}) in acetone at −50°C over a period of 45 min; (b) UV–vis spectra of the reversible acid–base reaction between **1a** and **1h** upon addition of $HClO_4$ (1 equiv) and TEA (1 equiv).

Interestingly, the addition of 1 equivalent of perchloric acid ($HClO_4$) to the solutions of complexes **1h–4h** and **7h** at −50°C resulted in immediate decay of the LMCT bands associated with the hydroperoxido adducts, yielding the corresponding copper(II) starting material. Subsequent addition of 1 equivalent of TEA fully restored the initial spectra. This reversible acid–base reaction could be repeated for at least three cycles, each showing complete recovery of the hydroperoxido complex (Figures 8b, S25–S28). Such behavior, previously reported for hydroperoxido species bearing BA ligand, indicates the existence of a clean equilibrium between the hydroperoxido adducts and the corresponding copper(II) species, which can be controlled by acid–base chemistry [47]. Additionally, it shows that one equivalent of acid or base is sufficient to drive the equilibrium completely in either direction.

2.8 | Reactivity of Copper(II) Cumylperoxido Complexes with External Substrates

Since the first structural characterization of a mononuclear copper(II) cumylperoxido complex by Kitajima and coworkers in 1993, the reactivity of alkylperoxo species has been extensively investigated [26]. These complexes were found to promote C–H bond activation of external substrates such as 1,4-cyclohexadiene (CHD), typically via O–O bond homolysis, as well as oxygen atom transfer reactions in the presence of triphenylphosphine [25, 27, 65]. In addition, they exhibit oxidative nucleophilic reactivity, including aldehyde deformylation [25, 30]. Accordingly, the reactivity of complexes **1c**, **2c**, and **7c** toward external substrates was investigated between −60°C and −30°C.

The electrophilic character of the cumylperoxido complexes was evaluated using thioanisole and cyclohexene as model compounds. The treatment of the solutions of **1c**, **2c**, and **7c** in acetone with 72 equivalents of substrate only resulted in minor spectral changes in the presence of thioanisole, while no detectable spectral changes were observed upon addition to cyclohexene. Consistent with these observations, product analysis showed no oxidation of cyclohexene, and only trace formation of methyl phenyl sulfoxide could be detected in ESI–MS.

The nucleophilic character of complexes **1c**, **2c**, and **7c** was evaluated through the oxidation of PhCOCl and the aldehyde deformylation of 2-PPA. As observed for the hydroperoxido analogs described above, addition of 72 equivalents of PhCOCl to the solutions of **1c**, **2c**, and **7c** in acetone resulted in pronounced changes in the absorption spectra, consistent with decay of the alkylperoxido intermediates (Figures S29–S31). Specifically,

10990682c, 0, Downloaded from https://chemistry-europe.onlinelibrary.wiley.com/doi/10.1002/ejic.70203, Wiley Online Library on [14/05/2026]. See the Terms and Conditions (https://onlinelibrary.wiley.com/terms-and-conditions) on Wiley Online Library for rules of use; OA articles are governed by the applicable Creative Commons License

TABLE 3 | Summary of the reactivity of the hydroperoxido and cumylperoxido copper(II) complexes.

Complex	Reactivity toward external substrates	Reference
1h	PhCOCl	This work
2h	PhCOCl	This work
3h	PhCOCl	This work
4h	PhCOCl	This work
7h	PhCOCl	This work
$[Cu^{II}(Me_6\text{-tren})(OOH)]^+$	No reactivity	[60]
$[Cu^{II}(BA)(OOH)]^+$	No reactivity	[47]
$[Cu^{II}(^iPr_3\text{-tren})(OOH)]^+$	PhCOCl, 2-PPA, CCA[a]	[52]
$[Cu^{II}(TMPA)(OOH)]^+$	Dimethyl sulfide	[22]
1c	PhCOCl, 2-PPA	This work
2c	PhCOCl, 2-PPA	This work
7c	PhCOCl, 2-PPA	This work
$[Cu^{II}(Me_6\text{-tren})(OOC(CH_3)_2Ph)]^+$	No reactivity	[60]
$[Cu^{II}(^iPr_3\text{-tren})(OOC(CH_3)_2Ph)]^+$	CHD[b], indene, cyclohexene, toluene[c], tetrahydrofuran,[c] cyclohexane[c]	[61]
$[Cu^{II}(TIPT_3tren)(OOC(CH_3)_2Ph)]^+$	Benzyl alcohol, TEMPOH[d]	[62]
$[Cu^{II}(TMPA)(OOC(CH_3)_2Ph)]^+$	CHD[b]	[63]
$[Cu^{II}(CHDAP)(OOC(CH_3)_2Ph)]^+$	PhCOCl, 2-PP, CHD[b]	[30]

[a]CCA = cyclohexylcarboxaldehyde.
[b]CHD = 1,4-cyclohexadiene.
[c]C–H bonds activation only observed in supercritical CO_2.
[d]TEMPOH = 2,2,6,6-tetramethylpiperidine-1-ol.

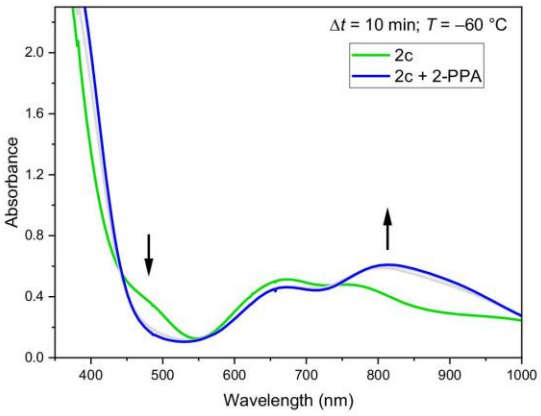
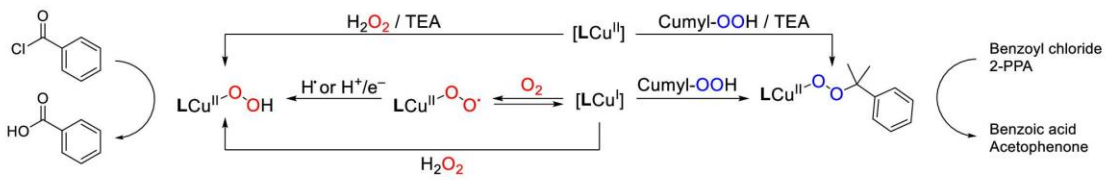


FIGURE 9 | UV–vis spectra of the reaction of **2c** (9.0×10^{-4} mol L^{-1}) with 2–PPA (6.5×10^{-2} mol L^{-1}) in acetone at −60°C over a period of 10 min.

the absorption bands at around 460 nm drastically decreased, while the bands related to d–d transitions shifted toward those of the initial copper(II) complexes. In all cases, the analysis of the products confirmed the formation of benzoic acid and benzoic anhydride.

Since the CHDAP-based alkylperoxido complex (CHDA*P* = N, N′-dicyclohexyl-2,11-diaza3,3pyridinophane) was reported to promote aldehyde deformylation, the reactivity of complexes **1c**, **2c**, and **7c** was investigated toward the oxidation of 2-PPA. In the CHDAP system, addition of 2-PPA led to a first-order decay of the absorption band assigned to the cumylperoxido species [30]. Similarly, treatment of **1c**, **2c**, and **7c** with 72 equivalents of 2-PPA resulted in pronounced spectral changes, consistent with decay of the oxygenated intermediates and partial regeneration of the initial Cu(II) complexes (Figures 9, S32, and S33). Whereas complexes **1c** and **2c** reacted rapidly with both substrates at −60°C, complex **7c** required a higher temperature (−30°C) to react with 2–PPA. Product analysis of the reaction mixtures revealed the formation of acetophenone in all cases. When the reaction was carried out using a stoichiometric amount



SCHEME 4 | Schematic summary of the reactivity of the copper(I) and copper(II) complexes reported in this work toward O_2, H_2O_2, and cumyl–OOH, and the reactivity of hydroperoxido and cumylperoxido species toward external substrates.

10990682c, 0, Downloaded from https://chemistry-europe.onlinelibrary.wiley.com/doi/10.1002/ejic.70203, Wiley Online Library on [14/05/2026]. See the Terms and Conditions (https://onlinelibrary.wiley.com/terms-and-conditions) on Wiley Online Library for rules of use; OA articles are governed by the applicable Creative Commons License

of 2-PPA with respect to the copper complexes, quantitative formation of acetophenone (>94%) was obtained in all cases. Although the mechanism of aldehyde oxidation by Cu(II)–alkylperoxido complexes is still to be clarified, the kinetic investigation performed on the related CHDAP system revealed a negative entropy value and second-order kinetics, suggesting that the oxidation of 2-PPA proceeds via a bimolecular mechanism [30]. Overall, these findings demonstrated that the cumylperoxido complexes do not exhibit significant electrophilic oxidative reactivity but instead undergo nucleophilic oxidation and efficiently promote aldehyde deformylation under the investigated conditions (Table 3).

3 | Summary and Conclusion

In summary, a new class of copper complexes was successfully synthesized by combining the tren backbone with various aryl substituents. Mononuclear copper(II) hydroperoxido and alkylperoxido complexes were prepared and characterized using spectroscopic techniques. Superoxido intermediates were detected when electron-donating and sterically hindered ligands were employed. The formation of hydroperoxido species was achieved either through the reaction of the copper(II) complexes with H_2O_2 and TEA or by oxidation of the corresponding copper(I) complexes with O_2 and H_2O_2 in the absence of a base. The hydroperoxido complexes exhibited reactivity toward benzoyl chloride but remained unreactive in electrophilic oxidation or aldehyde deformylation reactions under the studied conditions. Moreover, an acid–base controlled equilibrium between the hydroperoxido adducts and the corresponding copper(II) species was observed. Reaction of copper(I) precursors with cumene hydroperoxide afforded the corresponding cumylperoxido complexes, which exhibited enhanced stability in the presence of electron-withdrawing ligands. Alternatively, complexes **1c**, **2c**, and **7c** could also be generated from the analogous copper(II) complexes upon exposure to cumyl–OOH in the presence of TEA. These intermediates displayed pronounced reactivity toward benzoyl chloride and efficiently promoted aldehyde deformylation. The reactivity of the copper(I) and copper(II) complexes toward O_2, H_2O_2, and cumyl–OOH, as well as the reactivity of the oxygenated hydroperoxido and cumylperoxido species, is summarized in Scheme 4.

Overall, this work demonstrated that even small modifications in ligand architecture can lead to significant changes in the reactivity of the copper complexes and in the stability of the corresponding reactive intermediates. These findings, together with previous results on copper complexes based on tren ligands, provide valuable insights into ligand design and contribute to a deeper understanding of structure–reactivity relationships in copper–oxygen chemistry.

Acknowledgments

We acknowledge the German Academic Scholarship Foundation (Studienstiftung des deutschen Volkes) for financial support. No grant ID exists. We also acknowledge Friedemann Dreßler for the scientific discussions and valuable suggestions.

Open Access funding enabled and organized by Projekt DEAL.

Funding

This study was supported by Studienstiftung des Deutschen Volkes.

Conflicts of Interest

The authors declare no conflicts of interest.

References

1. C. E. Elwell, N. L. Gagnon, B. D. Neisen, et al., "Copper–Oxygen Complexes Revisited: Structures, Spectroscopy, and Reactivity," *Chemical Reviews* 117 (2017): 2059–2107.

2. J. De Tovar, R. Leblay, Y. Wang, et al., "Copper–oxygen Adducts: New Trends in Characterization and Properties towards C–H Activation," *Chemical Science* 15 (2024): 10308–10349.

3. E. I. Solomon, D. E. Heppner, E. M. Johnston, et al., "Copper Active Sites in Biology," *Chemical Reviews* 114 (2014): 3659–3853.

4. J. P. Klinman, "The Copper-Enzyme Family of Dopamine β-Monooxygenase and Peptidylglycine α-Hydroxylating Monooxygenase: Resolving the Chemical Pathway for Substrate Hydroxylation," *The Journal of Biological Chemistry* 281 (2006): 3013–3016.

5. K. D. Karlin, S. Kaderli, and A. D. Zuberbühler, "Kinetics and Thermodynamics of Copper(I)/Dioxygen Interaction," *Accounts of Chemical Research* 30 (1997): 139–147.

6. C. Würtele, E. Gaoutchenova, K. Harms, M. C. Holthausen, J. Sundermeyer, and S. Schindler, "Crystallographic Characterization of a Synthetic 1: 1 End-On Copper Dioxygen Adduct Complex," *Angewandte Chemie International Edition* 45 (2006): 3867–3869.

7. S. Itoh, "Mononuclear Copper Active-Oxygen Complexes," *Current Opinion in Chemical Biology* 10 (2006): 115–122.

8. B. F. Gherman, D. E. Heppner, W. B. Tolman, and C. J. Cramer, "Models for Dioxygen Activation by the CuB Site of Dopamine β-Monooxygenase and Peptidylglycine α-Hydroxylating Monooxygenase," *JBIC Journal of Biological Inorganic Chemistry* 11 (2006): 197–205.

9. L. Q. Hatcher and K. D. Karlin, *Advances in Inorganic Chemistry* (Elsevier, 2006) pp.131–184.

10. B. Kim and K. D. Karlin, "Ligand–Copper(I) Primary O_2 -Adducts: Design, Characterization, and Biological Significance of Cupric–Superoxides," *Accounts of Chemical Research* 56 (2023): 2197–2212.

11. L. M. Mirica, X. Ottenwaelder, and T. D. P. Stack, "Structure and Spectroscopy of Copper–Dioxygen Complexes," *Chemical Reviews* 104 (2004): 1013–1046.

12. S. Y. Quek, S. Debnath, S. Laxmi, M. Van Gastel, T. Krämer, and J. England, "Sterically Stabilized End-On Superoxocopper(II) Complexes and Mechanistic Insights into Their Reactivity with O–H, N–H, and C–H Substrates," *Journal of the American Chemical Society* 143 (2021): 19731–19747.

13. S. Debnath, S. Laxmi, O. M. C. Stepanic, et al., "A Four-Coordinate End-On Superoxocopper(II) Complex: Probing the Link between Coordination Number and Reactivity," *Journal of the American Chemical Society* 146 (2024): 23704–23716.

14. S. Paria, T. Ohta, Y. Morimoto, H. Sugimoto, T. Ogura, and S. Itoh, "Structure and Reactivity of Copper Complexes Supported by a Bulky Tripodal N_4 Ligand: Copper(I)/Dioxygen Reactivity and Formation of a Hydroperoxide Copper(II) Complex," *Zeitschrift Fur Anorganische Und Allgemeine Chemie* 644 (2018): 780–789.

15. Y. Kobayashi, K. Ohkubo, T. Nomura, et al., "Copper(I)-Dioxygen Reactivity in a Sterically Demanding Tripodal Tetradentate Tren Ligand: Formation and Reactivity of a Mononuclear Copper(II) End-On Superoxo Complex," *European Journal of Inorganic Chemistry* 2012 (2012): 4574–4578.

10990682c, 0, Downloaded from https://chemistry-europe.onlinelibrary.wiley.com/doi/10.1002/ejic.70203, Wiley Online Library on [14/05/2026]. See the Terms and Conditions (https://onlinelibrary.wiley.com/terms-and-conditions) on Wiley Online Library for rules of use; OA articles are governed by the applicable Creative Commons License

16. L. Ciano, G. J. Davies, W. B. Tolman, and P. H. Walton, "Bracing Copper for the Catalytic Oxidation of C–H Bonds," *Nature Catalysis* 1 (2018): 571–577.

17. D. Maiti, H. R. Lucas, A. A. N. Sarjeant, and K. D. Karlin, "Aryl Hydroxylation from a Mononuclear Copper-Hydroperoxo Species," *Journal of the American Chemical Society* 129 (2007): 6998–6999.

18. P. Chen and E. I. Solomon, "Oxygen Activation by the Noncoupled Binuclear Copper Site in Peptidylglycine α-Hydroxylating Monooxygenase. Reaction Mechanism and Role of the Noncoupled Nature of the Active Site," *Journal of the American Chemical Society* 126 (2004): 4991–5000.

19. T. Tano, Y. Okubo, A. Kunishita, et al., "Redox Properties of a Mononuclear Copper(II)-Superoxide Complex," *Inorganic Chemistry* 52 (2013): 10431–10437.

20. T. Fujii, S. Yamaguchi, Y. Funahashi, et al., "Mononuclear Copper(ii)–hydroperoxo Complex Derived from Reaction of Copper(i) Complex with Dioxygen as a Model of DβM and PHM," *Chemical Communications* (2006): 4428–4430.

21. S. Kim, J. W. Ginsbach, J. Y. Lee, et al., "Amine Oxidative N-Dealkylation via Cupric Hydroperoxide Cu-OOH Homolytic Cleavage Followed by Site-Specific Fenton Chemistry," *Journal of the American Chemical Society* 137 (2015): 2867–2874.

22. S. Yamaguchi and H. Masuda, "Basic Approach to Development of Environment-Friendly Oxidation Catalyst Materials. Mononuclear Hydroperoxo Copper(II) Complexes," *Science and Technology of Advanced Materials* 6 (2016): 34–47.

23. A. Wada, M. Harata, K. Hasegawa, et al., "Structural and Spectroscopic Characterization of a Mononuclear Hydroperoxo-Copper(II) Complex with Tripodal Pyridylamine Ligands," *Angewandte Chemie International Edition* 37 (1998): 798–799.

24. T. Abe, Y. Morimoto, K. Mieda, et al., "Geometric Effects on O O Bond Scission of Copper(II)-Alkylperoxide Complexes," *Journal of Inorganic Biochemistry* 177 (2017): 375–383.

25. H. Oh, W.-M. Ching, J. Kim, W.-Z. Lee, and S. Hong, "Hydrogen Bond-Enabled Heterolytic and Homolytic Peroxide Activation Within Nonheme Copper(II)-Alkylperoxo Complexes," *Inorganic Chemistry* 58 (2019): 12964–12974.

26. N. Kitajima, T. Katayama, K. Fujisawa, Y. Iwata, and Y. Morooka, "Synthesis, Molecular Structure, and Reactivity of (alkylperoxo) copper(II) Complex," *Journal of the American Chemical Society* 115 (1993): 7872–7873.

27. A. Kunishita, H. Ishimaru, S. Nakashima, T. Ogura, and S. Itoh, "Reactivity of Mononuclear Alkylperoxo Copper(II) Complex. O–O Bond Cleavage and C–H Bond Activation," *Journal of the American Chemical Society* 130 (2008): 4244–4245.

28. B. D. Neisen, N. L. Gagnon, D. Dhar, A. D. Spaeth, and W. B. Tolman, "Formally Copper(III)–Alkylperoxo Complexes as Models of Possible Intermediates in Monooxygenase Enzymes," *Journal of the American Chemical Society* 139 (2017): 10220–10223.

29. A. Kunishita, J. Teraoka, J. D. Scanlon, et al., "Aromatic Hydroxylation Reactivity of a Mononuclear Cu(II)–Alkylperoxo Complex," *Journal of the American Chemical Society* 129 (2007): 7248–7249.

30. B. Kim, D. Jeong, and J. Cho, "Nucleophilic Reactivity of Copper(ii)–alkylperoxo Complexes," *Chemical Communications* 53 (2017): 9328–9331.

31. M. Kol, R. R. Schrock, R. Kempe, and M. Davis, "Synthesis of Molybdenum and Tungsten Complexes That Contain Triamidoamine Ligands of the Type $(C_6F_5NCH_2CH_2)_3$ N and Activation of Dinitrogen by Molybdenum," *Journal of the American Chemical Society* 116 (1994): 4382–4390.

32. G. E. Greco and R. R. Schrock, "Synthesis of Triamidoamine Ligands of the Type $(ArylNHCH_2\ CH_2)_3$ N and Molybdenum and Tungsten Complexes That Contain an $[(ArylNCH_2\ CH_2)_3\ N]^{3-}$ Ligand," *Inorganic Chemistry* 40 (2001): 3850–3860.

33. G. W. Anderson and R. Paul, "N, N′-Carbonyldiimidazole, a New Reagent for Peptide Synthesis," *Journal of the American Chemical Society* 80 (1958): 4423–4423.

34. S. C. Lee and R. H. Holm, "Synthesis and Characterization of an Asymmetric Bridged Assembly Containing the Unsupported [FeIII-O-CuII] Bridge: An Analog of the Binuclear Site in Oxidized Cytochrome c Oxidase," *Journal of the American Chemical Society* 115 (1993): 11789–11798.

35. M. Schatz, M. Becker, O. Walter, G. Liehr, and S. Schindler, "Reactivity towards Dioxygen of a Copper(I) Complex of Tris(2-Benzylaminoethyl)amine," *Inorganica Chimica Acta* 324 (2001): 173–179.

36. A. W. Addison, T. N. Rao, J. Reedijk, J. Van Rijn, and G. C. Verschoor, "Synthesis, Structure, and Spectroscopic Properties of Copper(II) Compounds Containing Nitrogen–sulphur Donor Ligands; the Crystal and Molecular Structure of Aqua[1,7-Bis(N-Methylbenzimidazol-2′-Yl)-2,6-Dithiaheptane]copper(II) Perchlorate," *Journal of The Chemical Society-Dalton Transactions* (1984): 1349–1356.

37. J. Haak and G. E. Cutsail, "Distinguishing between Aquo and Hydroxo Coordination in Molecular Copper Complexes by ^{1}H and ^{17}O ENDOR Spectroscopy," *Dalton Transactions* 54 (2025): 728–744.

38. M. C. Carrasco, K. J. Dezarn, F. S. T. Khan, and S. Hematian, "Protonation of the Oxo-Bridged Heme/Copper Assemblies: Modeling the Oxidized State of the Cytochrome c Oxidase Active Site," *Journal of Inorganic Biochemistry* 225 (2021): 111593.

39. M. Asahi, S. Yamazaki, S. Itoh, and T. Ioroi, "Acid-Base and Redox Equilibria of a Tris(2-Pyridylmethyl)amine Copper Complex; Their Effects on Electrocatalytic Oxygen Reduction by the Complex," *Electrochimica Acta* 211 (2016): 193–198.

40. S. Schindler, "Reactivity of Copper(I) Complexes Towards Dioxygen," *European Journal of Inorganic Chemistry* 2000 (2000): 2311–2326.

41. M. Becker, F. W. Heinemann, and S. Schindler, "Reversible Binding of Dioxygen by a Copper(I) Complex with Tris(2-Dimethylaminoethyl) amine (Me_6Tren) as a Ligand," *Chemistry - A European Journal* 5 (1999): 3124–3129.

42. M. Weitzer, S. Schindler, G. Brehm, et al., "Reversible Binding of Dioxygen by the Copper(I) Complex with Tris(2-Dimethylaminoethyl) amine (Me_6Tren) Ligand," *Inorganic Chemistry* 42 (2003): 1800–1806.

43. J. Will, C. Würtele, J. Becker, O. Walter, and S. Schindler, "Synthesis, Crystal Structures and Reactivity towards Dioxygen of Copper(I) Complexes with Tripodal Aliphatic Amine Ligands," *Polyhedron* 171 (2019): 448–454.

44. M. Amirnasr, G. Kickelbick, and S. Dehghanpour, "Synthesis, Characterization, and X-Ray Crystal Structures of Bis[*N* -(3,3-Diphenylallylidene)quinolin-8-Amine- κN,κN^8]copper(1+) Tetraphenylborate(1−) ($[Cu(dpa\text{-}Qa)_2]BPh_4$) and Bis[N, N ′-Bis(3,3-Diphenylallylidene)-[1,1′-Biphenyl]-2,2′-Diamine- κN,κN ′]copper(1+) Perchlorate ($[Cu(bdpa\text{-}Bda)_2]ClO_4 \cdot 3\,H_2O$," *Helvetica Chimica Acta* 89 (2006): 274–284.

45. B. S. Lim and R. H. Holm, "Molecular Heme–Cyanide–Copper Bridged Assemblies: Linkage Isomerism, Trends in ν_{CN} Values, and Relation to the Heme- a_3 /Cu_B Site in Cyanide-Inhibited Heme–Copper Oxidases," *Inorganic Chemistry* 37 (1998): 4898–4908.

46. Z. Tyeklar, R. R. Jacobson, N. Wei, N. N. Murthy, J. Zubieta, and K. D. Karlin, "Reversible Reaction of Dioxygen (and Carbon Monoxide) with a Copper(I) Complex. X-Ray Structures of Relevant Mononuclear Cu(I) Precursor Adducts and the Trans-(.mu.-1,2-Peroxo) dicopper(II) Product," *Journal of the American Chemical Society* 115 (1993): 2677–2689.

47. S. Kim, C. Saracini, M. A. Siegler, N. Drichko, and K. D. Karlin, "Coordination Chemistry and Reactivity of a Cupric Hydroperoxide Species Featuring a Proximal H-Bonding Substituent," *Inorganic Chemistry* 51 (2012): 12603–12605.

10990682c, 0, Downloaded from https://chemistry-europe.onlinelibrary.wiley.com/doi/10.1002/ejic.70203, Wiley Online Library on [14/05/2026]. See the Terms and Conditions (https://onlinelibrary.wiley.com/terms-and-conditions) on Wiley Online Library for rules of use; OA articles are governed by the applicable Creative Commons License

48. M. Schatz, V. Raab, S. P. Foxon, et al., "Combined Spectroscopic and Theoretical Evidence for a Persistent End-On Copper Superoxo Complex," *Angewandte Chemie International Edition* 43 (2004): 4360–4363.

49. S. Paria, Y. Morimoto, T. Ohta, et al., "Copper(I)–Dioxygen Reactivity in the Isolated Cavity of a Nanoscale Molecular Architecture," *European Journal of Inorganic Chemistry* 2018 (2018): 1976–1983.

50. K. Komiyama, H. Furutachi, S. Nagatomo, et al., "Dioxygen Reactivity of Copper(I) Complexes with Tetradentate Tripodal Ligands Having Aliphatic Nitrogen Donors: Synthesis, Structures, and Properties of Peroxo and Superoxo Complexes," *Bulletin of the Chemical Society of Japan* 77 (2004): 59–72.

51. C. X. Zhang, S. Kaderli, M. Costas, et al., "Copper(I)−Dioxygen Reactivity of $[(L)Cu^{I}]^{+}$ (L = Tris(2-Pyridylmethyl)amine): Kinetic/Thermodynamic and Spectroscopic Studies Concerning the Formation of $Cu-O_2$ and Cu_2-O_2 Adducts as a Function of Solvent Medium and 4-Pyridyl Ligand Substituent Variations," *Inorganic Chemistry* 42 (2003): 1807–1824.

52. B. Kim, D. Jeong, T. Ohta, and J. Cho, "Nucleophilic Reactivity of a Copper(II)-Hydroperoxo Complex," *Communications Chemistry* 2 (2019): 81–87.

53. J. S. Woertink, L. Tian, D. Maiti, et al., "Spectroscopic and Computational Studies of an End-on Bound Superoxo-Cu(II) Complex: Geometric and Electronic Factors That Determine the Ground State," *Inorganic Chemistry* 49 (2010): 9450–9459.

54. M. Bhadra, W. J. Transue, H. Lim, et al., "A Thioether-Ligated Cupric Superoxide Model with Hydrogen Atom Abstraction Reactivity," *Journal of the American Chemical Society* 143 (2021): 3707–3713.

55. C. E. Campi, K. Parkatzidis, A. Anastasaki, and S. Schindler, "Unusual Stability of an, *End-on*, Superoxido Copper(II) Complex under Ambient Conditions," *Chemistry – A European Journal* 30 (2024): e202401634.

56. J. C. Páez-Franco, M. R. Zermeño-Ortega, C. M. De La O-Contreras, et al., "Relevance of Fluorinated Ligands to the Design of Metallodrugs for Their Potential Use in Cancer Treatment," *Pharmaceutics* 14 (2022): 402–438.

57. L. H. Doerrer and H. V. R. Dias, "Fluorinated Ligands and Their Effects on Physical Properties and Chemical Reactivity," *Dalton Transactions* 52 (2023): 7770–7771.

58. D. Maiti, D. Lee, K. Gaoutchenova, et al., "Reactions of a Copper(II) Superoxo Complex Lead to C–H and O–H Substrate Oxygenation: Modeling Copper-Monooxygenase C–H Hydroxylation," *Angewandte Chemie International Edition* 47 (2008): 82–85.

59. B. Kim, M. T. Brueggemeyer, W. J. Transue, et al., "Fenton-Like Chemistry by a Copper(I) Complex and H_2O_2 Relevant to Enzyme Peroxygenase C–H Hydroxylation," *Journal of the American Chemical Society* 145 (2023): 11735–11744.

60. Y. J. Choi, K.-B. Cho, M. Kubo, et al., "Spectroscopic and Computational Characterization of CuII–OOR (R = H or Cumyl) Complexes Bearing a Me6-Tren Ligand," *Dalton Transactions* 40 (2011): 2234–2241.

61. Y. Lee, B. Kim, S. Kim, et al., "Influence of Solvents on Catalytic C–H Bond Oxidation by a Copper(II)–Alkylperoxo Complex," *ACS Catalysis* 14 (2024): 3524–3532.

62. S. Paria, T. Ohta, Y. Morimoto, et al., "Generation, Characterization, and Reactivity of a Cu^{II}–Alkylperoxide/Anilino Radical Complex: Insight into the O–O Bond Cleavage Mechanism," *Journal of the American Chemical Society* 137 (2015): 10870–10873.

63. T. Tano, M. Z. Ertem, S. Yamaguchi, et al., "Reactivity of Copper(ii)-Alkylperoxo Complexes," *Dalton Transactions* 40 (2011): 10326–10336.

64. I. Castillo, A. P. Torres-Flores, D. F. Abad-Aguilar, A. Berlanga-Vázquez, M. Orio, and D. Martínez-Otero, "Cellulose Depolymerization with LPMO-Inspired Cu Complexes," *ChemCatChem* 13 (2021): 4700–4704.

65. I. Shimizu, Y. Morimoto, G. Velmurugan, et al., "Characterization and Reactivity of a Tetrahedral Copper(II) Alkylperoxido Complex," *Chemistry – A European Journal* 25 (2019): 11157–11165.

Supporting Information

Additional supporting information can be found online in the Supporting Information section. Experimental details are based on published procedures (31, 32, and additional references cited in supporting information).

10990682c, 0, Downloaded from https://chemistry-europe.onlinelibrary.wiley.com/doi/10.1002/ejic.70203, Wiley Online Library on [14/05/2026]. See the Terms and Conditions (https://onlinelibrary.wiley.com/terms-and-conditions) on Wiley Online Library for rules of use; OA articles are governed by the applicable Creative Commons License

3.3 Additional Published Research Articles

In addition to the two articles presented above, which describe the main focus of this research, contributions were also made to other publications, although not as a first author. These works are listed here to provide a more comprehensive overview of the research activities carried out during the PhD and of the expertise acquired in different fields related to copper-mediated dioxygen activation:

- K. Parkatzidis, N. P. Truong, R. Whitfield, C. E. Campi, B. Grimm-Lebsanft, S. Buchenau, M. A. Rübhausen, S. Harrisson, D. Konkolewicz, S. Schindler, A. Anastasaki, *J. Am. Chem. Soc.* **2023**, *145*, 1906 (DOI: https://doi.org/10.1021/jacs.2c11757);

- B. Sánchez-Eguía, C. Sánchez-López, M. Flores-Álamo, N. Schuth, V. M. Ugalde-Saldívar, V. Gómez-Vidales, C. E. Campi, J. R. Álvarez-Idaboy, L. Quintanar, L. Gasque, *Molecules* **2026**, *31*, 1245 (DOI: https://doi.org/10.3390/molecules31081245).

4. References

[1] C. Liu, H. Xu, *J. Inorg. Biochem.* **2002**, *88*, 77.

[2] R. H. Holm, P. Kennepohl, E. I. Solomon, *Chem. Rev.* **1996**, *96*, 2239.

[3] Y. Zhang, J. Zheng, *Molecules* **2020**, *25*, 3366.

[4] J. A. Tainer, V. A. Roberts, E. D. Getzoff, *Curr. Opin. Biotechnol.* **1991**, *2*, 582.

[5] M. M. Harding, M. W. Nowicki, M. D. Walkinshaw, *Crystallogr. Rev.* **2010**, *16*, 247.

[6] J. Liu, S. Chakraborty, P. Hosseinzadeh, Y. Yu, S. Tian, I. Petrik, A. Bhagi, Y. Lu, *Chem. Rev.* **2014**, *114*, 4366.

[7] P. Kuleta, J. Lasham, M. Sarewicz, I. Ekiert, V. Sharma, R. Ekiert, A. Osyczka, *Proc. Natl. Acad. Sci. U.S.A.* **2021**, *118*, e2026169118.

[8] E. M. Stone, L. Chantranupong, G. Georgiou, *Biochem.* **2010**, *49*, 10582.

[9] T. Shimizu, D. Huang, F. Yan, M. Stranava, M. Bartosova, V. Fojtíková, M. Martínková, *Chem. Rev.* **2015**, *115*, 6491.

[10] R. A. Festa, D. J. Thiele, *Curr. Biol.* **2011**, *21*, 877.

[11] W. Kaim, J. Rall, *Angew. Chem. Int. Ed.* **1996**, *35*, 43.

[12] E. I. Solomon, D. E. Heppner, E. M. Johnston, J. W. Ginsbach, J. Cirera, M. Qayyum, M. T. Kieber-Emmons, C. H. Kjaergaard, R. G. Hadt, L. Tian, *Chem. Rev.* **2014**, *114*, 3659.

[13] J. A. Tainer, E. D. Getzoff, J. S. Richardson, D. C. Richardson, *Nature* **1983**, *306*, 284.

[14] J. Osredkar, N. Sustar, *J. Clin. Toxicol.* **2011**, *3*, 1.

[15] Y. Fu, L. Hou, K. Han, C. Zhao, H. Hu, S. Yin, *Clin. Nutr.* **2025**, *48*, 161.

[16] J. Gale, E. Aizenman, *Eur. J. Neurosci.* **2024**, *60*, 3505.

[17] A. Członkowska, T. Litwin, P. Dusek, P. Ferenci, S. Lutsenko, V. Medici, J. K. Rybakowski, K. H. Weiss, M. L. Schilsky, *Nat. Rev. Dis. Primers* **2018**, *4*, 21.

[18] Z. Tümer, L. B. Møller, *Eur. J. Hum. Genet.* **2010**, *18*, 511.

[19] J. T. Rubino, K. J. Franz, *J. Inorg. Biochem.* **2012**, *107*, 129.

[20] I. A. Koval, P. Gamez, C. Belle, K. Selmeczi, J. Reedijk, *Chem. Soc. Rev.* **2006**, *35*, 814.

[21] K. I. Tishchenko, E. K. Beloglazkina, A. G. Mazhuga, N. V. Zyk, *Ref. J. Chem.* **2016**, *6*, 49.

[22] P. M. Colman, H. C. Freeman, J. M. Guss, M. Murata, V. A. Norris, J. A. M. Ramshaw, M. P. Venkatappa, *Nature* **1978**, *272*, 319.

[23] N. Ito, S. E. V. Phillips, C. Stevens, Z. B. Ogel, M. J. McPherson, J. N. Keen, K. D. S. Yadav, P. F. Knowles, *Nature* **1991**, *350*, 87.

[24] A. Volbeda, W. G. J. Hol, *J. Mol. Biol.* **1989**, *2*, 249.

[25] M. Pascaly, I. Jolk, B. Krebs, *Chem. Unserer Zeit* **1999**, *33*, 334.

[26] K. Piontek, M. Antorini, T. Choinowski, *J. Biol. Chem.* **2002**, *277*, 37663.

[27] T. Bertrand, C. Jolivalt, P. Briozzo, E. Caminade, N. Joly, C. Madzak, C. Mougin, *Biochem.* **2002**, *41*, 7325.

[28] A. Messerschmidt, A. Rossi, R. Ladenstein, R. Huber, M. Bolognesi, G. Gatti, A. Marchesini, R. Petruzzelli, A. Finazzi-Agró, *J. Mol. Biol.* **1989**, *206*, 513.

[29] S. Iwata, C. Ostermeier, B. Ludwig, H. Michel, *Nature* **1995**, *376*, 660.

[30] T. Tsukihara, H. Aoyama, E. Yamashita, T. Tomizaki, H. Yamaguchi, K. Shinzawa-Itoh, R. Nakashima, R. Yaono, S. Yoshikawa, *Science* **1995**, *269*, 1069.

[31] H. B. Gray, B. G. Malmström, R. J. P. Williams, *J. Biol. Inorg. Chem.* **2000**, *5*, 551.

[32] J. A. Guckert, M. D. Lowery, E. I. Solomon, *J. Am. Chem. Soc.* **1995**, *117*, 2817.

[33] M. J. Ettinger, *Biochem.* **1974**, *13*, 1242.

[34] J. P. Klinman, *J. Biol. Chem.* **2006**, *281*, 3013.
[35] J. A. Tainer, E. D. Getzoff, K. M. Beem, J. S. Richardson, D. C. Richardson, *J. Mol. Biol.* **1982**, *160*, 181.
[36] J. De Tovar, R. Leblay, Y. Wang, L. Wojcik, A. Thibon-Pourret, M. Réglier, A. J. Simaan, N. Le Poul, C. Belle, *Chem. Sci.* **2024**, *15*, 10308.
[37] F. Escalettes, N. J. Turner, *ChemBioChem* **2008**, *9*, 857.
[38] G. Vaaje-Kolstad, Z. Forsberg, J. S. Loose, B. Bissaro, V. G. Eijsink, *Curr. Opin. Struct. Biol.* **2017**, *44*, 67.
[39] E. Gonzalez-Lopez, K. E. Vrana, *J. Neurochem.* **2020**, *152*, 157.
[40] K. Yoshizawa, N. Kihara, T. Kamachi, Y. Shiota, *Inorg. Chem.* **2006**, *45*, 3034.
[41] R. E. Cowley, L. Tian, E. I. Solomon, *Proc. Natl. Acad. Sci. U.S.A.* **2016**, *113*, 12035.
[42] J. J. Liu, D. E. Diaz, D. A. Quist, K. D. Karlin, *Isr. J. Chem.* **2016**, *56*, 738.
[43] T. V. Vendelboe, P. Harris, Y. Zhao, T. S. Walter, K. Harlos, K. El Omari, H. E. M. Christensen, *Sci. Adv.* **2016**, *2*, e1500980.
[44] P. Wu, F. Fan, J. Song, W. Peng, J. Liu, C. Li, Z. Cao, B. Wang, *J. Am. Chem. Soc.* **2019**, *141*, 19776.
[45] G. Vaaje-Kolstad, B. Westereng, S. J. Horn, Z. Liu, H. Zhai, M. Sørlie, V. G. H. Eijsink, *Science* **2010**, *330*, 219.
[46] A. G. Contato, C. A. Conte-Junior, *Eng* **2025**, *6*, 177.
[47] L. Rieder, M. Sørlie, *Biochem.* **2023**, *62*, 3170.
[48] D. A. Quist, D. E. Diaz, J. J. Liu, K. D. Karlin, *J. Biol. Inorg. Chem.* **2017**, *22*, 253.
[49] G. C. Schröder, W. B. O'Dell, S. P. Webb, P. K. Agarwal, F. Meilleur, *Chem. Sci.* **2022**, *13*, 13303.
[50] B. Wang, X. Zhang, W. Fang, C. Rovira, S. Shaik, *Acc. Chem. Res.* **2022**, *55*, 2280.
[51] S. M. Jones, W. J. Transue, K. K. Meier, B. Kelemen, E. I. Solomon, *Proc. Natl. Acad. Sci. U.S.A.* **2020**, *117*, 11916.
[52] E. I. Solomon, U. M. Sundaram, T. E. Machonkin, *Chem. Rev.* **1996**, *96*, 2563.
[53] T. Klabunde, C. Eicken, J. C. Sacchettini, B. Krebs, *Nat. Struct. Mol. Biol.* **1998**, *5*, 1084.
[54] Y. Matoba, T. Kumagai, A. Yamamoto, H. Yoshitsu, M. Sugiyama, *J. Biol. Chem.* **2006**, *281*, 8981.
[55] A. Volbeda, W. G. J. Hol, *J. Mol. Biol.* **1989**, *209*, 249.
[56] M. Rolff, J. Schottenheim, H. Decker, F. Tuczek, *Chem. Soc. Rev.* **2011**, *40*, 4077.
[57] S. Itoh, H. Kumei, M. Taki, S. Nagatomo, T. Kitagawa, S. Fukuzumi, *J. Am. Chem. Soc.* **2001**, *123*, 6708.
[58] N. Fujieda, K. Umakoshi, Y. Ochi, Y. Nishikawa, S. Yanagisawa, M. Kubo, G. Kurisu, S. Itoh, *Angew. Chem. Int. Ed.* **2020**, *59*, 13385.
[59] S. Yamazaki, S. Itoh, *J. Am. Chem. Soc.* **2003**, *125*, 13034.
[60] I. Kipouros, A. Stańczak, J. W. Ginsbach, P. C. Andrikopoulos, L. Rulíšek, E. I. Solomon, *Proc. Natl. Acad. Sci. U.S.A.* **2022**, *119*, e2205619119.
[61] I. Kipouros, A. Stańczak, E. M. Dunietz, J. W. Ginsbach, M. Srnec, L. Rulíšek, E. I. Solomon, *J. Am. Chem. Soc.* **2023**, *145*, 22866.
[62] R. Trammell, K. Rajabimoghadam, I. Garcia-Bosch, *Chem. Rev.* **2019**, *119*, 2954.
[63] C. E. Elwell, N. L. Gagnon, B. D. Neisen, D. Dhar, A. D. Spaeth, G. M. Yee, W. B. Tolman, *Chem. Rev.* **2017**, *117*, 2059.
[64] S. Itoh, *Acc. Chem. Res.* **2015**, *48*, 2066.

[65] L. M. Mirica, X. Ottenwaelder, T. D. P. Stack, *Chem. Rev.* **2004**, *104*, 1013.
[66] K. D. Karlin, S. Kaderli, A. D. Zuberbühler, *Acc. Chem. Res.* **1997**, *30*, 139.
[67] S. Schindler, *Eur. J. Inorg. Chem.* **2000**, *11*, 2311.
[68] M. Weitzer, M. Schatz, F. Hampel, F. W. Heinemann, S. Schindler, *Dalton Trans.* **2002**, 686.
[69] R. M. Roat-Malone, *Bioinorganic Chemistry: A Short Course*, John Wiley & Sons, **2007**.
[70] K. Yamaguchi, *J. Mass Spectrom.* **2003**, *38*, 473.
[71] N. Kitajima, K. Fujisawa, Y. Morooka, K. Toriumi, *J. Am. Chem. Soc.* **1989**, *111*, 8975.
[72] K. Fujisawa, M. Tanaka, Y. Moro-oka, N. Kitajima, *J. Am. Chem. Soc.* **1994**, *116*, 12079.
[73] P. Chen, D. E. Root, C. Campochiaro, K. Fujisawa, E. I. Solomon, *J. Am. Chem. Soc.* **2003**, *125*, 466.
[74] N. W. Aboelella, E. A. Lewis, A. M. Reynolds, W. W. Brennessel, C. J. Cramer, W. B. Tolman, *J. Am. Chem. Soc.* **2002**, *124*, 10660.
[75] N. W. Aboelella, S. V. Kryatov, B. F. Gherman, W. W. Brennessel, V. G. Young, R. Sarangi, E. V. Rybak-Akimova, K. O. Hodgson, B. Hedman, E. I. Solomon, C. J. Cramer, W. B. Tolman, *J. Am. Chem. Soc.* **2004**, *126*, 16896.
[76] S. Paria, Y. Morimoto, T. Ohta, S. Okabe, H. Sugimoto, T. Ogura, S. Itoh, *Eur. J. Inorg. Chem.* **2018**, *2018*, 1976.
[77] K. D. Karlin, N. Wei, B. Jung, S. Kaderli, A. D. Zuberbuehler, *J. Am. Chem. Soc.* **1991**, *113*, 5868.
[78] K. D. Karlin, N. Wei, B. Jung, S. Kaderli, P. Niklaus, A. D. Zuberbuehler, *J. Am. Chem. Soc.* **1993**, *115*, 9506.
[79] S. T. Prigge, B. A. Eipper, R. E. Mains, L. M. Amzel, *Science* **2004**, *304*, 864.
[80] C. Würtele, E. Gaoutchenova, K. Harms, M. C. Holthausen, J. Sundermeyer, S. Schindler, *Angew. Chem. Int. Ed.* **2006**, *45*, 3867.
[81] M. Schatz, V. Raab, S. P. Foxon, G. Brehm, S. Schneider, M. Reiher, M. C. Holthausen, J. Sundermeyer, S. Schindler, *Angew. Chem. Int. Ed.* **2004**, *43*, 4360.
[82] B. Kim, K. D. Karlin, *Acc. Chem. Res.* **2023**, *56*, 2197.
[83] S. Fukuzumi, Y.-M. Lee, W. Nam, *Dalton Trans.* **2019**, *48*, 9469.
[84] S. Debnath, S. Laxmi, O. McCubbin Stepanic, S. Y. Quek, M. Van Gastel, S. DeBeer, T. Krämer, J. England, *J. Am. Chem. Soc.* **2024**, *146*, 23704.
[85] D. A. Quist, M. A. Ehudin, K. D. Karlin, *Inorg. Chim. Acta* **2019**, *485*, 155.
[86] M. Weitzer, S. Schindler, G. Brehm, S. Schneider, E. Hörmann, B. Jung, S. Kaderli, A. D. Zuberbühler, *Inorg. Chem.* **2003**, *42*, 1800.
[87] S. Y. Quek, S. Debnath, S. Laxmi, M. Van Gastel, T. Krämer, J. England, *J. Am. Chem. Soc.* **2021**, *143*, 19731.
[88] S. Kim, J. Y. Lee, R. E. Cowley, J. W. Ginsbach, M. A. Siegler, E. I. Solomon, K. D. Karlin, *J. Am. Chem. Soc.* **2015**, *137*, 2796.
[89] M. Bhadra, J. Y. C. Lee, R. E. Cowley, S. Kim, M. A. Siegler, E. I. Solomon, K. D. Karlin, *J. Am. Chem. Soc.* **2018**, *140*, 9042.
[90] D. E. Diaz, D. A. Quist, A. E. Herzog, A. W. Schaefer, I. Kipouros, M. Bhadra, E. I. Solomon, K. D. Karlin, *Angew. Chem. Int. Ed.* **2019**, *58*, 17572.
[91] P. Pirovano, A. M. Magherusan, C. McGlynn, A. Ure, A. Lynes, A. R. McDonald, *Angew. Chem. Int. Ed.* **2014**, *53*, 5946.
[92] T. Abe, Y. Hori, Y. Shiota, T. Ohta, Y. Morimoto, H. Sugimoto, T. Ogura, K. Yoshizawa, S. Itoh, *Commun. Chem.* **2019**, *2*, 12.

[93] W. D. Bailey, N. L. Gagnon, C. E. Elwell, A. C. Cramblitt, C. J. Bouchey, W. B. Tolman, *Inorg. Chem.* **2019**, *58*, 4706.
[94] T. Fujii, S. Yamaguchi, Y. Funahashi, T. Ozawa, T. Tosha, T. Kitagawa, H. Masuda, *Chem. Commun.* **2006**, 4428.
[95] J. Will, C. Würtele, J. Becker, O. Walter, S. Schindler, *Polyhedron* **2019**, *171*, 448.
[96] C. E. Campi, C. Würtele, S. Schindler, *Eur. J. Inorg. Chem.* **2026**, e70203.
[97] A. Kunishita, M. Kubo, H. Sugimoto, T. Ogura, K. Sato, T. Takui, S. Itoh, *J. Am. Chem. Soc.* **2009**, *131*, 2788.
[98] R. Davydov, A. E. Herzog, R. J. Jodts, K. D. Karlin, B. M. Hoffman, *J. Am. Chem. Soc.* **2022**, *144*, 377.
[99] M. Bhadra, W. J. Transue, H. Lim, R. E. Cowley, J. Y. C. Lee, M. A. Siegler, P. Josephs, G. Henkel, M. Lerch, S. Schindler, A. Neuba, K. O. Hodgson, B. Hedman, E. I. Solomon, K. D. Karlin, *J. Am. Chem. Soc.* **2021**, *143*, 3707.
[100] B. Kim, D. Jeong, T. Ohta, J. Cho, *Commun. Chem.* **2019**, *2*, 81.
[101] S. Paria, T. Ohta, Y. Morimoto, H. Sugimoto, T. Ogura, S. Itoh, *Z. Anorg. Allg. Chem.* **2018**, *644*, 780.
[102] S. Yamaguchi, H. Masuda, *Sci. Technol. Adv. Mater.* **2005**, *6*, 34.
[103] S. Kim, C. Saracini, M. A. Siegler, N. Drichko, K. D. Karlin, *Inorg. Chem.* **2012**, *51*, 12603.
[104] K. Sagar, M. Kim, T. Wu, S. Zhang, E. L. Bominaar, M. A. Siegler, M. Hendrich, I. Garcia-Bosch, *Eur. J. Inorg. Chem.* **2024**, *27*, e202300774.
[105] A. Wada, M. Harata, K. Hasegawa, K. Jitsukawa, H. Masuda, M. Mukai, T. Kitagawa, H. Einaga, *Angew. Chem. Int. Ed.* **1998**, *37*, 798.
[106] T. Osako, S. Nagatomo, T. Kitagawa, C. J. Cramer, S. Itoh, *J. Biol. Inorg. Chem.* **2005**, *10*, 581.
[107] T. Osako, S. Nagatomo, Y. Tachi, T. Kitagawa, S. Itoh, *Angew. Chem. Int. Ed.* **2002**, *114*, 4501.
[108] G. Roelfes, V. Vrajmasu, K. Chen, R. Y. N. Ho, J. U. Rohde, C. Zondervan, R. M. La Crois, E. P. Schudde, M. Lutz, A. L. Spek, R. Hage, B. L. Feringa, E. Münck, L. Que, *Inorg. Chem.* **2003**, *42*, 2639.
[109] F. Li, K. K. Meier, M. A. Cranswick, M. Chakrabarti, K. M. Van Heuvelen, E. Münck, L. Que, *J. Am. Chem. Soc.* **2011**, *133*, 7256.
[110] B. D. Neisen, N. L. Gagnon, D. Dhar, A. D. Spaeth, W. B. Tolman, *J. Am. Chem. Soc.* **2017**, *139*, 10220.
[111] N. Kitajima, T. Katayama, K. Fujisawa, Y. Iwata, Y. Morooka, *J. Am. Chem. Soc.* **1993**, *115*, 7872.
[112] T. Abe, Y. Morimoto, K. Mieda, H. Sugimoto, N. Fujieda, T. Ogura, S. Itoh, *J. Inorg. Biochem.* **2017**, *177*, 375.
[113] H. Oh, W.-M. Ching, J. Kim, W.-Z. Lee, S. Hong, *Inorg. Chem.* **2019**, *58*, 12964.
[114] S. Paria, T. Ohta, Y. Morimoto, T. Ogura, H. Sugimoto, N. Fujieda, K. Goto, K. Asano, T. Suzuki, S. Itoh, *J. Am. Chem. Soc.* **2015**, *137*, 10870.
[115] T. Tano, K. Mieda, H. Sugimoto, T. Ogura, S. Itoh, *Dalton Trans.* **2014**, *43*, 4871.
[116] A. Kunishita, H. Ishimaru, S. Nakashima, T. Ogura, S. Itoh, *J. Am. Chem. Soc.* **2008**, *130*, 4244.
[117] Y. J. Choi, K.-B. Cho, M. Kubo, T. Ogura, K. D. Karlin, J. Cho, W. Nam, *Dalton Trans.* **2011**, *40*, 2234.
[118] T. Tano, M. Z. Ertem, S. Yamaguchi, A. Kunishita, H. Sugimoto, N. Fujieda, T. Ogura, C. J. Cramer, S. Itoh, *Dalton Trans.* **2011**, *40*, 10326.
[119] B. Kim, D. Jeong, J. Cho, *Chem. Commun.* **2017**, *53*, 9328.

[120] M. Becker, F. W. Heinemann, S. Schindler, *Chem. Eur. J.* **1999**, *5*, 3124.
[121] J. Astner, M. Weitzer, S. P. Foxon, S. Schindler, F. W. Heinemann, J. Mukherjee, R. Gupta, V. Mahadevan, R. Mukherjee, *Inorg. Chim. Acta* **2008**, *361*, 279.
[122] Y. Lee, B. Kim, S. Kim, E. W. H. Ng, S. Ariyasu, O. Shoji, S. Yoon, H. Hirao, J. Cho, *ACS Catal.* **2024**, *14*, 3524.
[123] A. Kunishita, J. Teraoka, J. D. Scanlon, T. Matsumoto, M. Suzuki, C. J. Cramer, S. Itoh, *J. Am. Chem. Soc.* **2007**, *129*, 7248.
[124] S. Mandal, R. Mukherjee, *Inorg. Chim. Acta* **2006**, *359*, 4019.
[125] D. Maiti, A. A. Narducci Sarjeant, K. D. Karlin, *J. Am. Chem. Soc.* **2007**, *129*, 6720.
[126] L. Chaloner, M. S. Askari, A. Kutteh, S. Schindler, X. Ottenwaelder, *Eur. J. Inorg. Chem.* **2011**, *27*, 4204.
[127] S. Kim, J. W. Ginsbach, J. Y. Lee, R. L. Peterson, J. J. Liu, M. A. Siegler, A. A. Sarjeant, E. I. Solomon, K. D. Karlin, *J. Am. Chem. Soc.* **2015**, *137*, 2867.
[128] B. Kim, M. T. Brueggemeyer, W. J. Transue, Y. Park, J. Cho, M. A. Siegler, E. I. Solomon, K. D. Karlin, *J. Am. Chem. Soc.* **2023**, *145*, 11735.
[129] N. Singh, N. K. Botcha, T. M. Jones, M. Z. Ertem, J. Niklas, E. R. Farquhar, O. G. Poluektov, A. Mukherjee, *J. Inorg. Biochem.* **2019**, *197*, 110674.
[130] A. Kunishita, J. D. Scanlon, H. Ishimaru, K. Honda, T. Ogura, M. Suzuki, C. J. Cramer, S. Itoh, *Inorg. Chem.* **2008**, *47*, 8222.
[131] D. Maiti, A. A. Narducci Sarjeant, K. D. Karlin, *Inorg. Chem.* **2008**, *47*, 8736.
[132] I. Castillo, A. P. Torres-Flores, D. F. Abad-Aguilar, A. Berlanga-Vázquez, M. Orio, D. Martínez-Otero, *ChemCatChem* **2021**, *13*, 4700.
[133] T. Fujii, A. Naito, S. Yamaguchi, A. Wada, Y. Funahashi, K. Jitsukawa, S. Nagatomo, T. Kitagawa, H. Masuda, *Chem. Commun.* **2003**, 2700.
[134] S. Muthuramalingam, K. Anandababu, M. Velusamy, R. Mayilmurugan, *Inorg. Chem.* **2020**, *59*, 5918.
[135] S. Kumari, S. Muthuramalingam, A. K. Dhara, U. P. Singh, R. Mayilmurugan, K. Ghosh, *Dalton Trans.* **2020**, *49*, 13829.
[136] I. Shimizu, Y. Morimoto, G. Velmurugan, T. Gupta, S. Paria, T. Ohta, H. Sugimoto, T. Ogura, P. Comba, S. Itoh, *Chem. Eur. J.* **2019**, *25*, 11157.
[137] K. Parkatzidis, N. P. Truong, R. Whitfield, C. E. Campi, B. Grimm-Lebsanft, S. Buchenau, M. A. Rübhausen, S. Harrisson, D. Konkolewicz, S. Schindler, A. Anastasaki, *J. Am. Chem. Soc.* **2023**, *145*, 1906.
[138] K. Matyjaszewski, J. Xia, *Chem. Rev.* **2001**, *101*, 2921.
[139] K. Matyjaszewski, *Macromol.* **2012**, *45*, 4015.
[140] C. Boyer, N. A. Corrigan, K. Jung, D. Nguyen, T.-K. Nguyen, N. N. M. Adnan, S. Oliver, S. Shanmugam, J. Yeow, *Chem. Rev.* **2016**, *116*, 1803.